Stationary Waves in the Stratosphere-Troposphere Circulation

by

Lei Wang

A thesis submitted in conformity with the requirements
for the degree of Doctor of Philosophy

Department of Physics
University of Toronto

© Copyright by Lei Wang 2010

Stationary Waves in the Stratosphere-Troposphere Circulation

Lei Wang

Doctor of Philosophy

Department of Physics
University of Toronto

2010

Abstract

Stationary wave theory elucidates the dynamics of the time mean zonally asymmetric component of the atmospheric circulation and separates it from the dynamics of the zonal mean climatological flow. This thesis focuses on the dynamics of stationary wave nonlinearity and its applications in stationary wave modelling and the stationary wave response to climate change.

Stationary wave nonlinearity describes the self-interaction of stationary waves and is important in maintaining the observed zonally asymmetric atmospheric general circulation. Stationary wave nonlinearity is examined in quasi-geostrophic barotropic dynamics in both the presence and absence of transient waves. Stationary wave nonlinearity is shown to account for most of the difference between the linear and full nonlinear stationary waves, particularly if the zonal-mean flow adjustment to the stationary waves is taken into account. Wave activity analysis shows that stationary wave nonlinearity in this setting is associated with Rossby wave critical layer reflection. A time-integration type nonlinear stationary wave modelling technique is tested in this simple barotropic setting and is shown to be able to predict stationary wave nonlinearity and capture the basic features of the full nonlinear stationary wave.

A baroclinic nonlinear stationary wave model is then developed using this technique and is applied to the problem of the stationary wave response to climate change. Previous stationary wave modelling has largely focused on the tropospheric circulation, but the stationary wave field extends into the stratosphere and plays an important dynamical role there. This stationary wave model is able to represent the stratospheric stationary wave field and is used to analyze the Northern Hemisphere stationary wave response to climate change simulated by the Canadian Middle Atmosphere Model (CMAM). In the CMAM simulation changes to the zonal mean basic state alone can explain much of the stationary wave response, which is largely controlled by changes of the zonal mean circulation in the Northern Hemisphere subtropical upper troposphere. However, details of the stratospheric wave driving response are also sensitive to other aspects of the zonal-mean response and to the heating response. Many climate change related effects appear to contribute robustly to an increased wave activity flux into the stratosphere.

Acknowledgments

First and foremost, I'm especially grateful to my supervisor, Professor Paul J. Kushner, for his constant guidance, support, and encouragement. Paul has been steering my research in the right direction and making tremendous efforts to help me tackle both scientific and practical problems. With his outstanding management skills, he has built an actively interactive and well organized research team, a dominant factor contributing to my great study experiences during these years. He has also generously supported me to attend conferences and summer schools, which have largely broadened my knowledge in atmospheric sciences.

I'm also truly grateful to my Ph.D. committee, Professors Theodore G. Shepherd and Kimberly Strong, who have been advising on this project throughout my graduate studies. Their excellent education skills have been very helpful in preparing me for an academic career. Ted's insightful comments during the departmental defense have significantly improved this thesis. My external examiner, Professor Walter A. Robinson (North Carolina State University), has helped widen and deepen the understanding of the dynamical aspects of this thesis through his expert appraisal and informative feedbacks during the final defense. I would like to acknowledge other members of my thesis committee, Professors Kaley A. Walker, W. Richard Peltier and Dylan B. A. Jones, for their careful review and constructive criticism to this thesis.

Professor Mingfang Ting (Lamont-Doherty Earth Observatory) and Doctor Heiner Körnich (Stockholm University) have provided helpful resources and useful discussions at various stages of this project. Also, I have benefited greatly from regular meetings and occasional discussions with Paul's postdocs, Michael Sigmond and Chris Fletcher. This thesis has been improved through careful review and proofreading by Isla Simpson (Chapter 1), Chris Fletcher (Chapter 3), Karen Smith (Chapter 4), Lawrence Mudryk (Chapter 5). I am also thankful to many other graduate students and postdocs in the atmospheric physics group and physics department who together have built a warm and active atmosphere around.

Finally, this thesis is dedicated to my parents, Wang Jingzhou and Wang Mingzhu (王荆州和王明珠), who keep encouraging and supporting me to pursue my ideals. I could never express my appreciation for what they have done for me. It is also impossible for me to adequately appreciate my wife, Liang Shuang, who has brought me to a brand new view of the world through frequent scientific and philosophical discussions.

Table of Contents

Acknowledgments iv

Table of Contents v

List of Tables vii

List of Figures viii

1 Introduction 1

1.1 Characteristics and significance of stationary waves 1

1.2 Stationary wave modelling 6

1.3 Evaluating stationary waves simulated by GCMs 13

1.4 Stationary wave response to climate change 15

1.5 Conclusion 17

2 Interpreting Stationary Wave Nonlinearity in Barotropic Dynamics 25

2.1 Introduction 25

2.2 Numerical models and diagnostics 26

2.3 Zonal wind response 30

2.4 Strongly damped (SD) case 31

2.5 Weakly nonlinear asymptotic theory for the SD case 34

2.6 Weakly damped (WD) case 36

2.7 Nonlinear stationary wave model 39

2.8 Summary and discussion.....40

3 A Stratosphere-Troposphere Stationary Wave Model.....50

3.1 Introduction.....50

3.2 Stationary wave model construction for observational analysis.....51

3.3 NH stationary wave maintenance in ERA-40.....57

3.4 Stationary wave model construction for GCM analysis.....62

4 Diagnosing the Stratosphere-Troposphere Stationary Wave Response to Climate Change in a General Circulation Model.....74

4.1 Introduction.....74

4.2 Applying the stationary wave model to the CMAM simulation.....75

4.3 Stationary Wave Response in the CMAM CCM.....76

4.4 Stationary wave model diagnoses.....79

4.5 Analysis of the stationary wave response using the stationary wave model.....80

4.6 Analysis of the EP-flux response using the stationary wave model.....85

4.7 Summary and discussion.....91

5 Conclusions.....109

5.1 Summary.....109

5.2 Future research topics.....113

Bibliography.....122

Copyright Acknowledgements.....134

List of Tables

Table 1.1: Comparison of two types of stationary wave models ---------- 19

Table 2.1: Notation ---------- 43

Table 3.1: Damping profiles in the stationary wave model ---------- 64

Table 3.2: Damping settings in Table 3.1 for ERA-40 and CMAM cases ---------- 65

Table 3.3: Combinations of forcings used in studying the NH winter stationary wave maintenance in ERA-40 ---------- 66

Table 4.1: Climate change experiments ---------- 95

List of Figures

Figure 1.1: NH winter (January 1979–2002) (a, b) total and (c, d) zonally asymmetric streamfunction plots of ERA-40 (a, c) on 250 hPa pressure level and (b, d) 60°N longitude-height cross section. Contour intervals are 1.8×10^{7} m^2s^{-1} for the total streamfunction (a, b) and 6×10^{6} m^2s^{-1} for the stationary waves (c, d); positive values are plotted in solid and negative in dashed (hereafter for all contour plots). ---------- 20

Figure 1.2: Zonally averaged ERA-40 heat fluxes by (a) stationary waves ($\left[\overline{\upsilon}^{*}\overline{T}^{*}\right]$) and (b) transient waves ($\left[\overline{\upsilon'^{*}T'^{*}}\right]$) for NH January 1979–2002. Contours are labelled in K m s^{-1}. -- 21

Figure 1.3: The maximum amplitude for all latitudes in the stationary wave field for the NH DJF climatology. Data are based on climatological mean geopotential heights for the CCMVal-2 REF-B1 simulations, and for ERA-40 and NCEP data from 1980 to 1999. The black dashed curve is the mean of all the model curves. The CCMVal-2 REF-B1 simulations are forced by observed sea surface temperature (SST) and GHG and ODS forcing, aiming to test the ability of these comprehensive models to mimic the observed climate. ---------- 22

Figure 1.4: The annual cycle of stationary wave field zonal mean amplitude $\left[\sqrt{\left(\overline{Z_g}^{*}\right)^2}\right]$ on the 10 hPa pressure level in the CCMVal-2 REF-B1 simulations, ERA-40 and NCEP data. The contour interval is 100 m. Data are based on climatological mean geopotential heights (Z_g) for the CCMVal-2 models, ERA-40 and NCEP data from 1980 to 1999. ---------- 23

Figure 1.5: (Adopted from Figure 3 in Brandefelt and Körnich 2008; ©American Meteorological Society. Reprinted with permission.) NH winter (DJF) barotropic stationary wave (streamfunction averaged over 850–100 hPa) response to enhanced GHG forcing simulated by IPCC AR4 models (model names are labelled at top-left corner of each panel). These simulations are grouped according to the spatial correlation between their stationary wave response, with 7 simulations in Group S, 3 in Group B, 2 in Group N, and 4 ungrouped (groups are labelled at top-right corner of each panel and ungrouped simulations are not labelled). The contour interval is 1×10^{6} m^2s^{-1}; positive contours are solid, negative dotted,

and zero contour omitted. The gray shading represents 5% level by the Student's *t*-test. The stationary wave response pattern varies significantly among these models, although some common features exist, for example, most of the patterns consist of subtropical wave train structures of comparable spatial scale (zonal wavenumber-5 or so). ---------- 24

Figure 2.1: (a) Reference zonal wind, U_{ref} (solid), the SD case zonal wind, $[u]_{SD}$ (dashed), and the WD case zonal wind, $[u]_{WD}$ (dotted), for $\varepsilon = 2$, (b) SD zonal wind response (solid), WD zonal wind response (dashed), WD response to stationary wave forcing (dotted), WD response to transient wave forcing (dash-dotted). The units for zonal winds are m s^{-1}. ----- 44

Figure 2.2: Streamfunction (left panels) and associated wave activity flux and its divergence (right panels) of the stationary wave response for $\varepsilon = 2$; the Gaussian mountain is centered at the location of the triangle in each plot. (a,b) The DNS streamfunction response and its associated wave activity; (c,d) As in (a,b), for the classical linear model; (e,f) The DNS response minus the linear response in streamfunction and the associated wave activity; (g,h) Linear model response to zonally asymmetric stationary wave nonlinearity, and the associated wave activity. Contour intervals of streamfunction and wave activity divergence are 3×10^{6} m^2s^{-1}, and 1×10^{-5} m s^{-2}, respectively. Solid contours are positive, dashed negative, and dash-dotted zero. The arrows representing wave activity fluxes are four times longer in (f) and (h) than those in (b) and (d) for visibility. For this and subsequent plots, the critical lines are indicated by dash-dotted contours. ---------- 45

Figure 2.3: (a) The zonal mean zonal wind response for the weakly nonlinear asymptotic theory (2.7) and for DNS solutions $[u]_{SD} - U_{ref}$ for $\varepsilon = \{0.1, 0.2, 0.5, 1, 2\}$, ($h_0$={100, 200, 500, 1000, 2000} m) normalized by the reciprocal square of the mountain height. (b) Taylor (2001) diagram comparing the stationary wave response for the weakly nonlinear asymptotic theory (2.8) to the target field, which is the stationary wave in the DNS minus the stationary wave in the classical linear model (LIN(h); e.g., Figure 2.2e for $\varepsilon = 2$), for the cases in panel (a). In a Taylor diagram, the point 1 along the x axis corresponds to perfect agreement between the solutions, the orientation of the point is related to correlation between the fields (as indicated by the quarter circle labelled "correlation"), and the distance from the origin indicates amplitude relative to the amplitude of the target field. ---------- 46

Figure 2.4: (a) Streamfunction of the stationary wave response for $\varepsilon = 2$ for the DNS of the WD case; (b) Streamfunction response for the classical linear model, with τ_E =40 days. Contouring as in the corresponding plots in Figure 2.2. ---------- 47

Figure 2.5: Similar to Figure 2.2 for the WD case. (a,b) Shows the DNS minus the classical linear response (i.e., Figure 2.4a minus Figure 2.4b) and the associated wave activity. Following this is plotted the response diagnosed from the linear model to (c,d) zonally asymmetric stationary wave forcing, (e,f) zonally symmetric stationary wave forcing, (g,h) zonally asymmetric transient wave forcing, (i,j) combined zonally symmetric and zonally asymmetric stationary wave forcing, (k,l) zonally symmetric transient wave forcing. ------ 48

Figure 2.6: Taylor diagram of the linear and nonlinear stationary wave solutions compared with the target stationary wave solution in the DNS of the WD case. Shown are the response with $U = U_{ref}$ and no transient wave forcing (circles), with zonally asymmetric transient wave forcing (upward pointing triangles), with zonally symmetric stationary plus transient wave forcing (downward pointing triangles), and with zonally symmetric stationary plus transient wave forcing and zonally asymmetric transient wave forcing (diamonds). The star represents the latter case for the nonlinear model with damping increased to completely suppress transient waves. The black symbols represent the linear model with the prescribed stationary nonlinearity forcing, the grey ones are without the stationary wave nonlinearity forcing, and white symbols represent the nonlinear model. All runs have $\tau_E = 40$ days, except for the star case which has $\tau_E = 15$ days. ---------- 49

Figure 3.1: Taylor diagram of stationary wave solutions diagnosed by the stationary wave model compared with the ERA-40 NH winter (January 1979–2002) stationary wave climatological mean showing the effects of tuning the meridional variation of Newtonian cooling in the boundary layer when the nonlinear stationary wave model is forced by topography plus diabatic heating absent the longwave radiative component ($O + H - H_{LW}$) from the ERA-40: 1 $n = 0$, 2 $n = 1$, 3 $n = 2$, 4 $n = 3$, 5 $n = 4$, corresponding to a Newtonian cooling profile using (3.8) in the boundary layer ($1 > \sigma > \sigma_b$), where $\tau_s = 4$ days, $\tau_a = 20$ days, and $\sigma_b = 0.7$. The ▽ symbols represent the 250 hPa pressure level, the △ represent the 10 hPa

pressure level, the ○ symbols are the height-longitude cross section at 30°N, and the □ symbols are the height-longitude cross section at 60°N (hereafter for all Taylor diagrams). 67

Figure 3.2: Similar to Figure 3.1 but showing the effects of 1 fixing the zonal mean basic state as prescribed or 2 – 11 relaxing the zonal mean flow towards the prescribed basic state with a certain timescale. ---------- 68

Figure 3.3: Similar to Figure 3.1 but for comparison of the nonlinear stationary wave solution using the damping profiles in Table 3.2 for ERA-40 analysis (1) with the nonlinear stationary wave solutions using damping settings in Held et al. (2002; 2) and Chang (2009; 3). 4 is the linear solution using the same damping profiles as 1. ---------- 69

Figure 3.4: Similar to Figure 2.2e,f, (a) streamfunction and (b) associated wave activity flux (arrows) and its divergence (blue and red contours) of the difference between the nonlinear and linear stationary wave solutions, when the stationary wave model is forced by $O + H - H_{LW}$ from the ERA-40 NH winter (January 1979–2002) climatology. The black solid contour is the critical line for stationary waves. Contour intervals are 3×10^{6} m^2s^{-1} for streamfunction and 2×10^{-5} m s^{-2} for wave activity divergence. ---------- 70

Figure 3.5: Taylor diagram of stationary wave solutions diagnosed by the stationary wave model compared with the ERA-40 NH winter (January 1979–2002) stationary wave climatological mean showing the individual contribution of different combinations of forcings in the ERA-40: 1 $O + H - H_{LW}$ (i.e., topography plus diabatic heating without longwave radiative diabatic heating), 2 $O + H_{tropo}$ (topography plus tropospheric diabatic heating), 3 $O + H - H_{LW} + Trans$ (as in 1 plus the transient wave flux convergences), 4 $O + H$, 5 $O + H + Trans$. ---------- 71

Figure 3.6: Vertical profiles of (a) correlation and (b) relative amplitude examining effects of longwave radiative diabatic heating (H_{LW}) and transient wave flux convergences (*Trans*) in maintaining the NH winter (January 1979–2002) stationary wave field in the ERA-40. ---- 72

Figure 3.7: Similar to Figure 3.5 but for all the combinations of forcings listed in Table 3.3. Symbols “1” and “15” in ▽ overlap almost completely. ---------- 73

Figure 4.1: NH stationary wave streamfunction simulated by CMAM in the past (1960–1979; left column) and the future (2080–2099; middle column), along with the response (right column) on the 10 hPa pressure level for December (the first row, a–c), January (the second row, d–f), and February (the third row, g–i). Only north of 30°N is shown as the stationary wave amplitude in streamfunction is negligible equatorward of 30°N at 10 hPa. The streamfunction contour is 6×10^6 m^2s^{-1} for the past and the future, and 3×10^6 m^2s^{-1} for the response (hereafter for all streamfunction plots); positive values are plotted in solid / red and negative in dashed / blue (hereafter for all contour plots). The statistical significance of the response is indicated by gray shading at the 5% level by the Student's *t*-test, assuming independence of individual years of the detrended data (hereafter for all plots with statistical significance shading).---------- 96

Figure 4.2: NH wintertime (January and February) climatological mean stationary wave streamfunction simulated by CMAM in the past (1960–1979; left column) and the future (2080–2099; middle column), along with the response (right column). The first row (a–c) shows the 250 hPa pressure level, the second row (d–f) shows the 10 hPa pressure level, the third row (g–i) shows the pressure-longitude section at 30°N and the fourth row (j–l) shows the pressure longitude section at 60°N. Note that the 250 hPa plots cover the entire NH, while the 10 hPa plots only show north of 30°N (hereafter for all stereographic plots). ---- 97

Figure 4.3: Taylor diagram of the past (grey symbols), the future (white symbols) and the response (black symbols) of NH winter stationary waves diagnosed by the stationary wave model compared with their CMAM counterparts (the target; Figure 4.2). ---------- 98

Figure 4.4: Similar to Figure 4.2 but for the NH winter stationary wave streamfunction response to climate change in CMAM (1st column, (a, e, i, m), copied from the right column of Figure 4.2 for ease of comparison), and the response diagnosed by the stationary wave model, to ΔZM and ΔH (2nd column, (b, f, j, n)), to ΔZM (3rd column, (c, g, k, o)), and to ΔZM_a (last column, (d, h, l, p), referring to Figure 4.5c, g). ---------- 99

Figure 4.5: CMAM zonal mean zonal wind (upper row) and temperature (lower row) (a, e) in the past and their response to climate change, (b, f) ΔZM, plus three subsets of the response (c, g) ΔZM_a, (d, h) ΔZM_b, and (i) ΔZM_c, which satisfy $\Delta ZM = \Delta ZM_a + \Delta ZM_b + \Delta ZM_c$. Zonal

wind contour intervals are 10 m s^{-1} for the past (a) and 2 m s^{-1} for the response (b–d); temperature contour intervals are 10 K for the past (e) and 1 K for the response (f–i).----- 100

Figure 4.6: Similar to Figure 4.2 but for the response diagnosed by the stationary wave model, to ΔZM_b (left column, (a, d, g, j)), ΔZM_c (middle column, (b, e, h, k)), and ΔH (right column, (c, f, i, l)). ---------- 101

Figure 4.7: Taylor diagram of NH winter stationary wave response to the change in zonal mean basic state (ΔZM, white symbols) and the change in diabatic heating (ΔH, black symbols) compared with the total response to both changes ($\Delta ZM + \Delta H$, the target) diagnosed by the stationary wave model. ---------- 102

Figure 4.8: Taylor diagram of NH winter stationary wave response to three subsets of the change in the zonal mean basic state: ΔZM_a (white symbols), ΔZM_b (grey symbols), and ΔZM_c (black symbols) compared with the response to the total zonal mean changes (ΔZM, the target) diagnosed by the stationary wave model. ---------- 103

Figure 4.9: (a) The CMAM EP-flux (arrows) of the stationary waves in the past, (b) its response to climate change (Future – Past), and (c) the EP-flux response diagnosed by the stationary wave model (*FF – PP* or $\Delta ZM + \Delta H$). Zonal wind (black curves) contour intervals are 10 m s^{-1} for the past (a) and 2 m s^{-1} for the response (b–c); the contour interval of EP-flux divergence (blue and red curves) is 50 m^2s^{-2}.---------- 104

Figure 4.10: (a) Taylor diagram of NH winter stationary wave response to climate change diagnosed by the stationary wave model ($\Delta ZM + \Delta H$) using the "CMAM streamfunction" damping settings (black symbols; the same as the black symbols in Figure 4.3) and the "CMAM EP-flux" damping settings (white symbols) compared with the CMAM stationary wave response to climate change (the target). (b) Similar to Figure 4.7 but using the "CMAM EP-flux" damping settings.(c) Similar to Figure 4.8 but using the "CMAM EP-flux" damping settings. (d) Similar to (c) but for the stationary wave response to ΔZM_d (white symbols), ΔZM_e (grey symbols), and ΔZM_c (black symbols) compared with the response to the total zonal mean changes (ΔZM, the target; white symbols in (a) or the target "1" in (b)).---------- 105

Figure 4.11: Similar to Figure 4.9, but for (a) the CMAM stationary wave EP-flux (arrows) response to climate change (copied from Figure 4.9b for ease of comparison), and the EP-flux response diagnosed by the stationary wave model using the "CMAM EP-flux" damping settings to (b) $\Delta ZM + \Delta H$, (c) ΔZM, (d) ΔH, (e) ΔZM_a, (f) ΔZM_b, (g) ΔZM_c, (h) ΔZM_d, and (i) ΔZM_e. The contour interval of EP-flux divergence (blue and red curves) is 25 m^2s^{-2}. ------ 107

Figure 4.12: Similar to Figure 4.5 but for an alternative decomposition of ΔZM: (a, c) ΔZM_d, (b, d) ΔZM_e, which satisfy $\Delta ZM = \Delta ZM_d + \Delta ZM_e + \Delta ZM_c$. ---------- 108

Figure 5.1: Taylor diagrams of stationary waves in CCMVal-2 REF-B2 simulations (color circles) and the stationary wave solution diagnosed by the stationary wave model forced by $O + H - H_{LW} + Trans_{strat}$ (equivalent to symbol "15" in Figure 3.7; black circles) compared with the ERA-40 stationary wave climatological mean (a) on 250 hPa, (b) on 10 hPa, (c) at 30°N, (d) at 60°N. The NCEP stationary wave field (black diamonds) is included as a measure of the uncertainty in observations. All stationary wave fields are in geopotential height. Data are based on NH winter (January 1980–1999) climatological mean geopotential heights for the CCMVal-2 models, the stationary wave model in Section 3.3, ERA-40, and NCEP reanalysis. ---------- 120

Figure 5.2: Trends in the amplitude of the seasonal-mean stationary wave for the periods 1980–1999, 2000–2049, and 2050–2099 in the CCMVal-2 REF-B2 simulations, ERA-40 (shaded) and NCEP data from 1980 to 1999. The trends for model simulations and NCEP data are plotted in filled circles with the error bars representing the uncertainties in these trends, and the ERA-40 trend is plotted as the horizontal solid line with its uncertainty in grey shading. The linear trend is calculated using least square estimates, and the *t*-distribution is used to test the two-sided hypothesis that the true trend is within the estimated trend plus or minus an uncertainty for a given significance level (p=0.05 here). The multi-model mean trend (indicated as "x") is simply the average of the trends of individual models, where its error bar in magenta indicates the inter-model spread (based on the *t*-test at the 0.05 significance level), its thick error bar in dark grey represents the uncertainty due to the confidence intervals of individual models, and the black thin error bar represents the combination of the above two errors via root sum square. ---------- 121

Chapter 1

1 Introduction

1.1 Characteristics and significance of stationary waves

The time mean atmospheric general circulation is often divided into zonal mean and zonally asymmetric components, with the latter depending strongly on zonal variations in the lower boundary and the former only modestly doing so, because the dynamics of these two components are separable to a certain extent (e.g., Held 1983; Held et al. 2002). This zonally asymmetric component is usually called the "stationary wave field" or "stationary eddy field". The temporal and spatial decomposition is systematically used in this thesis, for example, the streamfunction ψ is decomposed as $\psi = \overline{\psi} + \psi'$ and $\psi = [\psi] + \psi^*$, where the time mean is indicated by " $^{-}$ ", the deviation from time mean is " $'$ ", the zonal mean is " [ ] " and the zonally asymmetric component " * " (following Peixoto and Oort 1992). The "time mean" refers to either the seasonal mean or long-term (e.g., 20 or 30 years) climatological mean of each season or month. The stationary wave field is then $\overline{\psi}^*$, i.e., the deviation from the zonal mean of the time mean flow, and this thesis focuses on the climatological mean of the Northern Hemisphere (NH) wintertime stationary wave field. The stationary wave field consists primarily of stationary Rossby waves and tropical stationary Kelvin waves, and the theoretical analysis in this thesis focuses on the extratropical stationary Rossby waves. The upper row in Figure 1.1 shows the NH January climatological mean (1979–2002) total streamfunction on the 250 hPa pressure level (Figure 1.1a) and the longitude-pressure cross section at 60°N (Figure 1.1b) from European

Centre for Medium-Range Weather Forecasts (ECMWF) reanalysis (ERA-40; Uppala et al. 2005). The stationary wave field is obtained by removing the zonal mean component of the streamfunction (Figure 1.1c–d). The positive and negative centres on these plots are related to the semi-permanent centres of action that were recognized from surface pressure charts in the early 20th century (e.g., Rossby 1939). The main centers of action in the NH winter, such as the Icelandic low, the Aleutian low, the Azores (or Bermuda) high, the Pacific high, and the Siberian high, all correspond to the positive and negative centres in Figure 1.1c–d. A spectral analysis reveals that the NH wintertime tropospheric stationary wave field is primarily comprised of the first three zonal wavenumbers of comparable amplitude (i.e., 35%, 24%, 22% for zonal wavenumbers 1, 2 and 3 respectively of the stationary wave field shown in Figure 1.1c) while the stratospheric stationary wave field is dominated by the zonal wavenumber-1 component (73% for the stationary wave field on 10 hPa) plus a minor wavenumber-2 component (18%) and a very small wavenumber-3 component (6%). The differences in the weightings of wavenumbers between the tropospheric and stratospheric stationary waves can be explained by the filtering effects of the zonal mean flow (Charney and Drazin 1961), which results in tropospheric small scale (large wavenumber) wave components being unable to propagate into the stratosphere. One can also observe from Figure 1.1d that the stationary wave amplitude increases in height, as it roughly follows the strength of the zonal mean flow (Simmons 1974) before the stationary waves break and are absorbed at a higher level. The observed stationary wave field has an almost barotropic vertical profile in the troposphere and extends baroclinically into the stratosphere (e.g., Figure 1.1d).

The stationary wave field is a principal field to explain in the atmospheric general circulation. In the troposphere, the stationary wave field is closely linked to regional climate due

to its positive correlation with the large scale zonal variations in temperature along with its connection with the centres of action mentioned above, and therefore changes in this field can have important societal and ecological impacts. For example, droughts and floods are often associated with stationary wave anomalies (e.g., Liu et al. 1998; Pan et al. 1999), ENSO (El Niño-Southern Oscillation) induces stationary wave anomalies which influence local climate (e.g., Held et al. 1989; Barlow et al. 2001; DeWeaver and Nigam 2004; Shaman and Tziperman 2005), and natural variability is also closely related to seasonal variations of stationary waves (e.g., Branstator 1992; Branstator and Frederiksen 2003).

The stationary wave field also plays a significant role in the wave driven zonal mean circulation, especially in the stratosphere. For example, the stratospheric stationary wave field contributes to more than half of the Eliassen-Palm flux (EP-flux, Eliassen and Palm 1961) and the Brewer-Dobson circulation (BDC) in NH winter (Rosenlof and Holton 1993; Yulaeva et al. 1994). The EP-flux and its convergence represent the propagation and absorption of wave activity, which results in a westward stress on the zonal mean zonal wind. The EP-flux in the stratosphere also describes the eddy driven circulation, in particular the poleward transport of mass and tracers. An important term that controls the BDC is the meridional flux of heat by the waves (the so-called "wave heat flux"), $\left[\overline{\upsilon^* T^*}\right] = \left[\bar{\upsilon}^* \bar{T}^*\right] + \left[\overline{\upsilon'^* T'^*}\right]$, which is proportional to the vertical component of the EP-flux and therefore represents the vertical propagation of the wave activity. The NH heat flux for the ERA-40 1979-2002 January climatological mean has been divided into stationary wave ($\left[\bar{\upsilon}^* \bar{T}^*\right]$, Figure 1.2a) and transient wave ($\left[\overline{\upsilon'^* T'^*}\right]$, Figure 1.2b) contributions. As can be seen from Figure 1.2, the climatological stationary waves and transient

waves contribute to the NH wintertime heat flux almost equally in the troposphere, while in the stratosphere stationary waves contribute twice as much as transients.

Stationary wave theory has progressed from a focus on the simple linear response to thermal and orographic forcing (e.g., Charney and Eliassen 1949; Hoskins and Karoly 1981) to a quantitative framework that accounts for nonlinear stationary wave effects, transient wave effects, and sensitivity to the zonal mean flow (e.g., Valdes and Hoskins 1991; Ting and Yu 1998; Joseph et al. 2004; Brandefelt and Körnich 2008; Chang 2009). This development has been based upon stationary wave models that solve for the stationary wave field in the presence of prescribed zonal mean and zonally asymmetric forcing fields. A key point is that the prescribed forcing fields are understood to fall outside the stationary wave theory itself.

A simple schematic example to start with, for purposes of illustration, is the barotropic quasigeostrophic (QG) vorticity equation for a flow that is independent of y or latitude (Charney and Eliassen 1949),

$$\frac{\partial \zeta}{\partial t} + u\frac{\partial \zeta}{\partial x} + \beta v = -\frac{f_0 u}{H}\frac{\partial h^*}{\partial x}, \tag{1.1}$$

where ζ represents the vorticity, u and v the winds in the zonal (x) and meridional (y) directions, β and f_0 are the meridional gradient and a representative value of the Coriolis parameter, H is a representative depth of the atmosphere, and h represents the topography. The stationary wave response to the zonally asymmetric topographic forcing (h^*) can be obtained by time averaging (1.1) and removing its zonal mean component, i.e.,

$$[\overline{u}]\frac{\partial \overline{\zeta}^*}{\partial x} + \beta \overline{v}^* = -\frac{f_0[\overline{u}]}{H}\frac{\partial h^*}{\partial x} - \left(\overline{u}^*\frac{\partial \overline{\zeta}^*}{\partial x}\right)^* - \overline{u'\frac{\partial \zeta'}{\partial x}}^* . \tag{1.2}$$

Then the stationary wave solution can be obtained by expressing all variables in terms of the streamfunction and taking the inverse of the linear operator on the forcing terms in (1.2) as

$$\overline{\psi}^* = \mathbf{L}^{-1}\left\{-\frac{f_0[\overline{u}]}{H}\frac{\partial h^*}{\partial x} - \left(\overline{u}^*\frac{\partial \overline{\zeta}^*}{\partial x}\right)^* - \overline{u'\frac{\partial \zeta'}{\partial x}}^*\right\}, \quad \text{where } \mathbf{L} = [\overline{u}]\frac{\partial^3}{\partial x^3} + \beta\frac{\partial}{\partial x}. \quad (1.3)$$

In the literature of stationary wave theory, the linear operator $\mathbf{L}$ represents the *basic state* (usually zonally symmetric) of the dynamics; $\frac{f_0[\overline{u}]}{H}\frac{\partial h^*}{\partial x}$ represents the *topographic forcing*; $\overline{u'\frac{\partial \zeta'}{\partial x}}^*$ is the zonally asymmetric component of the *transient wave flux* that is almost always treated as a zonally asymmetric forcing and prescribed in stationary wave models; and $\left(\overline{u}^*\frac{\partial \overline{\zeta}^*}{\partial x}\right)^*$ is the zonally asymmetric component of the *stationary wave flux* that is often prescribed traditionally in stationary wave models but can be predicted as will be discussed in Section 1.2. Another typical zonally asymmetric forcing term is the *diabatic heating* that appears in baroclinic systems. The diabatic heating primarily consists of sensible heating (e.g., turbulently transferred heat from the surface through the boundary layer), latent heating (e.g., condensational heat released by tropical convection and subtropical synoptic precipitation), and radiative heating or cooling of greenhouse gases (GHGs) in the atmosphere. The zonal variations in the diabatic heating come primarily from land-sea contrast and the zonal distribution of precipitation. These terms will be extensively used throughout this thesis.

The thesis first analyzes zonally asymmetric stationary wave flux convergences. Chapter 2 focuses on the so-called "*stationary wave nonlinearity*", also known as "*stationary nonlinearity*" (Ting 1994) or "*nonlinear self-interaction*", which arises primarily through advective terms in the equations of motion and becomes more important for larger amplitude

stationary waves (e.g., Ting et al. 2001 and references therein). For example, in barotropic QG dynamics, stationary wave nonlinearity involves the advection of the stationary wave vorticity by the stationary wave velocity. More specifically, the term $\left(\bar{u}^* \frac{\partial \bar{\zeta}^*}{\partial x}\right)^*$ in (1.3) represents a contribution to the advective stationary wave potential vorticity (PV) flux that is nonlinear in the stationary wave. Observed stationary wave amplitudes are sufficiently large that stationary wave nonlinearity is a leading order term in stationary wave dynamics, comparable in impact to topographic forcing (Valdes and Hoskins 1991; Ting 1994; Ting et al. 2001).

The content of the remainder of this chapter is as follows. In Section 1.2 the existing stationary wave models will be reviewed. To understand projections of the stationary wave response to climate change, it is necessary to understand how general circulation models (GCMs) represent stationary waves. This therefore will be reviewed in Section 1.3. Section 1.4 will then discuss the stationary wave response to climate change and this is followed in Section 1.5 by a summary of major aims of this thesis and publication plans.

1.2 Stationary wave modelling

Stationary wave models, like the Charney and Eliassen (1949) model considered in Section 1.1, are simplified atmospheric models that are used to diagnose the dynamics of the stationary wave field associated with a given zonal mean basic state and zonally asymmetric boundary (i.e., topography), thermal (i.e., diabatic heating), and mechanical forcings (i.e., stationary wave nonlinearity and transient wave flux convergence) (e.g., Smagorinsky 1953; Egger 1976; Hoskins and Karoly 1981; Nigam et al. 1988; Valdes and Hoskins 1991; Ting and Yu 1998; Branstator and Haupt 1998; Held et al. 2002; Chang 2009; Gritsun and Branstator, 2007). The various existing stationary wave models can be distinguished by their

dynamical and numerical features, although these two aspects are often closely related. Stationary wave models can be either linear or nonlinear in the wave fields such as the streamfunction ($\overline{\psi}^*$ in (1.3)). In linear stationary wave models, as in (1.3), the system is usually linearized about a zonal mean flow and nonlinear terms such as stationary and transient terms are treated as prescribed forcings (e.g., Nigam et al. 1986, 1988; Ting 1994; Körnich et al. 2006). Nonlinear stationary wave models try to predict nonlinear stationary wave terms (e.g., Valdes and Hoskins 1991, Jin and Hoskins 1995; Ringler and Cook 1997; Ting and Yu 1998; Held et al. 2002; Chang 2009), i.e., an example corresponding to (1.3) is

$$\mathbf{L}\left(\overline{\psi}^*\right)+\left(\overline{u}^*\frac{\partial\overline{\zeta}^*}{\partial x}\right)^*=-\frac{f_0\left[\overline{u}\right]}{H}\frac{\partial h^*}{\partial x}-\overline{u'\frac{\partial\zeta'}{\partial x}}^* \tag{1.4}$$

with the right hand side terms prescribed and left hand side terms to be predicted. It is not possible to solve (1.4) simply by matrix inversion and an iteration procedure was usually applied to obtain the stationary wave solution in early nonlinear stationary wave models (e.g., Valdes and Hoskins 1991). Although linear models have been helpful in improving the understanding of stationary wave dynamics and have been used widely for more than half a century, nonlinear stationary wave models that have been developed in the last 20 years have shown many advantages over linear stationary wave models such as robustness to the zonal mean basic state and zonally asymmetric forcings (as discussed below). Nonlinear stationary wave models will be used in this thesis.

Having roughly categorized the stationary wave models, some of the historical developments of such models will now be reviewed. The history of stationary wave modeling begins with Charney and Eliassen (1949) who solved the linearized barotropic QG equation in

the presence of topographic forcing alone, which is equivalent to $\overline{\psi}^* = \mathbf{L}^{-1}\left(-\frac{f_0[\overline{u}]}{H}\frac{\partial h^*}{\partial x}\right)$ (see (1.3)), and made the first attempt to numerically simulate the observed stationary wave field. The thermodynamically forced baroclinic stationary wave was first investigated quantitatively in Smagorinsky (1953) using diabatic heating derived from observations, although the importance of the zonally asymmetric component of diabatic heating to the stationary wave field had been recognized earlier by Rossby (1939, 1940). The linear operator used in these studies, which describes the dynamics of the climatological flow, can be represented as a matrix that depends on a prescribed zonal mean flow (idealized, observed, or simulated). Lindzen and Kuo (1969) developed a useful method based on the inversion of this matrix that led to the more widespread use of linear stationary wave models (e.g., Matsuno 1970; Shutts 1978; Hoskins and Karoly 1981; Hendon and Hartmann 1982; Lin 1982; Nigam et al. 1986, 1988; Valdes and Hoskins 1989; Held and Ting 1990; Qin and Robinson 1993; Ting 1994; Körnich et al. 2006; Brandefelt and Körnich 2008).

While the early literature on linear stationary wave models provided insightful understanding of the basic dynamics of the stationary wave field, the development of nonlinear stationary wave models continued. For example, the nonlinear stationary wave model of Valdes and Hoskins (1991) iterated the primitive equations to a steady state while fixing the zonal mean basic state. This nonlinear model is less sensitive to the zonal mean surface flow than corresponding linear models. This kind of approach is in fact equivalent to determining a linear operator linearized about a zonally asymmetric flow. Such an effort is challenging, especially when it involves linearizing about the observed zonally asymmetric climatological mean flow, because such a linear operator is often related to nearly neutrally stable low frequency modes

that can be easily excited by large scale stationary forcings (Simmons et al. 1983). This large sensitivity to small changes in forcing (e.g., Ting and Sardeshmukh 1993; Ting and Yu 1998) has limited the application of this kind of nonlinear stationary wave model.

While most stationary wave models initially used matrix inversion and iteration to solve the steady state equations, forward time integration methods began to be used around 1995 and have been used increasingly since then (e.g., Jin and Hoskins 1995; Rodwell and Hoskins 1996; Ting and Yu 1998; Held et al. 2002; Chang 2009). This trend appears to be driven by the fact that it is relatively easy to modify a dynamical core of a GCM to make a nonlinear stationary wave model, and by the availability of increasing computational power. In addition, time integration methods have the flexibility to become effectively linear models by reducing the amplitude of the forcing (e.g., Held et al. 2002).

The third numerical method to obtain stationary wave solutions from a system such as a GCM has been developed based on Fluctuation–Dissipation Theory (Leith 1975). This method empirically derives a linear operator by fitting the covariance statistics obtained from long GCM integrations (e.g., Branstator and Haupt 1998; Gritsun and Branstator, 2007). This kind of stationary wave model has been used mostly to diagnose the stationary wave response to diabatic heating forcing or to study low frequency variability (e.g., Branstator and Frederiksen 2003), and will not be discussed further in this thesis.

This thesis focuses on a technique that uses time integration of the (strongly) damped primitive equations (e.g., Ting and Yu 1998; Held et al. 2002; Chang 2009). Once enough damping is added to suppress baroclinic instability and obtain steady or quasi-steady stationary wave solutions, the resonance related to the linearization about the observed mean flow can also

often be avoided. This approach has been widely used in the literature and found to be more robust to the zonal mean flow and the zonally asymmetric forcings, despite the dependence on arbitrary damping added (Held et al. 2002).

The alternative way to obtain the nonlinear stationary wave solution without completely suppressing baroclinic instability is to integrate a model in time and simply terminate it before subtropical transients develop (Jin and Hoskins 1995; Hoskins and Rodwell 1995; Rodwell and Hoskins 1996). This is most useful for investigating the stationary wave response to tropical heating and might not work very well with other extra-tropical forcings that could induce baroclinic instability quickly.

Overall, nonlinear stationary wave models using time integration have several advantages over the classical linear models, which are summarized in Table 1.1. Here the time-integration nonlinear stationary wave models are compared with the linear stationary wave models that use matrix inversion. First, stationary wave nonlinearity is predicted instead of prescribed in nonlinear models, which is especially useful for diagnosing the nonlinear response to individual forcings in a way that linear models usually are not capable of doing. Second, linear models have shown moderate sensitivity to low level winds in the prescribed zonal mean basic state (e.g., Ting and Sardeshmukh 1993), while nonlinear models are relatively robust. Third, linear models are more sensitive to the prescribed zonally varying basic state as the linear operators are often close to singular and near-neutrally unstable eigen-modes that can be easily excited by stationary forcings (e.g., Simmons et al. 1983). Furthermore, such linear models can be sensitive to the damping formulation applied in the presence of certain forcings. For example, Ting and Held (1990) found the linear response to tropical diabatic heating highly dependent on the damping used, while Ting and Yu (1998) tested this sensitivity to damping for both linear and nonlinear

models and found that the latter is fairly robust but that the linear model gives an unrealistic large response for weak damping. Ting and Sardeshmukh (1993) also reported that the linear response to tropical heating is sensitive to the longitudinal location of the forcing when a zonally varying basic state is prescribed. Finally, linear models enforce proportionality to the amplitude of the forcing, while in general stationary waves are expected to become saturated as forcing amplitude increases, which can be captured by nonlinear models (see Chapter 2).

One principle aim in Chapter 2 is to improve the dynamical understanding of stationary wave nonlinearity and to evaluate the nonlinear stationary wave modeling technique of Ting and Yu (1998) and Held et al. (2002). This is first done in the classical setting of barotropic QG dynamics on the sphere, in which one will see that stationary wave nonlinear effects primarily involve stationary Rossby wave reflection at critical latitudes (Nigam and Held 1983; Held and Phillips 1987). The regional response to isolated forcing in the presence and absence of transient waves is considered in detail. The nonlinear effects of stationary and transient waves are considered separately in the zonal mean and zonally asymmetric flow. Understanding this elementary model problem is, in the author's view, a necessary step to understanding the baroclinic nonlinear stationary wave calculations of Ting and Yu (1998) and Held et al. (2002), which will be applied to the study of the three dimensional stationary waves and their response to climate change in Chapters 3 and 4. To the best of the author's knowledge, the results concerning zonally asymmetric stationary wave nonlinearity in the presence and absence of transient waves, applied to this simple system, have not previously been documented.

Nonlinear stationary wave models have been used to investigate the dynamics, maintenance and seasonal cycle of the observed stationary wave field and have improved understanding of stationary wave nonlinearity (e.g., Ting et al. 2001; Held et al. 2002; Chang

2009). However, the studies cited here analyzed, for the most part, the tropospheric stationary wave field, in part because the models have relatively poor stratospheric representation. On the other hand, stratospheric stationary wave modelling work (e.g., Lindzen, and Matsuno 1968; Matsuno 1970; Lin 1982; Robinson 1986; Nigam and Lindzen 1989; Wirth 1991; Harnik and Lindzen 2001) has focused on basic dynamical processes, usually with simplified dynamics. For example, only the first four zonal wavenumber components were considered in Nigam and Lindzen (1989) and stationary wave nonlinearity was often not taken into account in the above models. It could be appropriate to use a linear stationary wave model without taking into account stationary wave nonlinearity when the stationary wave amplitude is relatively weak and the zonal mean flow is relatively strong. This is the case, for example, for Harnik and Lindzen's (2001) study of the vertical reflection of stationary waves in Southern Hemisphere (SH) using a linear stationary wave model in QG baroclinic dynamics. By contrast, stationary wave nonlinearity is usually important in NH stationary wave modelling. Many stratospheric stationary wave models have an artificial lower boundary at the tropopause (around 100 hPa) and prescribe the tropospheric state in terms of a lower boundary condition such as a geopotential height anomaly on the lowest pressure level (e.g. Matsuno 1970; Wirth 1991). This kind of simplification is helpful in elucidating fundamental dynamical processes in the stratosphere, but a more realistic stationary wave modelling framework is required to quantitatively understand stratospheric climate variability and sensitivity to natural and anthropogenic forcing (see Figure 1.3 in Section 1.3). Therefore, a nonlinear stationary wave model that is similar to several previous studies (e.g., Ting and Yu 1998; Held et al. 2002; Chang 2009) but that has relatively good stratospheric representation and is able to accurately capture both tropospheric and stratospheric components of the observed or simulated stationary wave field will be developed in this thesis (see Chapter 3).

1.3 Evaluating stationary waves simulated by GCMs

To understand and accredit the stationary wave response to climate change, it is necessary to evaluate the ability of state-of-the-art climate models to capture the observed stationary wave field, which will be reviewed in this section. Boyle (2006) diagnosed the upper tropospheric (250 hPa) stationary waves simulated by the GCMs for the Intergovernmental Panel on Climate Change 4th Assessment Report (IPCC AR4, 2007), also known as the phase 3 of the Coupled Model Intercomparison Project (CMIP3) models, and compared them with National Centers for Environmental Prediction (NCEP) reanalysis (Kalnay et al. 1996) and ERA-40 (Uppala et al. 2005) for the period of 1980–2000. Chapter 4 (Butchart et al. 2010b) of the Chemistry Climate Model Validation Activity (CCMVal) 2010 (or CCMVal-2) report has a section on the stationary waves simulated by CCMVal-2 models with a focus on the stratospheric components for the period of 1980–1999.

Boyle (2006) found that the NH tropospheric stationary wave field is generally well simulated by the IPCC AR4 models. The spatial correlation between the NH extratropical stationary waves in these models and the observations on the 250 hPa pressure level is generally around 0.9 in each month except for around 0.8 for one model. This correlation drops to 0.6–0.8 in the spring and to 0.5–0.8 in the fall for about one third of the models. There is a bias towards the low amplitude in the NH winter stationary wave field and a bias towards the high amplitude in the NH summer stationary wave field for most of these models, resulting in a weaker annual cycle in the stationary wave amplitude than in the observations. The SH extratropical stationary wave field is relatively poorly simulated. The correlation for the SH counterparts is 0.7–0.8 on average and has a larger inter-model spread. The SH stationary wave amplitude is systematically underestimated by these models except for SH winter (JJA).

The IPCC AR4 GCMs are coupled ocean-atmosphere models and the stratospheric representation is normally poor in these models. On the other hand, the Chemistry Climate Models (CCMs) used for the recent CCMVal-2 Report (2010) usually are not coupled to an interactive ocean but have a relatively well resolved stratosphere and realistically represent stratospheric chemistry. CCMs are used mainly to quantify the evolution of stratospheric ozone under the influence of ozone depleting substance (ODS) emissions, GHG emissions, and other natural and anthropogenic forcings. Figure 1.3 shows the vertical profile of NH winter stationary wave maximum amplitudes in CCMVal-2 simulations compared with the ERA-40 and NCEP reanalyses. One can see that the stationary wave amplitudes in these simulations are generally realistic in the troposphere (but biased low in amplitude consistently with the IPCC AR4 simulations, see also Figure 5.1a) and start to diverge above the tropopause and become very different from each other and in many cases increasingly unrealistic in the stratosphere. For a closer look at the stratospheric stationary wave field, Figure 1.4 plots the seasonal cycle of the stationary wave amplitude on 10 hPa at all latitudes for CCMVal-2 simulations compared with NCEP and ERA-40 reanalyses. Many aspects of the stationary wave amplitude can be compared between individual models and observations, but here one of the fundamental characteristics in the observed stationary wave field is elaborated on. The observed NH stationary wave maximum amplitude is larger than the SH maximum due to the stronger zonal variations in the NH lower boundary (topography and land-sea contrast). However, most of the CCMVal-2 models simulate either the opposite, i.e., a SH stationary wave with a stronger peak than its NH counterpart (AMTRAC3, CAM3.5, CMAM, ULAQ, UMUKCA-UCAM, and WACCM), or comparable peaks in SH and NH stationary wave amplitude (CNRM-ACM and UMUKCA-METO), as can be seen in Figure 1.4. In summary, the CCMVal-2 models generally simulate the observed stationary wave field but some important features, especially for the stratospheric stationary

wave field, are not well captured in these models. This again calls for the aid of stratosphere-troposphere stationary wave models to evaluate and address these problems.

1.4 Stationary wave response to climate change

Given the large spread of the stationary waves simulated by state-of-the-art climate models, it is not surprising that the stationary wave response to climate forcing in these models is also model-dependent. This can be understood even using the simple example (1.3), considering it as a representative equation for upper tropospheric stationary wave dynamics. For example, the radiative warming in the low-latitude upper troposphere and the radiative cooling in the lower polar stratosphere by enhanced GHG forcing increases the meridional temperature gradient and thus is able to induce significant changes in zonal mean winds through thermal wind balance, which means the linear operator in (1.3) will respond to climate change and thus produce a stationary wave response; this will occur even if the zonally asymmetric forcing, as represented by h^*, is held fixed. In addition, all the zonally asymmetric forcings will respond to climate change to a certain extent. For example, the precipitation distribution and storm tracks that are closely related to the transient wave flux convergences are sensitive to climate change; changes in these fields will change the zonally asymmetric diabatic heating forcing which is not presented in (1.3) but is a leading order forcing term in baroclinic stationary wave dynamics.

The dynamics of the stationary wave response to climate change has been explored since the early 1990s but is still not well understood (e.g., Stephenson and Held 1993; Joseph et al. 2004; Brandefelt and Körnich 2008). For example, Stephenson and Held (1993), one of the earliest studies on this topic, found, using stationary wave modelling, that transient wave forcing and diabatic heating are the major factors controlling the stationary wave response to greenhouse gas increases in the GFDL (Geophysical Fluid Dynamics Laboratory) CGCM (coupled ocean-

atmosphere general circulation model). In a similar model at higher resolution, Joseph et al. (2004) showed that the change in the zonal mean basic state has a comparable impact as the zonally asymmetric forcings such as transients and diabatic heating on the total stationary wave response. More recently, Brandefelt and Körnich (2008) analyzed the stationary wave response in the IPCC AR4 simulations using a linear barotropic stationary wave model. Figure 1.5, adopted from Figure 3 of Brandefelt and Körnich (2008), shows the barotropic stationary wave response to enhanced GHG forcing. A large spread exists in the stationary wave response patterns predicted by these IPCC models, which are divided into three groups (Group S, Group B, Group N), except for four ungrouped simulations, based on the similarity between these response patterns (the correlation between any two group members is greater than 0.5 in each group, except that a single correlation is 0.46 in Group S). The stationary wave response in Group S and Group B corresponds to the positive phase of the Pacific-North American Oscillation (PNA; Wallace and Gutzler 1981) pattern, but is distinct over the North Atlantic and Eurasia. The response in Group N is similar to the response in Group S over the North Atlantic and Eurasia, but shows a negative phase of the PNA pattern. The linear barotropic stationary wave model diagnosis showed that the zonal mean flow change accounts for 50%, 37%, and 7% of the total stationary wave response in group S, N, B, respectively. Generally speaking, there is a great deal of spread among the models' stationary wave responses, and further work is needed to explain this spread in the troposphere (e.g., Figure 1.5) and in the stratosphere (e.g., CCMVal-2 simulations) for accurate prediction of future climate. Nonlinear stationary wave models that represent realistically the stratosphere and the troposphere might be helpful in this task.

In Chapter 4, the newly developed stationary wave model (Chapter 3) will be applied to understand the stratosphere-troposphere response to climate change in a particular CCM, the

Canadian Middle Atmosphere Model (CMAM; Scinocca et al. (2008)), with a view to extending the analysis to the stationary wave response in a larger set of CCMs involved in recent CCM intercomparison projects (CCMVal and CCMVal-2, see Eyring et al. (2007), Butchart et al. (2010b)). To the best knowledge of the author, there has been little work on understanding the full stratosphere-troposphere stationary wave response to climate change in a quantitative manner, in the context of climate assessments.

1.5 Conclusion

This chapter has reviewed the observations, dynamics and modelling of the NH wintertime stationary wave field, as well as how well this field is captured by state-of-the-art climate models. The dynamics of the stationary wave response to climate change has also been discussed. The remaining outstanding issues in the stationary wave literature have motivated the three major aims of this thesis. First, it is intended to investigate the stationary wave nonlinearity in relatively simple settings of QG dynamics, as a necessary step to understand the dynamics of the stationary wave nonlinearity and its significance in stationary wave modelling (Chapter 2). Second, a stationary wave model is to be developed in Chapter 3, which is able to predict the stationary wave nonlinearity internally and captures both the troposphere and the stratosphere. Finally, this stationary wave model will be applied to the problem of the stationary wave response to climate change (Chapter 4).

This thesis includes research that has been accepted by, or is to be submitted to, peer-reviewed journals. The CCMVal-2 part of Section 1.3 and some related results cited in Section 5.2 are a part of the author's contribution to Chapter 4 (Butchart et al. 2010b) of the CCMVal 2010 report. This has been published and a follow-on review paper is in preparation (Butchart et al. 2010c). Chapter 2 and the corresponding introductory part on the stationary wave nonlinearity

in Chapter 1 have been published on the Journal of the Atmospheric Sciences and are in press (See Wang and Kushner 2010). Chapters 3 and 4 plus part of the corresponding introductory text in Chapter 1 are in preparation for submission.

Table 1.1: Comparison of two types of stationary wave models

	Linear	*Nonlinear*
Numerical method	Matrix inversion	Time integration
Prescribed fields from observations or GCMs	Zonal mean basic state; Zonally asymmetric diabatic heating, topography, transients, stationary wave nonlinearity.	Zonal mean basic state; Zonally asymmetric diabatic heating, topography, transients.
Sensitivity to zonally symmetric basic state	Moderate, especially to lower-level winds	Robust
Sensitivity to zonally varying basic state	Resonant modes exist	Robust
Sensitivity to the amount of damping applied	Unrealistically large amplitude for weak damping	Robust in pattern; damping primarily modulates amplitude.
Sensitivity to forcing pattern	Unrealistically large for small changes in the forcing pattern	Robust
Sensitivity to forcing amplitude	Linearly proportional	Becomes saturated as forcing amplitude increases

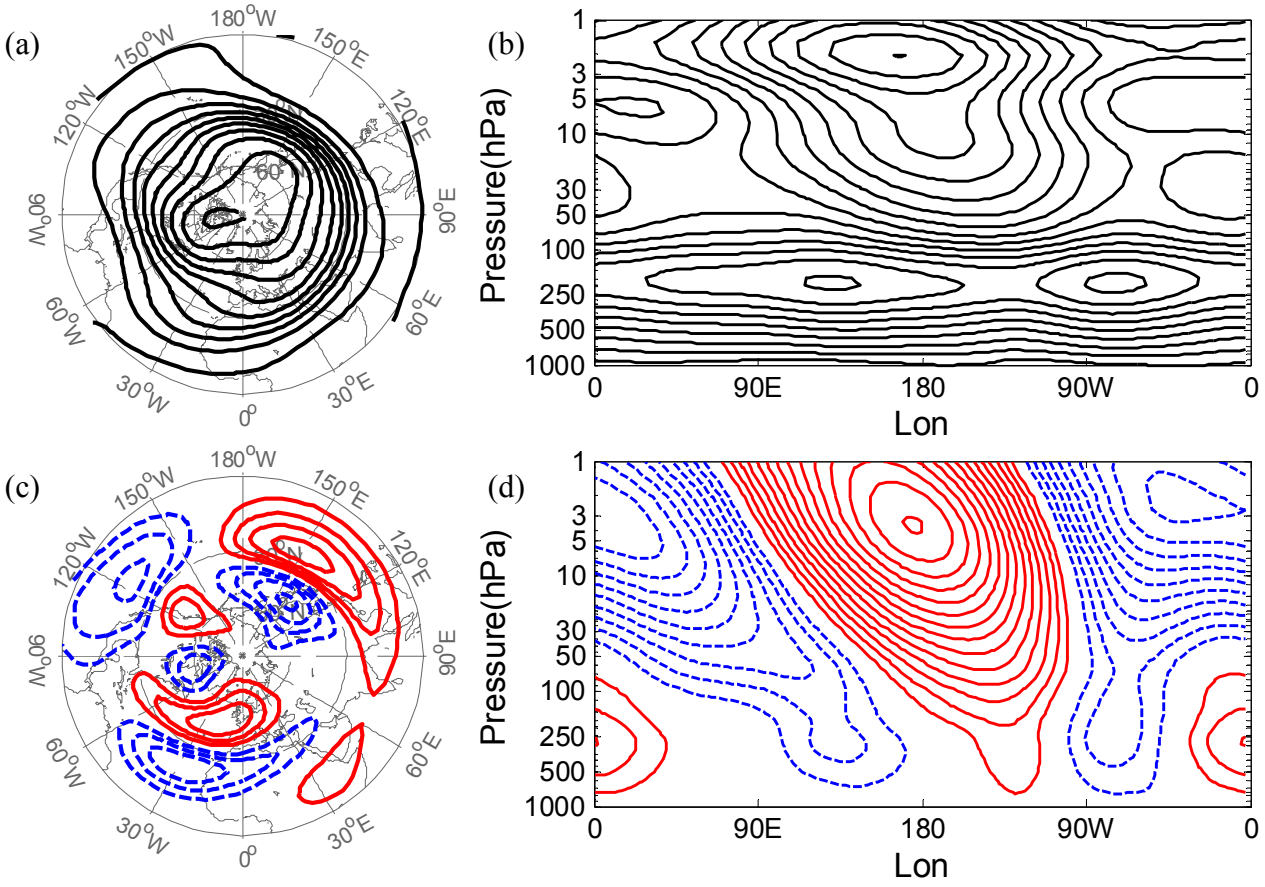

Figure 1.1: NH winter (January 1979–2002) (a, b) total and (c, d) zonally asymmetric streamfunction plots of ERA-40 (a, c) on 250 hPa pressure level and (b, d) 60°N longitude-height cross section. Contour intervals are 1.8×10^{7} m^2s^{-1} for the total streamfunction (a, b) and 6×10^{6} m^2s^{-1} for the stationary waves (c, d); positive values are plotted in solid and negative in dashed (hereafter for all contour plots).

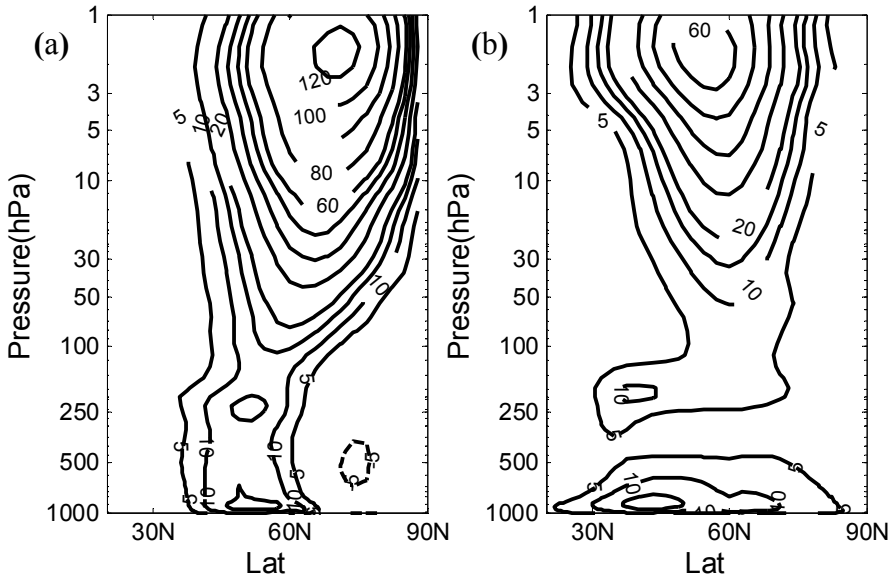

Figure 1.2: Zonally averaged ERA-40 heat fluxes by (a) stationary waves ($\left[\overline{\upsilon}^{*}\overline{T}^{*}\right]$) and (b) transient waves ($\left[\overline{\upsilon'^{*}T'^{*}}\right]$) for NH January 1979–2002. Contours are labelled in K m s^{-1}.

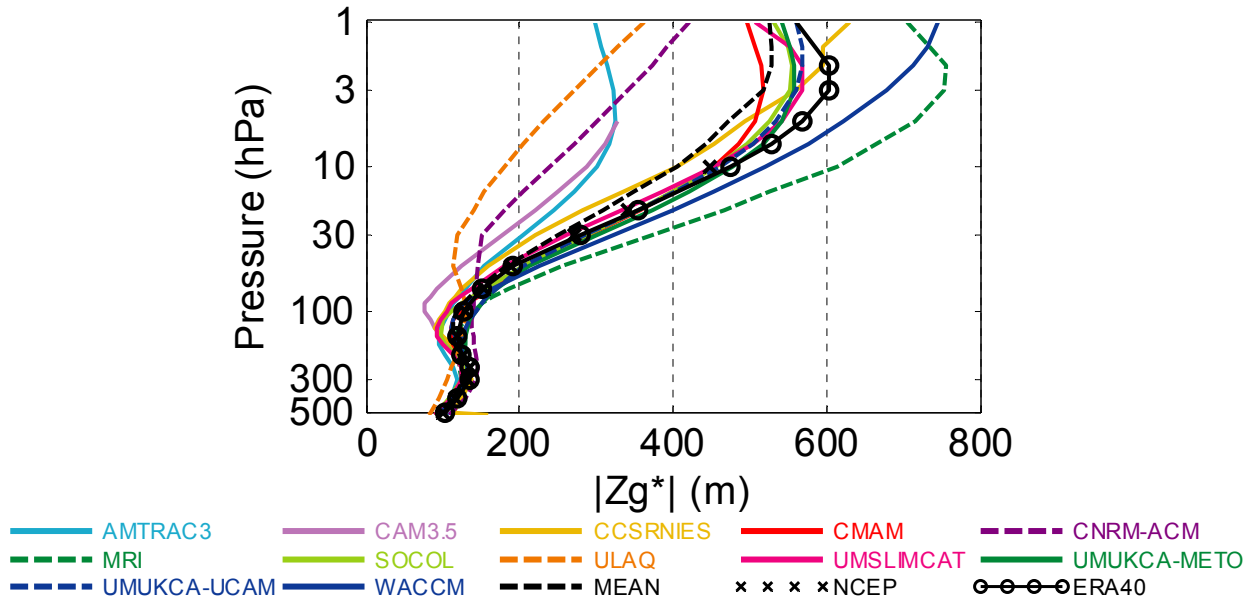

Figure 1.3: The maximum amplitude for all latitudes in the stationary wave field for the NH DJF climatology. Data are based on climatological mean geopotential heights for the CCMVal-2 REF-B1 simulations, and for ERA-40 and NCEP data from 1980 to 1999. The black dashed curve is the mean of all the model curves. The CCMVal-2 REF-B1 simulations are forced by observed sea surface temperature (SST) and GHG and ODS forcing, aiming to test the ability of these comprehensive models to mimic the observed climate.

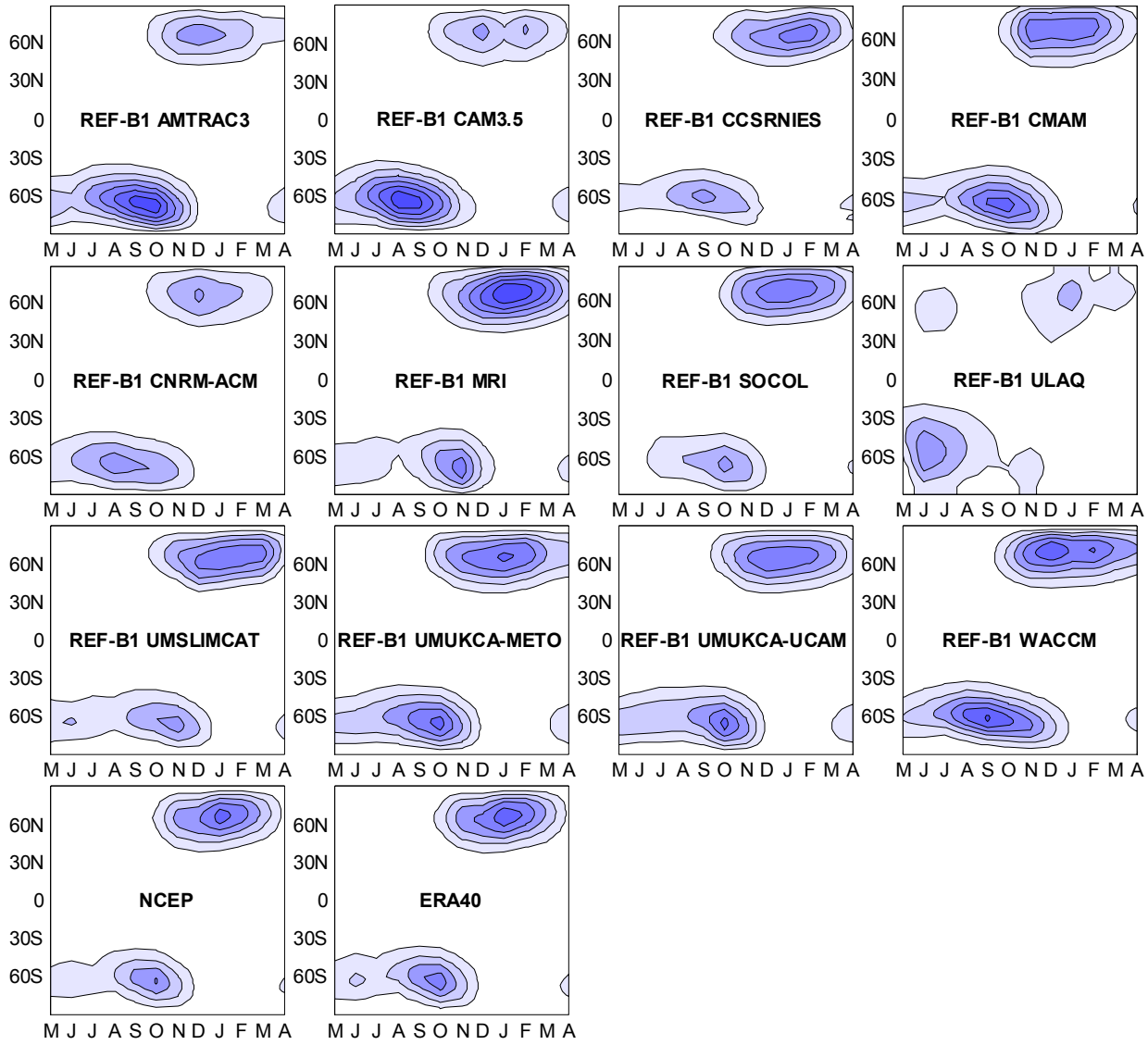

Figure 1.4: The annual cycle of stationary wave field zonal mean amplitude $\left[\sqrt{\left(\overline{Z_g}^*\right)^2}\right]$ on the 10 hPa pressure level in the CCMVal-2 REF-B1 simulations, ERA-40 and NCEP data. The contour interval is 100 m. Data are based on climatological mean geopotential heights (Z_g) for the CCMVal-2 models, ERA-40 and NCEP data from 1980 to 1999.

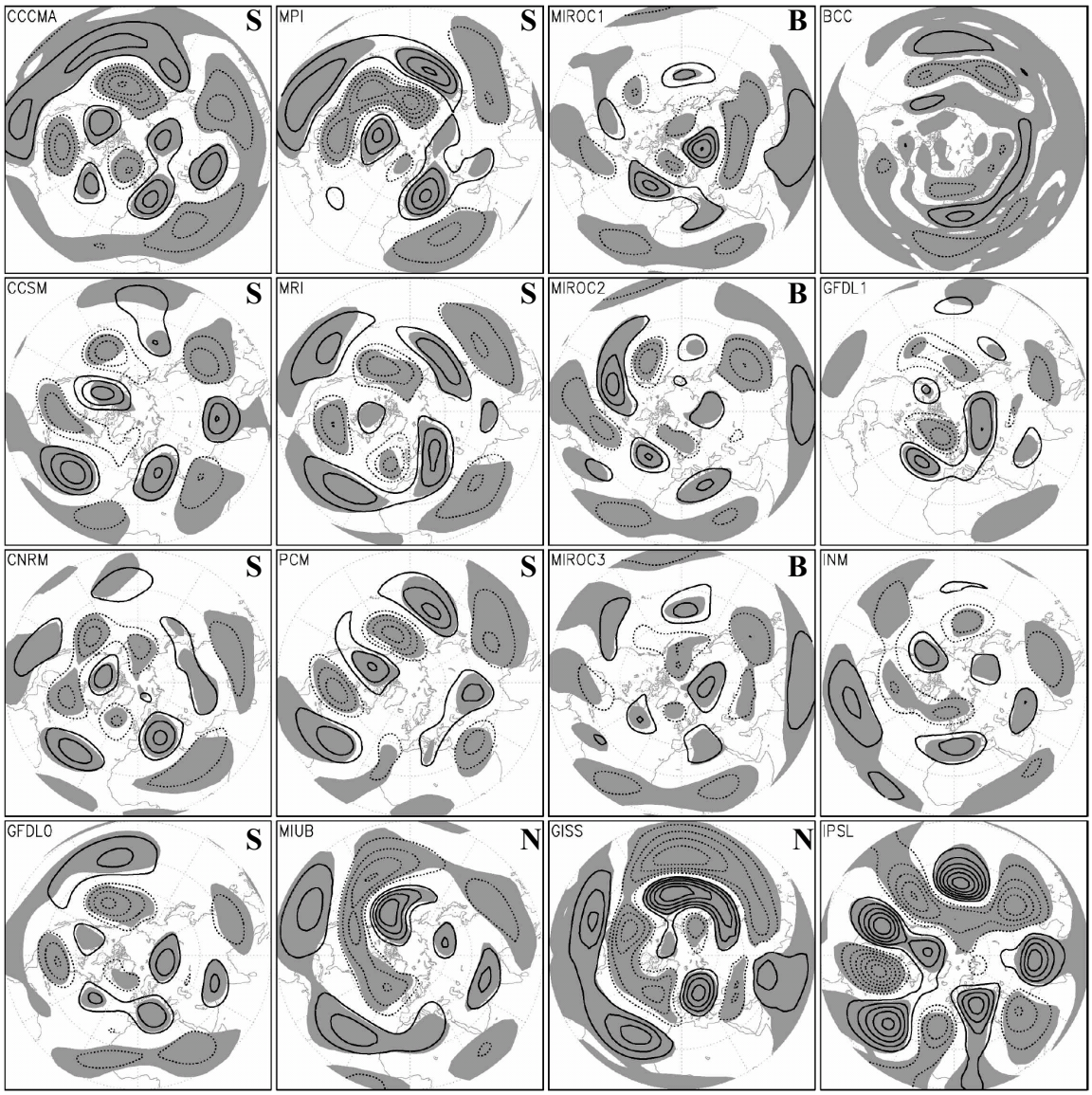

Figure 1.5: (Adopted from Figure 3 in Brandefelt and Körnich 2008; ©American Meteorological Society. Reprinted with permission.) NH winter (DJF) barotropic stationary wave (streamfunction averaged over 850–100 hPa) response to enhanced GHG forcing simulated by IPCC AR4 models (model names are labelled at top-left corner of each panel). These simulations are grouped according to the spatial correlation between their stationary wave response, with 7 simulations in Group S, 3 in Group B, 2 in Group N, and 4 ungrouped (groups are labelled at top-right corner of each panel and ungrouped simulations are not labelled). The contour interval is 1×10^{6} $m^{2}s^{-1}$; positive contours are solid, negative dotted, and zero contour omitted. The gray shading represents 5% level by the Student's *t*-test. The stationary wave response pattern varies significantly among these models, although some common features exist, for example, most of the patterns consist of subtropical wave train structures of comparable spatial scale (zonal wavenumber-5 or so).

Chapter 2

2 Interpreting Stationary Wave Nonlinearity in Barotropic Dynamics

2.1 Introduction

This chapter examines the dynamics of stationary wave nonlinearity in barotropic QG dynamics on the sphere and tests the nonlinear stationary wave modeling technique of Ting and Yu (1998) and Held et al. (2002) in this simple setting. As introduced in Chapter 1, stationary wave nonlinearity represents the nonlinear effects of the stationary wave mainly through self-advection of the zonally asymmetric flow (e.g., Valdes and Hoskins 1991; Ting 1994; Ting et al. 2001), which has not been fully understood. Barotropic QG dynamics is a compact system that contains the necessary elements for understanding stationary wave nonlinearity related to vorticity advection, and is easy to study both analytically and numerically. The local response to isolated topographic forcing is investigated in the presence and absence of transient waves, which allows us to focus on the nonlinear effects of stationary waves and transients in maintaining the time mean flow. One aim here is to use this approach to help understand the Ting-Yu type baroclinic nonlinear stationary wave modelling technique. This technique will then be implemented in Chapter 3 to build a stratosphere-troposphere stationary wave model, and will apply the model in Chapter 4 to study the stationary wave response to climate change.

After describing the set of dynamical equations and techniques (Section 2.2), the author diagnoses the zonal mean flow response in the presence and the absence of transient waves (Section 2.3) and analyzes the strongly damped case in which transient waves are absent and in

which the only nonlinearity arises from the stationary wave field itself (Section 2.4). The author also develops a weakly nonlinear asymptotic theory to explicitly account for the stationary wave nonlinear effects (Section 2.5). The more weakly damped case is then examined in which transient waves are important (Section 2.6) and a Ting-Yu type nonlinear stationary wave model that numerically predicts the stationary wave nonlinearity is tested (Section 2.7). In both the strongly damped and weakly damped cases, critical-layer reflection is important, but in the weakly damped case the adjustment of the zonal-mean basic state also needs to be accounted for to accurately reproduce the critical-layer reflection. Conclusions are presented in Section 2.8.

2.2 Numerical models and diagnostics

Barotropic vorticity dynamics on a rotating sphere in the presence of relaxation to a prescribed zonal flow is considered. The flow represents the boreal winter upper tropospheric wind, and in the presence of orography that generates a Rossby lee wave train. The system is first solved by direct nonlinear simulation (DNS) of the equation:

$$\frac{\partial \zeta}{\partial t} + \nabla \cdot \left\{ \left(f + \zeta + \frac{f_0 h}{H} \right) \mathbf{u} \right\} + \frac{1}{\tau_Z} \left([\zeta] - \zeta_{ref} \right) + \frac{1}{\tau_E} \zeta^* + \nu \nabla^8 \zeta = 0 \,, \tag{2.1}$$

where the notation, which is for the most part standard, is described in Table 2.1. Equation (2.1) is solved using a T85 ("T" represents the triangular truncation of the spherical harmonics; T85 is equivalent to about 1.4° in longitude and latitude) resolution pseudospectral model from the NOAA/GFDL Flexible Modeling System (FMS). The zonal asymmetry in the model arises from a mountain whose amplitude is determined by the parameter h_0; the amplitude of the associated potential vorticity perturbation is $(h_0/H)\, f_0$, where H = 10 km is a representative depth for the troposphere. Standard QG scaling (Vallis 2006) requires that the PV contribution from topography be comparable to or smaller than the relative vorticity, ζ, i.e., $f_0 h/H \sim f_0 h_0/H \sim \zeta \sim Z_0$,

where ζ and Z_0, from Table 2.1, provide scales for the topography and vorticity. The author defines a topographic amplitude parameter $\varepsilon = f_0 h_0 / Z_0 H$. For linear theory to be applicable, the PV contribution from topography needs to be small compared to ζ, i.e., $\varepsilon << 1$. Cases are tested in the range 100 m $\leq h_0 \leq$ 2 km, which corresponds to $0.1 \leq \varepsilon \leq 2$. In section 2.5, diagnostics are developed based on a small-parameter expansion of the equations in ε.

The response of a given field to this topography is defined as the solution with topography minus the solution without topography. In the absence of topography, the solution has the zonal jet given by U_{ref}, slightly spread out by hyperviscosity, and U_{ref} is taken as the basic background flow.

Two cases are considered in this study. In the strongly damped case (SD), it is set $\tau_Z = \tau_E$ = 5 days, which provides sufficiently strong damping to suppress transient waves that arise due to instability of the zonally asymmetric flow. The SD case represents a classical application of this model to the stationary wave problem and is useful for testing ideas. In the weakly damped case (WD), it is set τ_Z = 5 days and $\tau_E = \infty$, which allows transient waves and a transient zonal flow to develop. The WD case is qualitatively more realistic and perhaps more relevant to the observed general circulation, but is much more complex because of transient wave effects.

The time average of (2.1) has zonal mean component

$$\nabla \cdot \left\{ \left[\left(\bar{\zeta}^* + \frac{f_0 h^*}{H} \right) \bar{\mathbf{u}}^* \right] + \left[\overline{\zeta' \mathbf{u}'} \right] \right\} + \frac{1}{\tau_Z} \left(\left[\bar{\zeta} \right] - \zeta_{ref} \right) = 0 , \tag{2.2}$$

and zonally asymmetric component

$$\nabla \cdot \left\langle \left(f + \left[\bar{\zeta} \right] + \frac{f_0 [h]}{H} \right) \bar{\mathbf{u}}^* + \left(\bar{\zeta}^* + \frac{f_0 h^*}{H} \right) [\bar{\mathbf{u}}] + \left\{ \left(\bar{\zeta}^* + \frac{f_0 h^*}{H} \right) \bar{\mathbf{u}}^* + \overline{\zeta' \mathbf{u}'} \right\}^* \right\rangle + \frac{1}{\tau_E} \bar{\zeta}^* = 0 , \tag{2.3}$$

where the (relatively small) hyperviscous term is included. In the SD case, the transient wave vorticity flux $\overline{\zeta'\mathbf{u}'} = \mathbf{0}$ and these two equations represent a closed system which could in principle be solved by iteration (see Section 1.2) for the zonally symmetric and the zonally asymmetric components of the flow. In practice, the prognostic versions of these equations are used, along the lines of (2.4) below, to solve for these components of the flow. In the more realistic WD case, $\overline{\zeta'\mathbf{u}'} \neq \mathbf{0}$, and in the absence of an accurate mean-flow parameterization of the transient wave flux convergences one must integrate (2.1) by DNS and take its time average to get the stationary wave field. In particular, the day 200 to 1000 average fields are shown in the WD case.

In contrast to equations (2.2) and (2.3), stationary wave models represent so-called "anomaly models" in which only the stationary wave terms of the general form $\overline{A}^*$ for a field A are solved for and other fields are prescribed as consistently as possible with the original equations. Three types of stationary wave model are considered in this study. The linear stationary wave model (LIN-ANOM) integrates to a steady state the equation

$$\frac{\partial \zeta^*}{\partial t} + U \frac{\partial \left(\zeta^* + \frac{f_0 h^*}{H} \right)}{a \cos\theta \, \partial\lambda} + \upsilon^* \frac{\partial \left(f + Z + \frac{f_0 [h]}{H} \right)}{a \partial\theta} + \frac{1}{\tau_E} \zeta^* = F^*, \tag{2.4}$$

which is linear in the zonally asymmetric terms like ζ^*. Here, Z and U are prescribed time-independent and longitude-independent vorticity and zonal wind fields. The right-hand-side term F^* is a prescribed "forcing" that represents the zonally asymmetric component of the wave vorticity flux convergence and can include either or both of the stationary and transient wave contributions to this flux taken from the DNS solution of (2.1). These terms are not genuine external forcing but inherently dynamical quantities that are treated as forcing for diagnostic

purpose (see Section 1.1). In addition, τ_E is the wave damping timescale used in the linear model, which is used as a tuning parameter to stabilize the solution as necessary.

The second anomaly model considered is a nonlinear stationary wave model (NONLIN-ANOM) in which the equation

$$\frac{\partial \zeta^*}{\partial t} + U \frac{\partial \left(\zeta^* + \frac{f_0 h^*}{H} \right)}{a \cos\theta \, \partial \lambda} + \upsilon^* \frac{\partial \left(f + Z + \frac{f_0 [h]}{H} \right)}{a \partial \theta} + \nabla \cdot \left\{ \left(\zeta^* + \frac{f_0 h^*}{H} \right) \mathbf{u}^* \right\}^* + \frac{1}{\tau_E} \zeta^* = F^* \qquad (2.5)$$

is integrated to a "quasi-steady" state, which means that transients are suppressed to the extent that it is practicable while maintaining a reasonable solution (similar to Held et al. 2002; see Section 2.7). This equation corresponds to the Ting and Yu (1998) and Held et al. (2002) nonlinear baroclinic stationary wave model, whose performance will be evaluated in this simplified setting of barotropic dynamics. In this model, the zonal mean flow is again prescribed via U and Z, but now the zonally asymmetric forcing F^* is understood to represent only the transient wave contribution. In this model, the damping τ_E is again set to a minimum value that stabilizes the flow.

A final anomaly model used is a prognostic version of the zonal mean equation (2.2) to diagnose the zonal mean state in the presence of prescribed time averaged zonal mean wave vorticity flux convergence of either or both of the stationary and transient waves (ZONAL-ANOM). This calculation is a barotropic version of classical baroclinic calculations of the zonal mean circulation consistent with a prescribed wave forcing, which is commonly known as the "downward control" diagnostic in the stratospheric literature (Haynes et al. 1991).

Three principal types of diagnostics are shown to diagnose the wave response. First, the zonally asymmetric streamfunction ψ^* is displayed. Second, the propagation of Rossby-wave activity is plotted in the longitude-latitude plane using the Plumb (1985) wave activity flux, which for barotropic flow linearized about a zonally symmetric basic state reduces to

$$\mathbf{W} = \frac{\cos\phi}{2}\left(\upsilon^{*\,2} - \frac{\psi^*}{a\cos\phi}\frac{\partial \upsilon^*}{\partial \lambda}, \quad -u^*\upsilon^* - \frac{\psi^*}{a}\frac{\partial \upsilon^*}{\partial \phi} \right).$$

This wave activity flux is parallel to the local group velocity of stationary Rossby wave in the Wentzel-Kramers-Brillouin (WKB) limit for monochromatic waves, but has been found also useful for wave packets which are more relevant in this study. Finally, the author makes use of Taylor (2001) diagrams that combine information about the correlation and relative magnitude of two fields as a single point in a polar-coordinate plane; this allows to concisely representing the results of several sensitivity tests.

2.3 Zonal wind response

Figure 2.1a shows the reference zonal wind, U_{ref}, the SD case zonal wind, $[u]_{SD}$, and the WD case zonal wind, $[u]_{WD}$, for a mountain with a nominal h_0 = 2 km height. The NH jet is slowed down by the mountain in the SD case but is sharpened (with acceleration of the maximum and deceleration of the flanks) in the WD case. Figure 2.1b shows the zonal wind response for the SD case, which is almost entirely associated with the stationary wave forcing, with a much weaker contribution from hyperdiffusion. It also shows the WD response and the decomposition of the WD response into parts associated with the zonally symmetric components of the stationary wave vorticity flux and of the transient wave vorticity flux, using the ZONAL-ANOM model as discussed in Section 2.2. It is found that the stationary wave vorticity flux has a similar decelerating effect in the SD and WD cases, but that the transient wave vorticity flux in

the WD case is responsible for the sharpening of the jet. In this sense the weakly damped case provides a qualitative representation of the observed upgradient flux of transient wave momentum into the tropospheric jet stream. The distinct zonal mean response to the topography in the two cases has important implications for understanding stationary wave nonlinearity.

2.4 Strongly damped (SD) case

Figure 2.2a shows the stationary wave streamfunction $\overline{\psi}^*$ induced by the topography in the DNS of (2.1); Figure 2.2b shows the associated Plumb wave activity flux and its divergence. The response is highly structured and one can identify three distinct branches of wave activity propagation. First, wave activity diverges away from the topography into a weak convergence region eastward and poleward of the topography. Second, wave activity diverges away from the topography into a strong convergence region eastward and equatorward of the topography, in the vicinity of the critical line defined by the zero-contour of zonal wind. This low-latitude branch has a relatively shorter wavelength but greater amplitude. Third, wave activity diverges away from the critical line eastward of 150°E and propagates poleward before bending back equatorward. This part of the wave response evidently deviates from the classical great circle ray passing through the topography that is predicted by linear theory (Hoskins and Karoly, 1981).

The stationary wave modeling is used to separate linear and nonlinear effects in this solution. In the SD case, transient wave vorticity fluxes $\overline{\zeta'\mathbf{u}'} = \mathbf{0}$, so the sole source of nonlinearity in (2.2) and (2.3) is the stationary wave potential vorticity flux, which can be decomposed into zonally symmetric and zonally asymmetric components. The zonally asymmetric component is the “stationary wave nonlinearity” referred to in the stationary wave modeling literature (Ting et al. 2001); the zonally symmetric nonlinear term is a momentum flux

convergence, which, as discussed in Section 2.3, drives the zonal mean flow away from U_{ref}. The rest of the zonal-mean response comes from the zonal mean of the topography and the hyperdiffusion, which represent smaller terms.

As a test, one can use the linear model, LIN-ANOM, to closely reproduce the nonlinear solution by prescribing the zonal mean vorticity $Z = \left[\overline{\zeta}\right]_{SD}$, zonal wind $U = \left[\overline{u}\right]_{SD}$, and (zonally asymmetric) stationary wave nonlinearity

$$F^* = -\nabla \cdot \left\{ \left(\overline{\zeta}^*_{SD} + \frac{f_0 h^*}{H} \right) \overline{\mathbf{u}}^*_{SD} \right\}^* \tag{2.6}$$

from the DNS solution of (2.1). Doing so reproduces the DNS solution to a very high precision, with less than 1‰ in relative error between the DNS (2.1) and LIN-ANOM (2.4) solutions (not shown).

Next, one can solve the linear model (2.4) with $Z = \zeta_{ref}$, $U = U_{ref}$, $F^* = 0$, $\tau_E = 5$ days, which represents the classical solution of linear theory. The linear solution (Figure 2.2c–d) propagates from the topographic forcing region to the critical layer; has slightly greater amplitude, shorter wavelength, and does not propagate downstream as far as the original solution; and is more consistent with the expected great circle propagation pattern passing through the topography (although the author has not checked agreement with the great circle solution in detail).

Nonlinear effects are shown in Figure 2.2e, which plots the DNS solution (Figure 2.2a) minus the classical linear solution (Figure 2.2c); Figure 2.2f shows the wave activity associated with this wave streamfunction pattern (as opposed to the difference in wave activities). One can see that the high latitude branch and the low-latitude branch to the east of 150°E are associated

with nonlinear effects. In addition, another wave train pattern is seen emanating poleward of the critical line east of 150°W. Thus, the dominant nonlinear effect in this solution is critical layer reflection, which occurs in this highly damped setting through self-advection of stationary wave potential vorticity. Nonlinear reflection of Rossby wave trains is usually characterized with localized overturning PV contours associated with wave breaking (Brunet and Haynes 1996; Walker and Magnusdottir 2003 and references therein). Weak PV overturning is observed when the topographic forcing is strong, i.e., 2000 m and 1000 m, but nonlinear stationary wave reflection still exists with weaker topographic forcing even though the stationary wave does not homogenize the potential vorticity field (not shown because the patterns are similar to those in the 2000 m case except with smaller amplitude). In the discussion, the author returns to the issue of when critical layer reflection can be expected to occur.

One can now use the stationary wave model to separately diagnose the stationary wave response in terms of changes to zonally asymmetric forcing terms and of changes to the zonal mean basic state. Although both the zonally asymmetric forcing terms and the zonal mean basic state depend on the stationary wave field, it is found that such diagnostics can provide physical insight. In the SD case, one can find that it is the stationary wave nonlinearity that is most important: when the response to F^* is calculated from (2.6) with the zonal mean basic state corresponding to U_{ref}, one gets a pattern (Figure 2.2g–h) that accounts for the main features of Figure 2.2e–f; in particular, stationary wave nonlinearity generates the critical layer reflection term. The complementary case, in which the basic state is altered by the stationary wave forcing and F^* is set to zero, yields only a weak wave response (not shown). This solution is sometimes referred to a "quasi-linear" solution (e.g., Davey 1980; Haynes and McIntyre 1987).

2.5 Weakly nonlinear asymptotic theory for the SD case

To better understand stationary wave nonlinearity in the SD case, a weakly nonlinear asymptotic theory is developed to show how stationary wave nonlinearity arises as part of the rectified effect of the wave PV flux from the linear solution. In equations (2.2) and (2.3), one can see that the topographic forcing comes in as a term proportional to εZ_0; for topography to represent a small perturbation, it is required that $\varepsilon << 1$. A standard asymptotic analysis involving small-parameter expansion in ε is performed with the hyperviscosity term in (2.1) neglected. The variables are expressed as asymptotic series in the standard way: $\hat{\zeta} = \hat{\zeta}_0 + \varepsilon\hat{\zeta}_1 + \varepsilon^2\hat{\zeta}_2 + \cdots$ and $\hat{\mathbf{u}}=\hat{\mathbf{u}}_0+\varepsilon\hat{\mathbf{u}}_1+\varepsilon^2\hat{\mathbf{u}}_2+\cdots$, where the ^ variables are non-dimensional. It is also assumed that the advective and damping timescales are comparable: $\tau_Z \sim \tau_E \sim \zeta^{1} \sim Z_0^{-1}$. Then to $O(\varepsilon^0 = 1)$, the leading order vorticity and winds are: $\zeta_0 = \zeta_{ref}$, $\mathbf{u}_0 = (U_{ref}, 0)$, $\mathbf{u}_0^* = \mathbf{0}$, where ζ_0 is the dimensional version of $\hat{\zeta}_0$, $\mathbf{u}_0$ is the dimensional version of $\hat{\mathbf{u}}_0$, etc. To $O(\varepsilon)$,

$$O(\varepsilon):\ [\mathbf{u}_1] = \mathbf{0},\ [\zeta_1]=0,\ U_{ref}\frac{\partial\zeta_1^*}{a\cos\theta\,\partial\lambda} + \upsilon_1^*\frac{\partial}{a\partial\theta}\left(f + \left[\zeta_{ref}\right]\right) + \frac{1}{\tau}\zeta_1^* = -\frac{f_0 U_{ref}}{H}\frac{\partial h^*}{a\cos\theta\,\partial\lambda},$$

where again all fields and coordinates are understood to be dimensional. The contribution to the zonal mean flow at this order is zero, and the zonally asymmetric flow satisfies the classical linear stationary wave equation. Nonlinear terms come in at $O(\varepsilon^2)$. The dimensional zonal equation is

$$O(\varepsilon^2):\ \nabla\cdot\left[\left(\zeta_1^* + \frac{f_0 h^*}{H}\right)\mathbf{u}_1^*\right] = -\frac{1}{\tau}[\zeta_2], \tag{2.7}$$

showing that the zonally symmetric component at second order is driven by the wave PV flux associated with the first order fields including topography, and the dimensional zonally asymmetric equation is

$$O\left(\varepsilon^2\right):\ U_{ref}\frac{\partial\zeta_2^*}{a\cos\theta\,\partial\lambda}+\upsilon_2^*\frac{\partial\left(f+\left[\zeta_{ref}\right]\right)}{a\partial\theta}+\frac{1}{\tau}\zeta_2^*=-\frac{f_0v_1^*}{H}\frac{\partial[h]}{a\partial\theta}-\nabla\cdot\left\{\left(\zeta_1^*+\frac{f_0h^*}{H}\right)\mathbf{u}_1^*\right\}^*, \quad (2.8)$$

showing that stationary wave nonlinearity, in the sense of Ting and Yu (1998), comes in as the zonally asymmetric component of this wave PV flux.

In Figure 2.3, the accuracy of the weakly nonlinear asymptotic solution given by (2.7) and (2.8) is tested as the mountain height increases. Figure 2.3a shows the zonal mean winds predicted by the solution for mountains of various height. The wave solution's Taylor diagram is plotted in Figure 2.3b, in which the target point refers to the stationary wave in the DNS minus the stationary wave in the classical linear model (e.g., Figure 2.2e for h_0 = 2000 m). As the forcing magnitude decreases, the second order correction approaches this target field, illustrated by a series of arrows in Figure 2.3b. The Taylor diagram gives a good measure of how well a linear prognostic theory can estimate the self-nonlinearity of the stationary wave response to various forcing amplitudes. The solution remains reasonably good as long as $\varepsilon = f_0h_0/Z_0H < 1/2$, which corresponds to a 500 m mountain for a depth of 10 km.

In sum, for the SD case, the linear response to isolated topography involves transmission of the wave packet to the critical latitude, and absorption of the wave activity there. The nonlinear response involves reflection of the wave activity, and this is captured by the stationary wave nonlinearity, which is here the wave potential vorticity flux. The zonally symmetric contribution to the solution is relatively small. Furthermore, it is found that the stationary wave

nonlinearity can be reasonably predicted in terms of the wave vorticity flux from the linear solution. By contrast, several differences will be seen in the WD case.

2.6 Weakly damped (WD) case

The aim in this section is to see how transient waves affect the conclusions about the role of stationary wave nonlinearity of the SD case. The weakly nonlinear asymptotic theory of Section 2.5 has not been extended to this case because there is no well established statistical closure to describe the transient wave PV flux. The analysis will thus be limited to the numerical models described in Section 2.2. One can recall that in the WD case, as described in Section 2.3, the transient waves act to sharpen the jet (see Figure 2.1; the author has also noted a zonal wind response seen in the Southern Hemisphere polar region, associated with waves that propagate across the equator, but this will not be discussed further). The stationary wave streamfunction response in DNS is shown in Figure 2.4a. Similarly to the SD case, one can see Rossby wave reflection, and propagation into multiple branches. The WD stationary wave response has larger amplitude than the SD response and more wave energy propagates further downstream because of the removal of the damping on waves. But the more fundamental difference in the dynamics is seen when the interplay between the controlling factors in the solution is analyzed, as diagnosed by the LIN-ANOM model.

The WD case is more complex than the SD case because there is no predictive theory (closure) for the transient wave PV fluxes. A new notation is introduced to discuss separately the impacts of transient and stationary waves. The stationary nonlinear terms are referred to as S and the transient nonlinear terms as T. The linear model solution's dependence on S and T can be written schematically as

$$\psi^* = \mathbf{L}\left\{U\left([S],[T]\right), F^*\left(S^*, T^*\right)\right\},$$

where the zonal basic state U depends on the zonal components of the stationary and transient wave nonlinearity, $[S]$ and $[T]$, and the zonally asymmetric forcing F^* depends on the zonally asymmetric component of the stationary and transient wave forcing, S^* and T^*. In the linear calculation, the dependence on $[S]$ and $[T]$ is included by changing the zonal mean basic state to be in balance with these terms, according to the zonal mean equation (2.2). The classical linear case corresponds to $\mathbf{L}\{U([S]=0,[T]=0), F^*(S^*=0,T^*=0)\}$; note that $U([S]=0,[T]=0)$ corresponds to U_{ref}, apart from hyperdiffusion effects.

To obtain the linear solution from the LIN-ANOM model (2.4), it is necessary to add a weak damping on the waves to suppress resonant modes, which degrade the solution. Thus, in (2.4), for example, τ_E =40 days for $\varepsilon = 2$. The classical linear case is shown in Figure 2.4b; the only difference between Figure 2.4b and Figure 2.2c is the reduction of the wave damping, which serves to enhance the poleward branch and increase the amplitude of the solution. The nonlinearity of the solution, which is the difference between Figure 2.4a and Figure 2.4b, is shown in Figure 2.5a, and its corresponding wave activity is shown in Figure 2.5b, in which critical layer reflection is primarily visible around (150°E, 15°N). In the remainder of this section, the simplest possible dynamical description of the nonlinear solution is sought.

It is found that the individual contributions from the zonally asymmetric nonlinear terms in the operator $\mathbf{L}$ do not, in isolation, explain well the critical layer reflection in the WD case. This is in contrast to the SD case, in which S^* explained much of the nonlinearity. For example, Figure 2.5c–d shows the streamfunction and wave activity for $\mathbf{L}\{U([S]=0,[T]=0), F^*(S^*=S^*_{WD},T^*=0)\}$, which includes stationary wave nonlinearity. In contrast to the SD case, the

WD S^* alone does not account for critical layer reflection (compare Figure 2.5c–d to Figure 2.2e–f). The case $\mathbf{L}\{U([S]=0,[T]=0),\ F^*(S^*=0,T^*=T^*_{WD})\}$, (Figure 2.5g–h) in which only the zonally asymmetric transient wave nonlinearity is included, provides a solution which is largely of opposite sign to the previous case. The author finds that the S^* and T^* components in these cases are generally of opposite sign (not shown). This is consistent with the previous finding that $[S]$ and $[T]$ acted in opposite senses on the zonal jet (Section 2.3).

After some trial and error experimentation, two ways have been found to produce the key nonlinear effects. One way, corresponding to the operator $\mathbf{L}\{U([S]=[S]_{WD},[T]=0),\ F^*(S^*=S^*_{WD},T^*=0)\}$ (Figure 2.5i–j) is to include both the zonally symmetric and zonally asymmetric stationary nonlinear terms. This case produces significant reflection near (150°E, 15°N) and the overall feature of the wave activity pattern is fairly consistent with that in Figure 2.5b. The other way is to include the jet sharpening effect of the transient wave forcing, using $\mathbf{L}\{U([S]=0,[T]=[T]_{WD}),\ F^*(S^*=0,T^*=0)\}$ (Figure 2.5k–l). This change in the basic state alone can induce considerable reflection wave energy back to mid-latitudes, but the location of the reflection is much broader than that in Figure 2.5b and the pattern around the reflection area in streamfunction plot Figure 2.5k is not similar to that in Figure 2.5a. This effect is diminished when the zonal mean adjustment to the stationary wave forcing is reintroduced ($\mathbf{L}\{U([S]=[S]_{WD},[T]=[T]_{WD}),\ F^*(S^*=0,T^*=0)\}$, Figure 2.5e–f), again because of the opposite impact of the stationary and transient wave forcings on the zonal mean jet.

Thus, critical layer reflection downstream from the topography can be induced by the combination of stationary wave nonlinearity and its impact on the zonal mean basic state. The zonal mean basic state response to transients is able to induce pronounced reflection, but does not put the reflection in the right location. There is no evidence indicating the involvement of the

time mean zonally varying component of transient wave forcing in the reflection in this simulation.

2.7 Nonlinear stationary wave model

One applied goal of this study is to test the Ting and Yu (1998) and Held et al. (2002) nonlinear stationary wave modeling approach in the presence of transient wave forcing. In the NONLIN-ANOM model (2.5), the zonal flow and the zonally asymmetric transient wave nonlinearity T^* are prescribed, but the stationary nonlinearity is calculated internally instead of being prescribed. The damping τ_E acts to stabilize the flow. A linear damping is still required to suppress the transients generated internally, while an absolutely steady flow is achieved only with an unrealistically strong damping. The magnitude of the damping is chosen as a trade-off between the need to suppress transients and the need to maintain a good quality solution relative to the DNS. The 40-day damping used in the linear WD calculation appears suitable for a good solution to (2.5); it produces transient wave flux convergences that are an order of magnitude smaller than those found in the WD DNS. This is similar to the treatment in Held et al. (2002), in which weak transients are present that are not strong enough to significantly modify the solution.

Figure 2.6 shows a Taylor diagram comparing the LIN-ANOM model and the NONLIN-ANOM model in the WD case. The plotting symbols are grouped according to whether stationary wave nonlinearity is neglected ($F^*(S^*)$=0, gray symbols), prescribed from the WD DNS in the LIN-ANOM model ($F^*(S^*)= F^*(S^*_{WD})$, black symbols), or predicted with the NONLIN-ANOM model (white symbols). The sensitivity of neglecting, prescribing, or predicting stationary wave nonlinearity to the presence of the remaining nonlinear effects is explored in the figure. In all cases, neglecting stationary wave nonlinearity seriously degrades the agreement with the DNS. One can see that the NONLIN-ANOM model reproduces the effect

of prescribed stationary wave nonlinearity $F^*(S^*)$ in the LIN-ANOM model for various combinations of forcings fairly well, in terms of both correlation and amplitude. The LIN-ANOM model solutions with prescribed stationary wave nonlinearity (black symbols) are not exactly the true solutions that the NONLIN-ANOM model solutions should be because transient waves are not suppressed completely and extra linear damping has been introduced in both models, but the stationary wave solutions from these two models are similar (not shown but can be inferred from the Taylor diagram in Figure 2.6). Overall, this comparison supports the validity of the nonlinear stationary wave modeling technique, confirms the necessity of including the stationary wave nonlinearity in stationary wave modeling, and highlights the importance of zonal mean adjustment. All the nonlinear model integrations are with τ_E = 40 days, except for the one indicated by a star symbol which achieves complete suppression of the transient waves with τ_E = 15 days.

2.8 Summary and discussion

Simple barotropic QG dynamics has been used to improve the understanding of stationary wave nonlinearity in barotropic dynamics. It has been shown that stationary wave nonlinearity in this setting is primarily manifested as critical layer reflection in the absence and presence of transient waves. In the weakly damped case with transient waves, a combination of adjustments to the zonal mean and stationary wave nonlinearity are required to accurately reproduce the pattern of critical layer reflection in the DNS solution. Although including the zonal mean adjustment to the transient wave forcing also results in reflection (Figure 2.5k–l), presumably through a change in the refractive properties of the basic state (Karoly 1983; Hoskins and Ambrizzi 1993), the spatial distribution of the wave activity associated with this effect is not fully consistent with the reflection pattern of the DNS solution.

How general are the effects described here? In the cases shown here and additional cases that have been analyzed, local stationary wave activity reflection is found where stationary wave amplitudes are large enough to induce longitudinally localized easterlies and weak PV gradients. In fact, such reflection is even seen in cases where the zonal mean zonal wind is westerly at all latitudes (not shown). This is similar to what Waugh et al. (1994) saw for total (stationary plus transient) wave activity fluxes.

Additional cases (not shown) examining the sensitivity of these results to model resolution, dissipation and topographic amplitude have begun to be explored. For Integrations with resolution ranging from T21 (5.6°) to T170 (0.7°), the basic results concerning critical layer reflection are fairly robust across these resolutions although the solution varies somewhat from case to case. Varying the eddy dissipation ($1/\tau_E$) also has a relatively weak effect on reflectivity. On the other hand, the solutions are more sensitive to two types of parameter changes. First, in the regime of weak zonal mean dissipation ($1/\tau_Z$), the reflectivity weakens as the zonal mean dissipation is reduced. However, when $1/\tau_Z$ is set to zero, the critical layer becomes fully reflective so that the amount of equatorward propagating wave activity balances the poleward propagating wave activity. Second, the solution and reflectivity are relatively sensitive to topographic amplitude. For example, there is less reflection in the linear regime of small amplitude topography and the solution changes unpredictably as topography is increased in the nonlinear regime. A question for future investigation is whether stationary wave nonlinearity changes in any fundamental manner for these two parameter changes.

A weakly nonlinear asymptotic theory is also used to physically interpret stationary wave nonlinearity in the SD case. It is found that to leading order, stationary wave nonlinearity represents the PV flux associated with the linear response in the SD case. This theory not only

matches the nonlinear solution in the small forcing limit, but also expresses the ability to prognose a large portion of both zonally symmetric and asymmetric components of the nonlinear response to finite size forcing. An improved version of this approach might be extended to a multiple stage method to prognose the stationary wave response to an imposed forcing that includes a zonal flow adjustment to stationary wave forcing. This might potentially provide an advance over standard approaches in which the zonal mean is fixed (e.g., Valdes and Hoskins 1991), and avoid reported sensitivities to the zonal mean basic state used (Ting and Sardeshmukh 1993). However, it should be remembered that in the absence of a statistical closure for transient wave flux convergences, this theory does not extend to the WD case. The fact that stationary and transient wave effects oppose each other in this simple system suggests that care needs to be taken with such an approach in both barotropic and baroclinic systems.

The Ting-Yu nonlinear technique of stationary wave modeling is now being employed to calculate stationary wave nonlinearity in observations and climate simulations. The author has attempted to quantify its performance and found that the Ting-Yu approach works best when zonal mean adjustments are included and wave damping is used that does not entirely remove transients from the solution. These results suggest that in the presence of transient waves, like baroclinic waves in the troposphere or the transient planetary waves of the stratosphere, stationary wave models will be qualitatively more accurate if the zonal mean flow adjustment is accounted for explicitly.

Table 2.1: Notation

ζ	vorticity	ψ	streamfunction
τ_Z	damping timescale for zonal mean flow	τ_E	damping timescale for waves
[ ]	zonal mean	*	deviation from zonal mean
$\overline{}$	time mean	'	deviation from time mean
U	prescribed time-independent and zonally symmetric zonal wind		
Z, Z_0	prescribed time-independent and zonally symmetric vorticity and its representative value, 1×10^{-5} s^{-1}		
u	horizontal velocity, **u** = (u,υ), zonal and meridional winds respectively		
f, f_0	Coriolis parameter and its representative value, 1×10^{-4} s^{-1}		
ν	resolution dependent hyperdiffusion coefficient; ν = 2.7×10^{50} m^8 s^{-1} for the highest meridional mode with zero zonal mode in T85, corresponding to a 3 hours damping timescale on this mode		
ζ_{ref}	vorticity of a zonally symmetric reference zonal flow corresponding to $U_{ref} = 25\cos\theta - 30\cos^3\theta + 300\sin^2\theta\cos^6\theta$ m s^{-1} (Held 1985)		
h	topography, a Gaussian mountain centered at (λ_0,θ_0) with half-width $\Delta\lambda$ and $\Delta\theta$; $h = h_0 \exp\left(-\frac{(\lambda-\lambda_0)^2}{(\Delta\lambda)^2} - \frac{(\theta-\theta_0)^2}{(\Delta\theta)^2}\right)$, λ_0=90°, θ_0=30°, $\Delta\lambda$=$\Delta\theta$=22.5°, h^*=h-[h]		

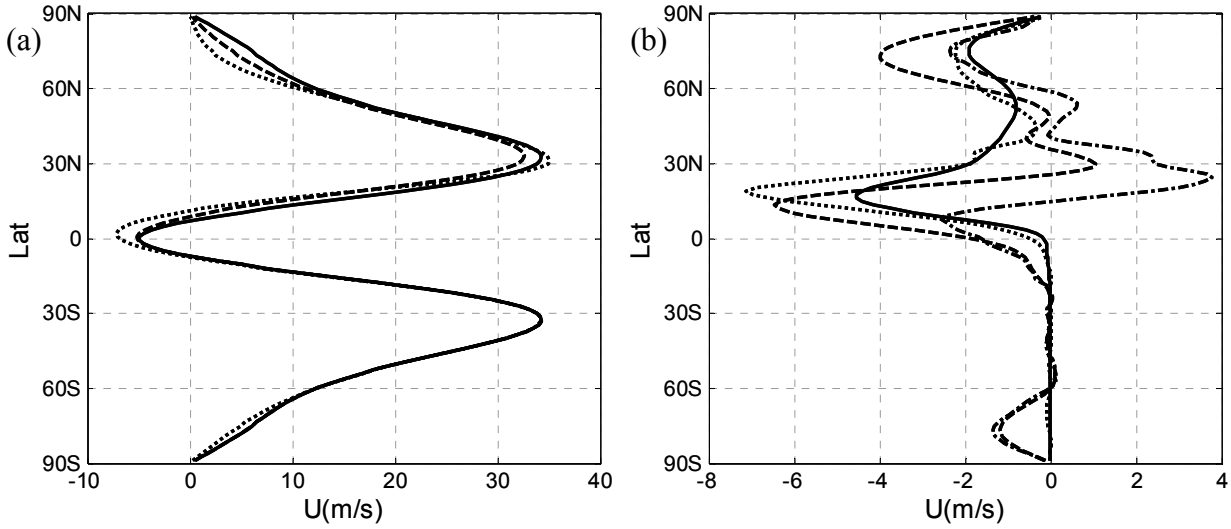

Figure 2.1: (a) Reference zonal wind, U_{ref} (solid), the SD case zonal wind, $[u]_{SD}$ (dashed), and the WD case zonal wind, $[u]_{WD}$ (dotted), for $\varepsilon = 2$, (b) SD zonal wind response (solid), WD zonal wind response (dashed), WD response to stationary wave forcing (dotted), WD response to transient wave forcing (dash-dotted). The units for zonal winds are m s^{-1}.

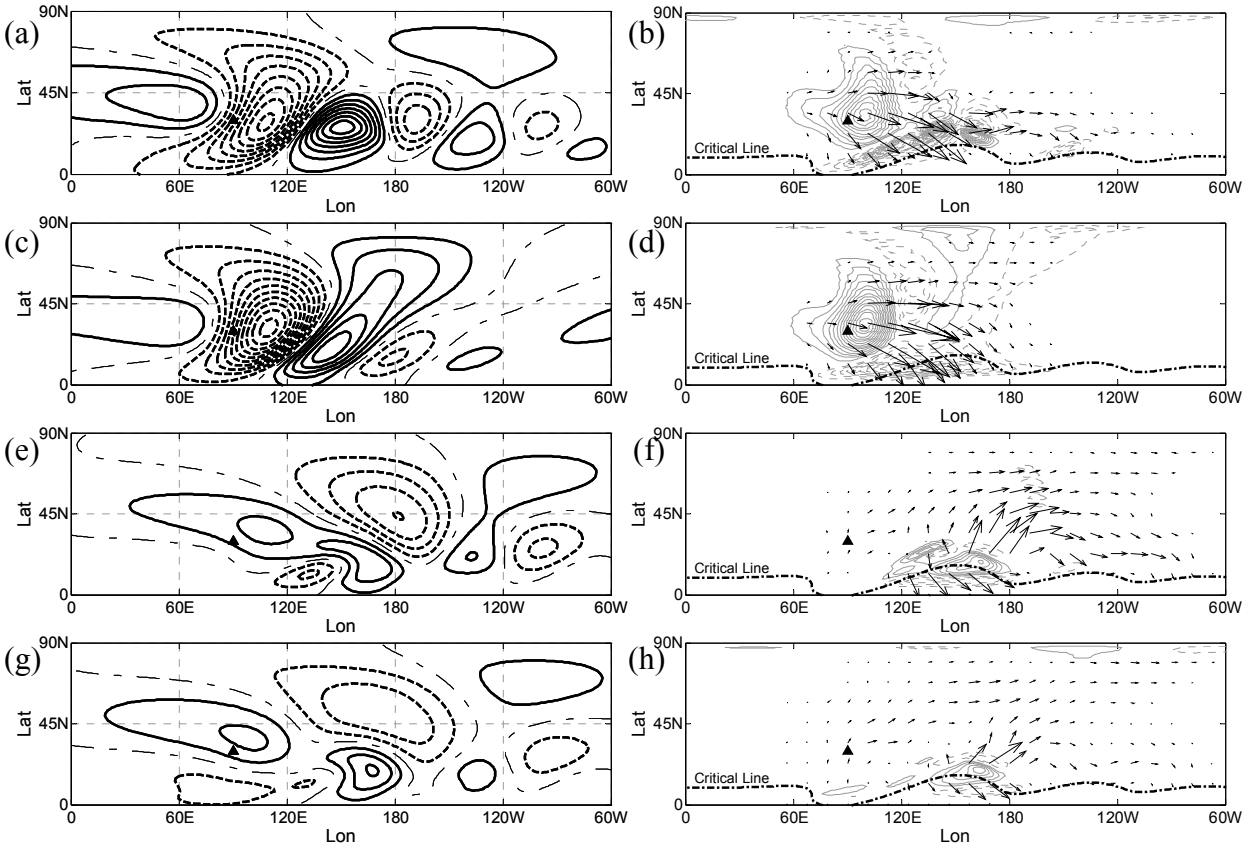

Figure 2.2: Streamfunction (left panels) and associated wave activity flux and its divergence (right panels) of the stationary wave response for $\varepsilon = 2$; the Gaussian mountain is centered at the location of the triangle in each plot. (a,b) The DNS streamfunction response and its associated wave activity; (c,d) As in (a,b), for the classical linear model; (e,f) The DNS response minus the linear response in streamfunction and the associated wave activity; (g,h) Linear model response to zonally asymmetric stationary wave nonlinearity, and the associated wave activity. Contour intervals of streamfunction and wave activity divergence are 3×10^{6} m^2s^{-1}, and 1×10^{-5} m s^{-2}, respectively. Solid contours are positive, dashed negative, and dash-dotted zero. The arrows representing wave activity fluxes are four times longer in (f) and (h) than those in (b) and (d) for visibility. For this and subsequent plots, the critical lines are indicated by dash-dotted contours.

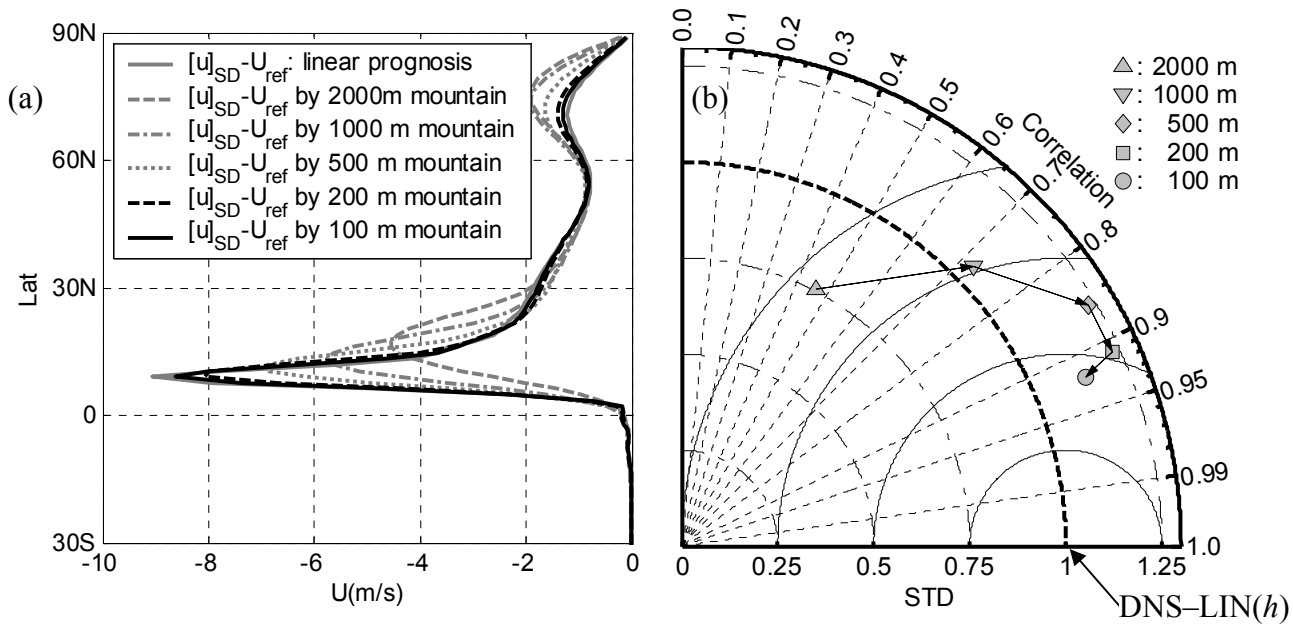

Figure 2.3: (a) The zonal mean zonal wind response for the weakly nonlinear asymptotic theory (2.7) and for DNS solutions $[u]_{SD} - U_{ref}$ for $\varepsilon = \{0.1, 0.2, 0.5, 1, 2\}$, ($h_0$={100, 200, 500, 1000, 2000} m) normalized by the reciprocal square of the mountain height. (b) Taylor (2001) diagram comparing the stationary wave response for the weakly nonlinear asymptotic theory (2.8) to the target field, which is the stationary wave in the DNS minus the stationary wave in the classical linear model (LIN(h); e.g., Figure 2.2e for $\varepsilon = 2$), for the cases in panel (a). In a Taylor diagram, the point 1 along the x axis corresponds to perfect agreement between the solutions, the orientation of the point is related to correlation between the fields (as indicated by the quarter circle labelled "correlation"), and the distance from the origin indicates amplitude relative to the amplitude of the target field.

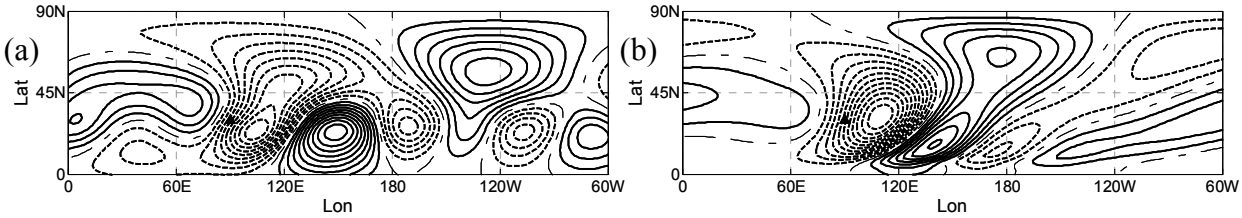

Figure 2.4: (a) Streamfunction of the stationary wave response for $\varepsilon = 2$ for the DNS of the WD case; (b) Streamfunction response for the classical linear model, with τ_E =40 days. Contouring as in the corresponding plots in Figure 2.2.

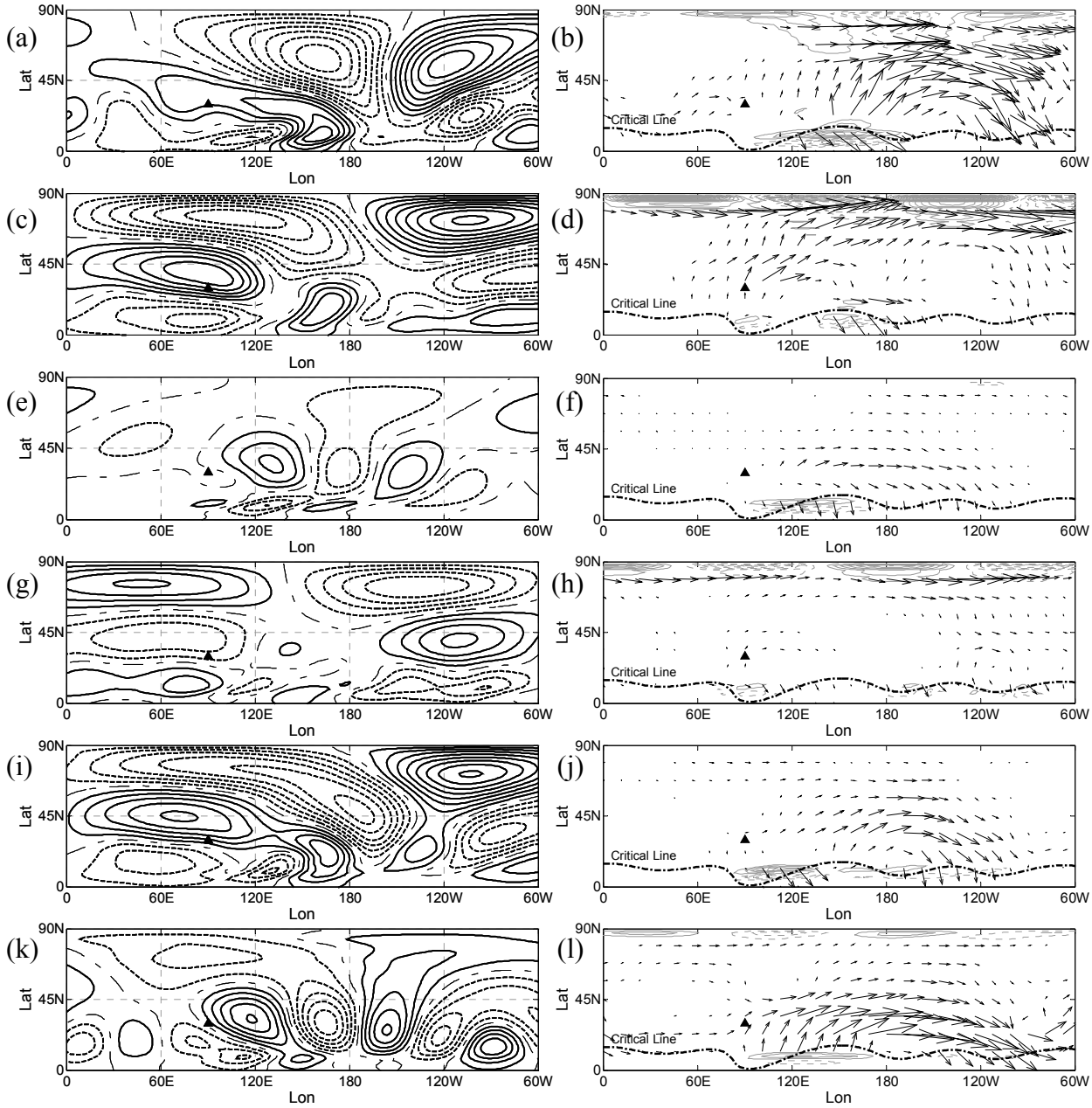

Figure 2.5: Similar to Figure 2.2 for the WD case. (a,b) Shows the DNS minus the classical linear response (i.e., Figure 2.4a minus Figure 2.4b) and the associated wave activity. Following this is plotted the response diagnosed from the linear model to (c,d) zonally asymmetric stationary wave forcing, (e,f) zonally symmetric stationary wave forcing, (g,h) zonally asymmetric transient wave forcing, (i,j) combined zonally symmetric and zonally asymmetric stationary wave forcing, (k,l) zonally symmetric transient wave forcing.

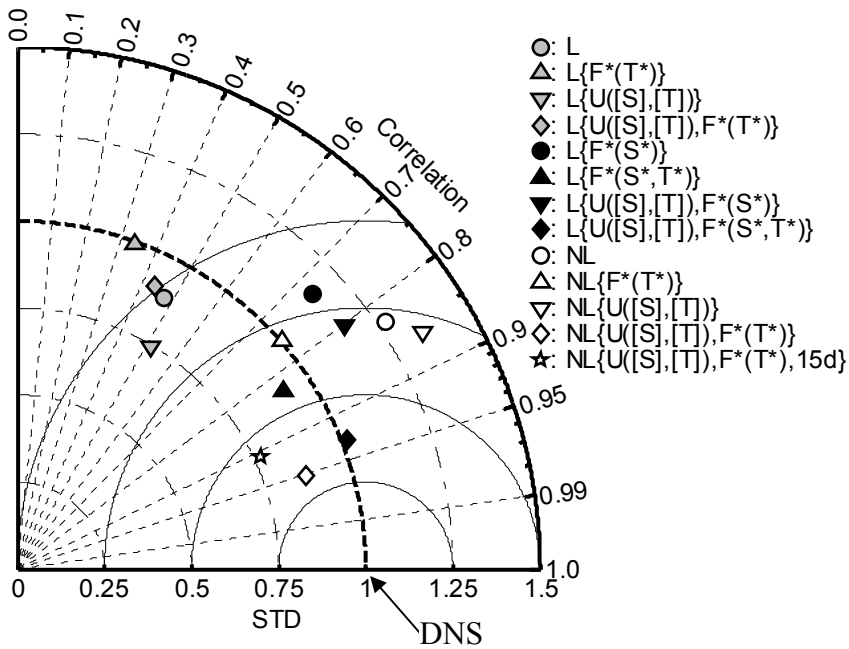

Figure 2.6: Taylor diagram of the linear and nonlinear stationary wave solutions compared with the target stationary wave solution in the DNS of the WD case. Shown are the response with $U = U_{ref}$ and no transient wave forcing (circles), with zonally asymmetric transient wave forcing (upward pointing triangles), with zonally symmetric stationary plus transient wave forcing (downward pointing triangles), and with zonally symmetric stationary plus transient wave forcing and zonally asymmetric transient wave forcing (diamonds). The star represents the latter case for the nonlinear model with damping increased to completely suppress transient waves. The black symbols represent the linear model with the prescribed stationary nonlinearity forcing, the grey ones are without the stationary wave nonlinearity forcing, and white symbols represent the nonlinear model. All runs have $\tau_E = 40$ days, except for the star case which has $\tau_E = 15$ days.

Chapter 3

3 A Stratosphere-Troposphere Stationary Wave Model

3.1 Introduction

In Chapter 1, an example of a stationary wave model has been introduced in barotropic QG dynamics and (1.3) is used to introduce four elements of a stationary wave model, i.e., the *zonal mean basic state*, *topographic forcing*, *stationary wave nonlinearity*, and *transient wave flux convergences*. In Chapter 2, the detailed effects of these elements on the stationary wave solution are examined. In this Chapter, baroclinic effects are to be considered. Stationary wave theory and modelling brings in several new effects: zonally asymmetric thermal forcing (*diabatic heating*) becomes a wave source term, baroclinic instability becomes a major source of tropospheric transient wave flux convergences, and stratospheric internal variability provides a pronounced contribution to stratospheric transient wave flux convergences. How to best combine these forcings into a stratosphere-troposphere stationary wave model still remains a challenge. Some tests addressing this issue will be discussed in Section 3.3 by considering the processes that maintain the NH winter stationary wave field in ERA-40 data. This will provide instructive information for further applications in studying stationary waves simulated by GCMs in Chapter 4. Before this testing, Section 3.2 will first focus on how to build a stratosphere-troposphere nonlinear stationary wave model using the Ting-Yu technique (see Sections 1.2 and 2.7). The damping and forcing settings of stationary wave models often depend on the input data, widely seen in the stationary wave modelling literature. Section 3.4 will discuss how these settings will be retuned for a CMAM simulation studied in Chapter 4.

Taylor diagrams have been found useful in Chapter 2 to summarize information in comparing modelling results to targeted fields, and therefore will be used intensively in this Chapter to evaluate the stationary wave model solutions against the ERA-40. The baroclinic stationary wave field has a three dimensional structure, while most studies focus on specific two-dimensional (2D) cross sections (e.g., 250 hPa pressure level) for the sake of visualization and convention. Here four 2D components of the stationary wave field are chosen, i.e., 250 / 10 hPa pressure levels and 30 / 60°N longitude-pressure cross sections as target fields to evaluate stationary wave model performance. The two pressure levels are chosen because the tropospheric stationary wave field has a nearly barotropic structure and its amplitude peaks in the upper troposphere, while the stratospheric stationary wave field is baroclinic but its structure is relatively simple and its maximum amplitude occurs usually near the 10 hPa level (e.g., Figure 1.1d, Figure 1.3, and Figure 4.2j–l). The 30°N cross section can illustrate the barotropic structure of the tropospheric stationary wave field and more importantly the topography is highest at this latitude, i.e., the Tibetan Plateau, for which the stationary wave response to the topography is significant and usually difficult to capture. The 60°N cross section best shows the baroclinic structure of the stratospheric stationary wave (e.g., Figure 1.1d) and the stratospheric stationary wave and its response to climate change are strongest at this latitude (e.g., Figure 4.2d–f).

3.2 Stationary wave model construction for observational analysis

A nonlinear stationary wave model is developed based on the GFDL FMS primitive equation spectral dynamical core (e.g., Held and Suarez 1994; Polvani and Kushner 2002). This model uses a weakly nonlinear technique that time integrates the damped primitive equations to a steady or quasi-steady state (e.g., Ting and Yu 1998; Held et al. 2002; Chang 2009). The

nonlinearity allowed in the model is via the stationary wave self-interaction, which involves quadratic advective nonlinearity and other nonlinear terms. The barotropic stationary wave nonlinearity has been introduced in Chapter 1 and some dynamical aspects of the Ting-Yu methods have been investigated in the barotropic dynamics setting in Chapter 2 to better understand how they capture stationary wave nonlinearity.

The primitive equations that GFDL FMS spectral dry dynamical core (or dry GCM) solves for in spherical coordinates are well known and can be found in many textbooks, but are reproduced here for completeness and clarity.

$$\frac{Du}{Dt} = 2\Omega\sin(\theta)\upsilon + \frac{u\upsilon\tan(\theta)}{a} - \frac{1}{\rho a\cos(\theta)}\frac{\partial p}{\partial\lambda} - k_\upsilon u + \nu\nabla^2 u \tag{3.1}$$

$$\frac{D\upsilon}{Dt} = -2\Omega\sin(\theta)u - \frac{u^2\tan(\theta)}{a} - \frac{1}{\rho a}\frac{\partial p}{\partial\theta} - k_\upsilon\upsilon + \nu\nabla^2\upsilon \tag{3.2}$$

$$\frac{DT}{Dt} = \frac{\kappa T\omega}{p} + \frac{Q}{c_p} - k_T\left\{T - T_{eq}(\theta, p)\right\} + \nu\nabla^2 T \tag{3.3}$$

$$\frac{\partial p_s}{\partial t} = -\nabla\cdot\int_0^{p_s}\mathbf{u}dp \tag{3.4}$$

where

$$\frac{D}{Dt} = \frac{\partial}{\partial t} + \frac{u}{a\cos(\theta)}\frac{\partial}{\partial\lambda} + \frac{\upsilon}{a}\frac{\partial}{\partial\theta} + \omega\frac{\partial}{\partial p}, \tag{3.5}$$

and $\mathbf{u} = (u, \upsilon)$ represents horizontal winds, Ω the angular velocity of the Earth. The intermediate variable ω (vertical velocity in pressure coordinates) is diagnosed in the model. The temperature is relaxed to a zonally symmetric background equilibrium temperature field, T_{eq} in (3.3), with a relaxation time k_T. This Newtonian cooling damping varies in the vertical direction, is strongest at the surface and decreases gradually to a constant value in the free atmosphere ($\sigma < \sigma_b = 0.7$,

where $\sigma_b = p / p_s$). The Rayleigh friction in velocity equations (3.1) and (3.2) only applies to the boundary layer ($1 > \sigma > \sigma_b$). The numerical settings for the Newtonian cooling and the Rayleigh friction in this simple GCM are quoted here from Held and Suarez (1994):

$$k_T = k_a + \left(k_s - k_a\right)\max\left(0, \frac{\sigma - \sigma_b}{1 - \sigma_b}\right)\cos^4\phi\,, \tag{3.6}$$

$$k_v = k_f \max\left(0, \frac{\sigma - \sigma_b}{1 - \sigma_b}\right), \tag{3.7}$$

where $k_f = 1$ day^{-1}, $k_a = 1/40$ day^{-1}, $k_s = 1/4$ day^{-1}. The Rayleigh friction is latitude independent and has a damping timescale of 1 day at the surface ($\sigma = 1$) and the friction linearly decreases to zero at the top of the boundary layer ($\sigma_b = 0.7$). The Newtonian cooling coefficient has both meridional and vertical structure; it linearly decreases into the free atmosphere and then stays constant above, and decreases from the equator to the poles following $\cos^4$(latitude).

This dynamical core has a clear and simple structure in its source code and is well documented, publicly available, and widely used in many different research topics; in short, the author thinks this is an "elegant" model (a concept proposed by Held 2005). A stationary wave model is built with the following objectives which are easy to accomplish with this dynamical core: first, the stationary wave model should be well documented and publicly available; second, the stationary wave model should be easy for anyone to reproduce; third, the tuning steps in the stationary wave model should be made as clear as possible; and finally, known sensitivities and known robust tunings should be documented. To accomplish these objectives, the author builds a new stationary wave model and does not just extend previous models to the stratosphere, as most existing models either have an outdated dynamical core or are not well documented from the perspective outlined above.

To build the stationary wave model, the GCM damping settings in (3.6) and (3.7) are modified not only following the experience from previous studies but also exploring various aspects of the spatial variation of the damping profiles. Ting and Yu (1998) employ a damping timescale of 0.2 days and 1 day at the lowest two sigma levels, and then 15 days from $\sigma = 0.811$, for both the Rayleigh friction and the Newtonian cooling. Held et al. (2002) uses different settings for the Rayleigh friction and the Newtonian cooling, i.e., a uniform damping timescale of 15 days throughout the atmosphere for the Newtonian cooling, plus a damping timescale of 25 days for the Rayleigh friction throughout the atmosphere except for the lowest four sigma levels which are 0.3, 0.5, 1, and 8 days, respectively. Chang (2009) uses a Rayleigh friction profile very similar to that of Held et al. (2002) plus a Newtonian cooling damping timescale of 30 days in the free atmosphere ($\sigma < 0.7$) which decreases to 2 days at the surface.

From the cited studies one can see that tuning the damping profiles is a standard procedure in building this kind of time-integration stationary wave model and that different damping settings might apply for different applications. During the construction of this new stationary wave model, the author has tested the vertical variations of the damping profiles including both the damping timescales and the transition levels for boundary layer, tropopause, sponge layer near the model lid, and the like. The author has also tuned the meridional variations of the dampings, which is different from previous practice but is inspired by Held and Suarez (1994). For example, (3.6) is extended to

$$k_T = \frac{1}{\tau_a} + \left(\frac{1}{\tau_s} - \frac{1}{\tau_a} \right) \frac{\sigma - \sigma_b}{1 - \sigma_b} \cos^n \phi \tag{3.8}$$

for $1 > \sigma > 0.7$, where the timescales (τ) are reciprocals of the damping rates. In addition, the effects of the power exponent n have been tested in shaping the meridional profile of the Newtonian cooling and in controlling the stationary wave model solution.

Figure 3.1 shows the Taylor diagram of NH stationary wave solutions corresponding to n = {0, 1, 2, 3, 4} in (3.8), when all other damping components are fixed and the stationary wave model is forced by topography plus diabatic heating absent its long wave radiative component (the reasons for using this combination of forcings are discussed in Section 3.3) from ERA-40. To calculate the spatial correlation, the streamfunction fields are weighted by area, $\cos^2(\phi)$, and log-pressure depth of each level, $\Delta\log(p)$; the amplitude is measured in terms of the spatial standard deviation of the stationary wave field. As the damping timescale in the boundary layer increases (n from 0 to 4), the stationary wave amplitude increases monotonically but the pattern correlation between the stationary wave solution and the ERA-40 NH January 1979–2002 stationary wave field does not increase systematically, for example, the stationary wave field on 250 hPa pressure level (symbol "▽" in Figure 3.1) and longitude-pressure cross sections near the North Pole (not shown). This kind of trade-off is quite typical in tuning the damping parameters, and one has to compromise at a certain point to control the overall quality of the stationary wave solution, in the balance of qualities of different components as well as in the pattern correlation and amplitude. Diffusion is also considered a tunable parameter in many stationary wave models (e.g., Ting and Yu 1998; Ting et al. 2001; Held et al. 2002; Chang 2009) and is usually set to a significantly larger value than those used in GCMs in order to partially suppress the internally developed transient waves in stationary wave models. A sponge layer is also used at the model lid in order to suppress possible stationary wave reflection by the rigid lid at the top. The damping profiles used in the stationary wave model developed here are summarized in Table 3.1.

Another issue related to this stationary wave modelling technique is the way to deal with the zonal mean basic state. Ting and Yu (1998) prescribed the zonal mean basic state and kept it

fixed. On the other hand, Held et al. (2002) and Chang (2009) relaxed the zonal mean flow towards the prescribed basic state on a timescale of 3 days in order to allow the zonal mean flow to adjust slightly to a flow more consistent with wave driving of the zonal mean flow. Held et al. (2002) found that there is no significant difference if the zonal mean is fixed at a prescribed state. However, tests have shown that fixing the zonal mean basic state is superior to relaxing the zonal mean flow with a wide range of timescales from 0.1 to 15 days (Figure 3.2). The relaxed zonal mean case approaches the fixed zonal mean case (symbol "1" in Figure 3.2) as the relaxation timescale is reduced, as especially evident for 10 hPa and 60°N (symbols "△" and "□" in Figure 3.2). The damping profiles are fixed at the values for the ERA-40 case in Table 3.2 for this test, and extra tests with other damping profiles also support the results here (not shown). On the other hand, as mentioned in Section 2.7, this stationary wave modelling technique allows internally generated transients of relatively small amplitude in the stationary wave model, and it is found that transients can only be completely suppressed with unrealistically strong dampings that degrade the stationary wave solution, whether or not the zonal mean flow is fixed or relaxed. Therefore, the author keeps the zonal mean basic state fixed in the new stationary wave model.

Pretreatments, typically smoothing, of forcings are also common in the stationary wave modelling literature. For example, Grose and Hoskins (1979) smooth the realistic topography using a scale-selective filter in spectral space, Ting et al. (2001) also uses a smoothed topography, while many other studies simply interpolate topography to their model resolution (e.g., Held et al. 2002; Chang 2006). Two versions of topography have been tried, T20 (6°) and T42 (2.8°), with the latter the same as the model resolution and the former much smoother. The stationary wave solution in the ERA-40 is more realistic with the smoothed topography, although the differences in the stationary wave solutions are fairly small (the difference in correlation is less than 0.15 in

all combinations of forcings). Thus the smoothed (T20) topography is used for ERA-40 diagnoses. The ERA-40 diagnoses in Section 3.3 are also reproduced with unsmoothed topography, and there is no fundamental impact on the findings (not shown).

The stationary wave model resolution is T42 in the horizontal and 42 levels in the vertical, with 18 levels above 100 hPa and the highest full level at 0.4 hPa, which are chosen to match the resolutions of current comprehensive climate models and to well resolve stationary wave and forcing fields. Unlike the troposphere-focussed stationary wave models in previous studies, a hybrid sigma-to-pressure vertical coordinate, instead of a sigma coordinate, is adopted to avoid numerical artefacts in the stratosphere over large topography. The use of hybrid vertical coordinates is common in most CCMs. The model uses linear damping on the waves including Rayleigh friction and Newtonian cooling as discussed above. For a comparison with the damping profiles using in previous studies, Figure 3.3 shows the comparison of the stationary wave solution using the damping settings in Table 3.2 (symbol “1” in Figure 3.3) with the solutions using damping profiles in Held et al. (2002) and Chang (2009). These stationary wave solutions using different damping profiles are comparable while the settings in Table 3.2 work with the ERA-40 diabatic heating better as a result of extensive tuning. The linear stationary wave solution (symbol “4” in Figure 3.3) will be discussed in the next section.

3.3 NH stationary wave maintenance in ERA-40

The ERA-40 has been chosen to test the stationary wave model because its vertical coverage includes the entire stratosphere. The period 1979–2002 is used to examine the maintenance of the NH wintertime stationary wave field because the quality of the stratospheric reanalysis has been improved since satellite observations started to be used extensively in 1979. This section will focus on the January climatology, as this is when the NH stationary wave

amplitude peaks in its annual cycle. As mentioned in Chapter 1 and this chapter, stationary wave theory categorizes the zonally asymmetric forcings of the stationary wave field into diabatic heating, topographic forcing, stationary wave nonlinearity and transient wave flux convergences (e.g., Nigam et al. 1988; Ting 1994; Held et al. 2002; Chang 2009). This stationary wave model is able to calculate the stationary wave nonlinearity internally and thus only needs to prescribe the other three forcings.

In Chapter 2, the dynamical nature and significance of stationary wave nonlinearity has been discussed in barotropic QG dynamics. Similarly to the approaches in Chapter 2, the wave activity diagnosis is applied here to the difference between the nonlinear and linear stationary wave solutions on 250 hPa, a representative level for the tropospheric stationary wave. The nonlinear solution is the symbol "▽" in Figure 3.3 and the linear solution (symbol "▽" in Figure 3.3) is obtained by eliminating the stationary wave nonlinearity in the stationary wave model. Figure 3.4 shows the streamfunction and wave activity (Plumb (1985) flux) of this difference. The difference in streamfunction is comparable to the stationary wave itself in amplitude (see Figure 1.1c), confirming the importance of stationary wave nonlinearity in the baroclinic case. Wave activity reflection in the vicinity of the critical line is evident at 90°E, 180°, 150°W, 60°W and 30°W. These reflections are dynamically consistent with the reflections seen in the barotropic cases in Chapter 2. The barotropic component of the tropospheric stationary wave, i.e., averaged over 850–100 hPa, has similar structures in both streamfunction and wave activity (not shown). The amplitude of the linear solution is considerably weaker than the amplitude of the nonlinear solution in the stratosphere and at 60°N (symbol "4" versus symbol "1", symbols "△" and "□", in Figure 3.3).

An important issue is how best to incorporate diabatic heating H in the stationary wave model. The diabatic heating H is the sum of the convective, condensational, radiative and other heating terms appearing in the thermodynamic equation. Among these terms the longwave radiative heating (H_{LW}) is particularly problematic to prescribe as a forcing, because it is strongly coupled to the local atmospheric state. In particular, stratospheric longwave heating is typically relaxational, implying that in regions where $H_{LW} > 0$, the local temperature is anomalously cool, and the converse. If a positive H_{LW} were imposed as a forcing, in the presence of Newtonian relaxation in the stationary wave model it would locally warm the atmosphere, leading to an opposite thermal response to what is physically expected.

The nonlinear stationary wave model is used to investigate the roles of the zonally asymmetric forcings from the ERA-40 in maintaining the observed stationary wave field. The forcings considered include orographic forcing (O), diabatic heating (H), diabatic heating with the longwave component removed ($H - H_{LW}$), and transient wave forcing (*Trans*). All possible combinations of these forcings have been investigated and several cases are included in the Taylor diagram in Figure 3.5, which, as in Section 3.2, includes symbols for the NH 250 hPa, the NH 10 hPa, the 30°N and the 60°N January stationary wave streamfunction field. The case in which orographic forcing and diabatic heating absent the longwave heating is applied ($O + H - H_{LW}$; symbol "1" in Figure 3.5) is able to best mimic the ERA-40 stationary wave field. Adding transients to this combination ($O + H - H_{LW} + Trans$; symbol "3" in Figure 3.5) degrades the solution somewhat, for reasons that have not been fully understood. But the result is consistent with the idea that transient wave flux convergences have a relaxational behaviour as well (Ting and Held 1990; Ting et al. 2001; see also the discussion below on Figure 3.6). Including the longwave heating ($O + H + Trans$; symbol "5" in Figure 3.5) degrades the solution even more,

similarly from $O + H - H_{LW}$ (symbol “1” in Figure 3.5) to $O + H$ (symbol “4” in Figure 3.5). Another case ($O + H_{tropo}$; symbol "2" in Figure 3.5) will be discussed in Section 3.4.

To further understand the role of longwave radiative heating and transient wave flux convergences, their individual contribution to the observed stationary wave field is investigated (in the absence of orographic forcing). Figure 3.6 shows the spatial correlation and the relative amplitude between the observed stationary wave field and the stationary wave model solution as a function of vertical level when the stationary wave model is forced by longwave radiative heating only (red curve in Figure 3.6). The longwave radiative heating in isolation generates a stationary wave pattern that is negatively correlated with the observed stationary wave field almost throughout the entire troposphere and stratosphere. Given the physical expectation of the effects of longwave heating and the consistent results of these tests, the study proceeds by excluding, where possible, prescribed longwave radiative diabatic heating as a forcing in the stationary wave model. In addition, Figure 3.5 suggests that transient wave flux effects are relatively small and that including them does not necessarily improve the solution. Not surprisingly, transient wave effects are complex. For example, Figure 3.6 also plots the vertical profile of the spatial correlation and the relative amplitude between the observed stationary wave field and the stationary wave solution by transient wave flux convergences only (dashed curve in Figure 3.6). This correlation is negative in the troposphere, consistent with previously reported similar dissipative behaviour of transient wave forcing (e.g., Ting and Held 1990; Ting et al. 2001), and positive in the stratosphere. However, this effect does not directly apply to the stratospheric stationary wave field when other forcings are present. For example, as discussed in Figure 3.5, adding transient wave forcing degrades the stationary wave solution, even in the stratosphere where transients alone induce a stationary wave pattern positively correlated with

observed stationary wave field. This indicates nonlinear interactions local in the stratosphere between the stationary wave components forced by different forcings or remote impacts from the degraded stationary wave solution by tropospheric transients. It can be inferred from Figure 3.7 that the latter is the case (see discussion below).

The nonlinear stationary wave maintenance in ERA-40 1979–2002 January climatological mean is summarized in Figure 3.7, and the combinations of the forcing terms are listed in Table 3.3. The combination that best mimics the ERA-40 stationary wave field is topography, diabatic heating absent its longwave radiative component, plus the stratospheric transient wave flux convergences ($O + H - H_{LW} + Trans_{strat}$; symbol "15" in Figure 3.7). It is evident here by comparing symbol "1" and symbol "15" that the local nonlinear interactions in the stratosphere between the stationary wave components forced by stratospheric transients and other forcings do not degrade the solution but enhance the amplitude of the stratospheric stationary wave. This indicates that the degrading of the stratospheric stationary wave seen in Figure 3.5 is caused by the remote influence from the troposphere. The individual contribution from each combination of forcings to the total stationary wave field is not described further here. It is worth mentioning, however, that nonlinear stationary wave solutions have moderate nonadditivity for different combinations of forcings (not shown), indicating nonlinear interaction between the stationary waves response to individual forcings is a major source of the total stationary wave nonlinearity (e.g., Held 1983; Held et al. 2002; Brandefelt and Körnich 2008).

In summary, the above results from ERA-40 stationary wave modelling have suggested a practical way to combine the zonally asymmetric stationary forcings into the stationary wave model developed here and also how to find the damping settings for given forcings. The

longwave radiative diabatic heating and tropospheric transient wave flux convergences both have a relaxational behaviour and should be excluded as forcings in the stationary wave model.

3.4 Stationary wave model construction for GCM analysis

The literature discussed in Section 3.2 suggests that the optimal stationary wave model tuning can often be data or model dependent. This section discusses some of the changes needed to apply the stationary wave model to analysis of GCM simulations. In particular, it focuses on the construction of a stationary wave model for the diagnosis of a CMAM simulation in the next chapter. Changes both to the damping settings of the model and to the externally prescribed fields need to be considered.

In Section 3.2, the optimal configuration of the stationary wave model required smoothed topography. By contrast, this seems unnecessary for the CMAM diagnosis: the best CMAM stationary wave solution is found using topography consistent with model resolution (not shown), and therefore the unsmoothed (T42) topography is used for CMAM diagnosis.

The detailed contributions to H of the longwave, shortwave, condensational, and other components (see Section 1.1), as well as the transient wave forcing terms, are not typically available from climate model output, including from the CMAM simulation. Practical approaches to address this problem will now be discussed.

Based on the stationary wave model testing with ERA-40 data (Section 3.2), it would be beneficial to exclude the longwave radiative diabatic heating H_{LW}, but since this term has not been separately archived, another practical approach is used. Given that longwave radiative heating dominates the stratosphere but is a minor component in the troposphere, an alternative solution to this problem is to apply the total diabatic heating only in the troposphere in the

stationary wave model. This approach is tested with reference to the ERA-40 data in Figure 3.5: $O + H_{tropo}$ (symbol "2"s in Figure 3.5) is compared with $O + H - H_{LW}$ (symbol "1"s in Figure 3.5) and one can see only a slight degradation of the stationary wave representation; it is also found that $O + H_{tropo}$ is superior to the solution $O + H$ with the total diabatic heating (symbol "4"s in Figure 3.5). Thus, this compromise only slightly influences the solution.

The stationary wave model testing with ERA-40 data has also revealed that the transient wave effects are complex in maintaining the observed stationary wave field (Section 3.3). Given the complexity and the fact that the daily sampled data required to calculate the transient wave flux convergences are often not available from the CCMs, and in particular from the CMAM that will be focused on, it is decided to neglect them in Chapter 4.

The damping settings for ERA-40 turn out not to be optimal for the application to the CMAM simulation and this leads to a modest retuning. The differences between the two settings are localized to a few critical areas, as seen in Table 3.2. The standard tuning of these damping settings is based on the optimization of the stationary wave streamfunction and produces a stationary wave model response in streamfunction which captures well that in the GCM. But the wave driving (i.e., the EP-flux) response for this tuning does not capture the GCM response to climate change, which involves detailed information on the vertical structure of the streamfunction (and hence the temperature). Section 4.6 describes another retuning of the stationary wave model that improves the temperature field with a modest cost to the streamfunction tuning. As can be seen in Table 3.1 and Table 3.2, thermal damping is strengthened in the stratosphere and a transition layer is applied from the troposphere to the stratosphere. These issues will be discussed further in the next chapter.

Table 3.1: Damping profiles in the stationary wave model

	Rayleigh friction timescale (days)	Newtonian cooling timescale (days)
Lower boundary ($\sigma = 1$)	τ_f	τ_s
Boundary layer ($1 > \sigma > \sigma_b$)	$\dfrac{1}{\dfrac{1}{\tau_{av}} + \left(\dfrac{1}{\tau_f} - \dfrac{1}{\tau_{av}}\right)\dfrac{\sigma - \sigma_b}{1 - \sigma_b}}$	$\dfrac{1}{\dfrac{1}{\tau_a} + \left(\dfrac{1}{\tau_s} - \dfrac{1}{\tau_a}\right)\dfrac{\sigma - \sigma_b}{1 - \sigma_b}\cos^n lat}$
Troposphere ($\sigma_b > \sigma > 0.1 = \sigma_{strat1}$)	τ_{av}	τ_a
Transition layer ($\sigma_{strat1} > \sigma > 0.05 = \sigma_{strat2}$)	$\dfrac{1}{\dfrac{1}{\tau_{strat}} + \left(\dfrac{1}{\tau_{av}} - \dfrac{1}{\tau_{stratv}}\right)\dfrac{\sigma - \sigma_{strat2}}{\sigma_{strat1} - \sigma_{strat2}}}$	$\dfrac{1}{\dfrac{1}{\tau_{strat}} + \left(\dfrac{1}{\tau_a} - \dfrac{1}{\tau_{strat}}\right)\dfrac{\sigma - \sigma_{strat2}}{\sigma_{strat1} - \sigma_{strat2}}}$
Stratosphere ($\sigma_{strat2} > \sigma > 0.01 = \sigma_{sp}$)	τ_{stratv}	τ_{strat}
Sponge layer ($\sigma_{sp} > \sigma$)	$\dfrac{1}{\dfrac{1}{\tau_{stratv}} + \left(\dfrac{1}{\tau_{spv}} - \dfrac{1}{\tau_{stratv}}\right)\left(\dfrac{\sigma_{sp} - \sigma}{\sigma_{sp}}\right)^8}$	$\dfrac{1}{\dfrac{1}{\tau_{strat}} + \left(\dfrac{1}{\tau_{sp}} - \dfrac{1}{\tau_{strat}}\right)\left(\dfrac{\sigma_{sp} - \sigma}{\sigma_{sp}}\right)^8}$
Model lid ($\sigma = 0$)	τ_{spv}	τ_{sp}

Table 3.2: Damping settings in Table 3.1 for ERA-40 and CMAM cases

		ERA40	CMAM streamfunction	CMAM EP-flux
Rayleigh friction timescale (days)	τ_f	1	1	1
	τ_{av}	7.5	7.5	7.5
	τ_{stratv}	7.5	7.5	7.5
	τ_{spv}	0.5	0.5	0.5
Newtonian cooling timescale (days)	τ_s	4	4	1
	τ_a	40	40	40
	τ_{strat}	40	40	15
	τ_{sp}	0.5	0.5	0.5
Top of the boundary layer	σ_b	0.8	0.7	0.7
Power exponent in (3.8), shaping the meridional profile of the Newtonian cooling	n	0	1	1

Table 3.3: Combinations of forcings used in studying the NH winter stationary wave maintenance in ERA-40

Runs	Topography (O)	Diabatic heating (H)		Transients (*Trans*)
		Total – Longwave radiative ($H - H_{LW}$)	Longwave radiative (H_{LW})	
1	✓	✓		
2	✓	✓	✓	
3	✓		✓	
4	✓	Troposphere only	Troposphere only	
5	✓	Stratosphere only	Stratosphere only	
6		✓		
7		✓	✓	
8			✓	
9	✓			
10				✓
11	✓			✓
12	✓	✓		✓
13	✓	✓	✓	✓
14	✓		✓	✓
15	✓	✓		Stratosphere only

The "✓" means the forcing is present and blank means absent; some forcings are applied only in the stratosphere or only in the troposphere.

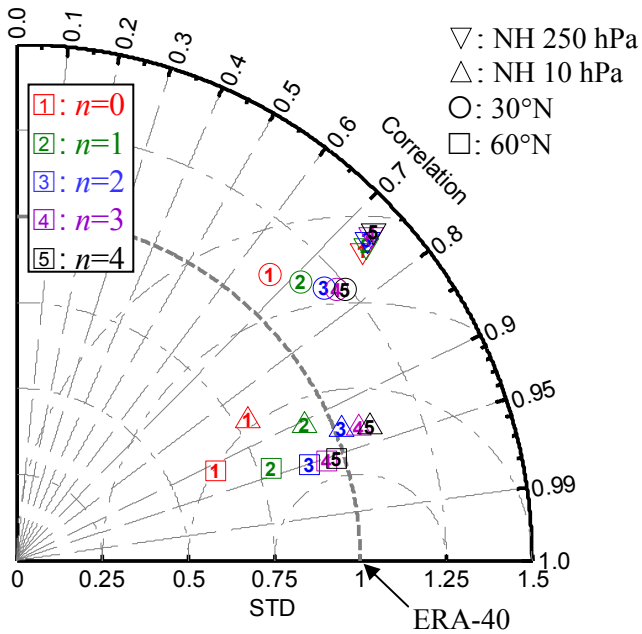

Figure 3.1: Taylor diagram of stationary wave solutions diagnosed by the stationary wave model compared with the ERA-40 NH winter (January 1979–2002) stationary wave climatological mean showing the effects of tuning the meridional variation of Newtonian cooling in the boundary layer when the nonlinear stationary wave model is forced by topography plus diabatic heating absent the longwave radiative component ($O + H - H_{LW}$) from the ERA-40: 1 $n = 0$, 2 $n = 1$, 3 $n = 2$, 4 $n = 3$, 5 $n = 4$, corresponding to a Newtonian cooling profile using (3.8) in the boundary layer ($1 > \sigma > \sigma_b$), where $\tau_s = 4$ days, $\tau_a = 20$ days, and $\sigma_b = 0.7$. The ▽ symbols represent the 250 hPa pressure level, the △ represent the 10 hPa pressure level, the ○ symbols are the height-longitude cross section at 30°N, and the □ symbols are the height-longitude cross section at 60°N (hereafter for all Taylor diagrams).

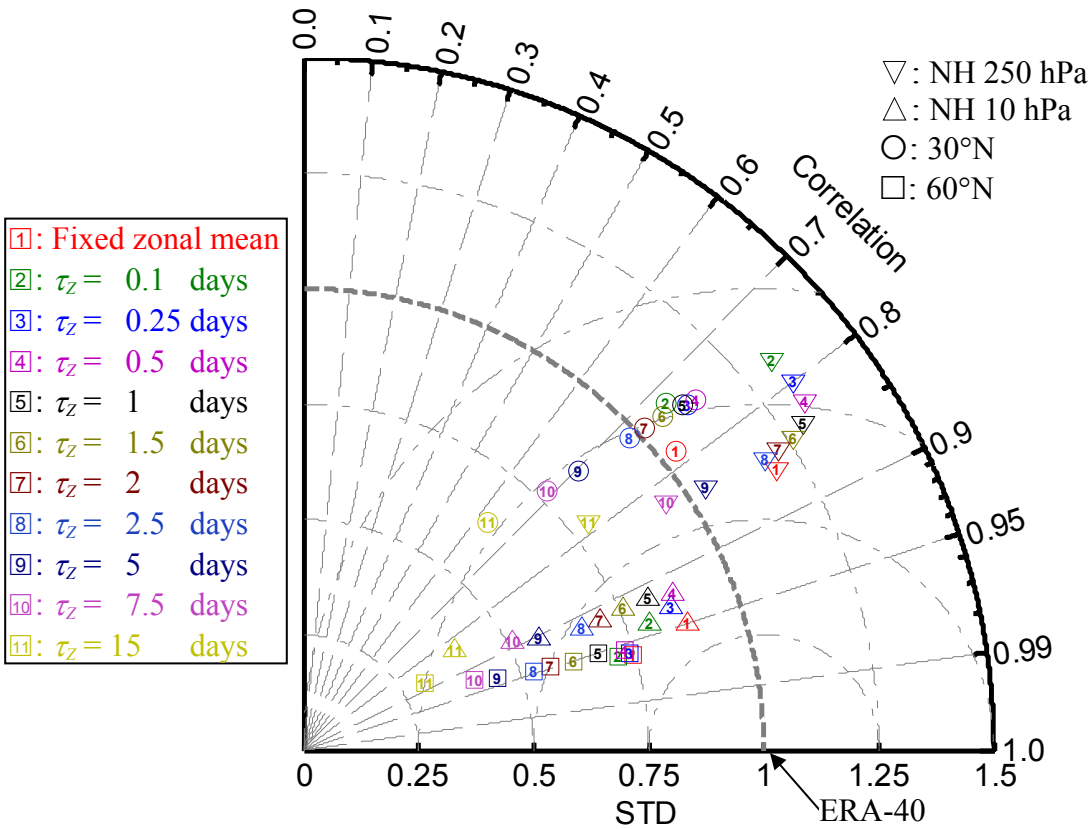

Figure 3.2: Similar to Figure 3.1 but showing the effects of 1 fixing the zonal mean basic state as prescribed or 2 – 11 relaxing the zonal mean flow towards the prescribed basic state with a certain timescale.

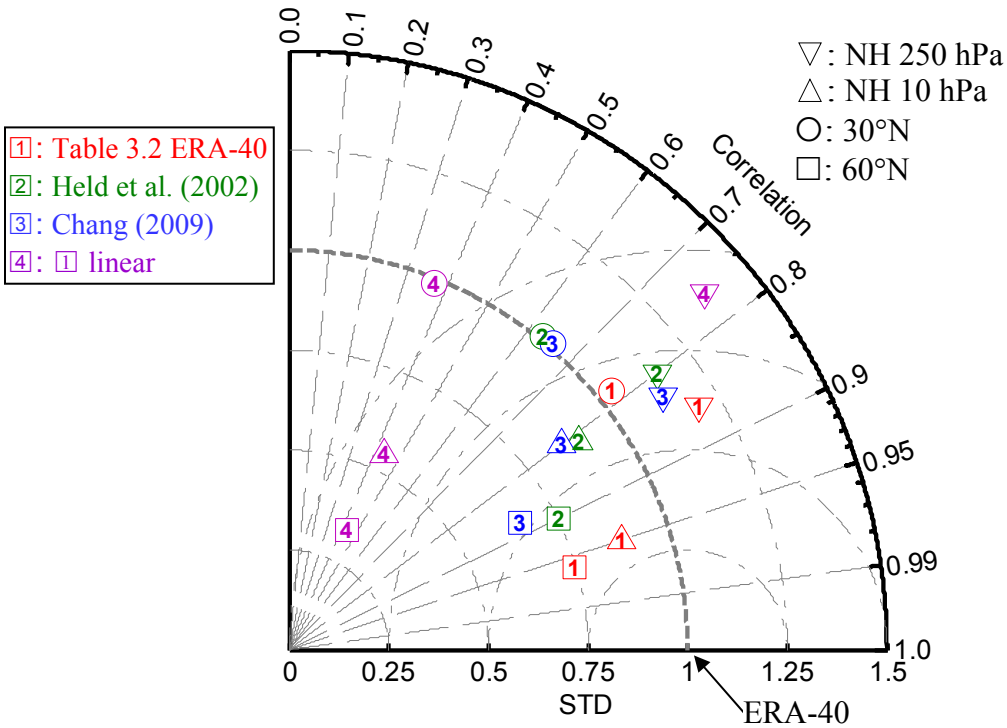

Figure 3.3: Similar to Figure 3.1 but for comparison of the nonlinear stationary wave solution using the damping profiles in Table 3.2 for ERA-40 analysis (1) with the nonlinear stationary wave solutions using damping settings in Held et al. (2002; 2) and Chang (2009; 3). 4 is the linear solution using the same damping profiles as 1.

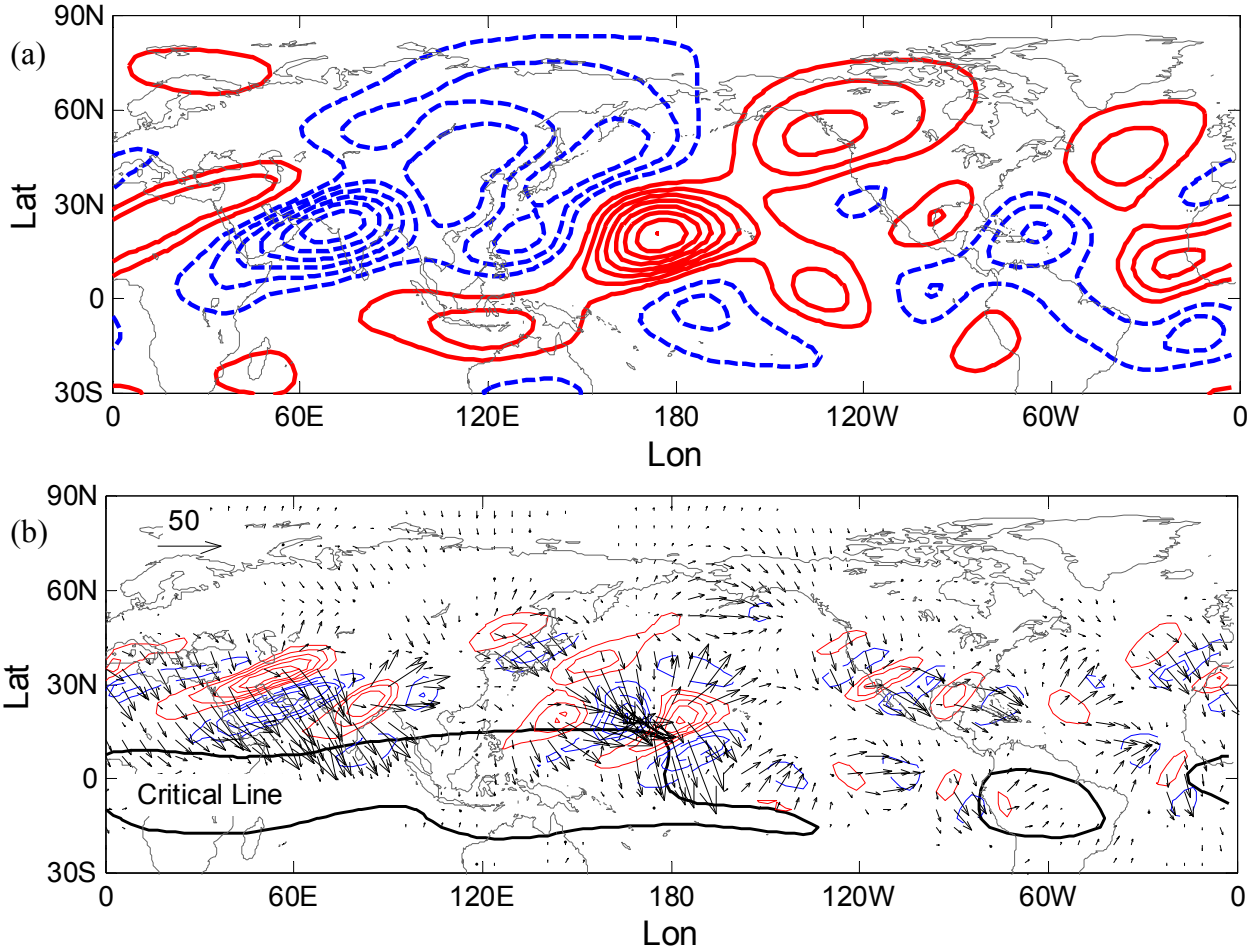

Figure 3.4: Similar to Figure 2.2e,f, (a) streamfunction and (b) associated wave activity flux (arrows) and its divergence (blue and red contours) of the difference between the nonlinear and linear stationary wave solutions, when the stationary wave model is forced by $O + H - H_{LW}$ from the ERA-40 NH winter (January 1979–2002) climatology. The black solid contour is the critical line for stationary waves. Contour intervals are 3×10^{6} m^2s^{-1} for streamfunction and 2×10^{-5} m s^{-2} for wave activity divergence.

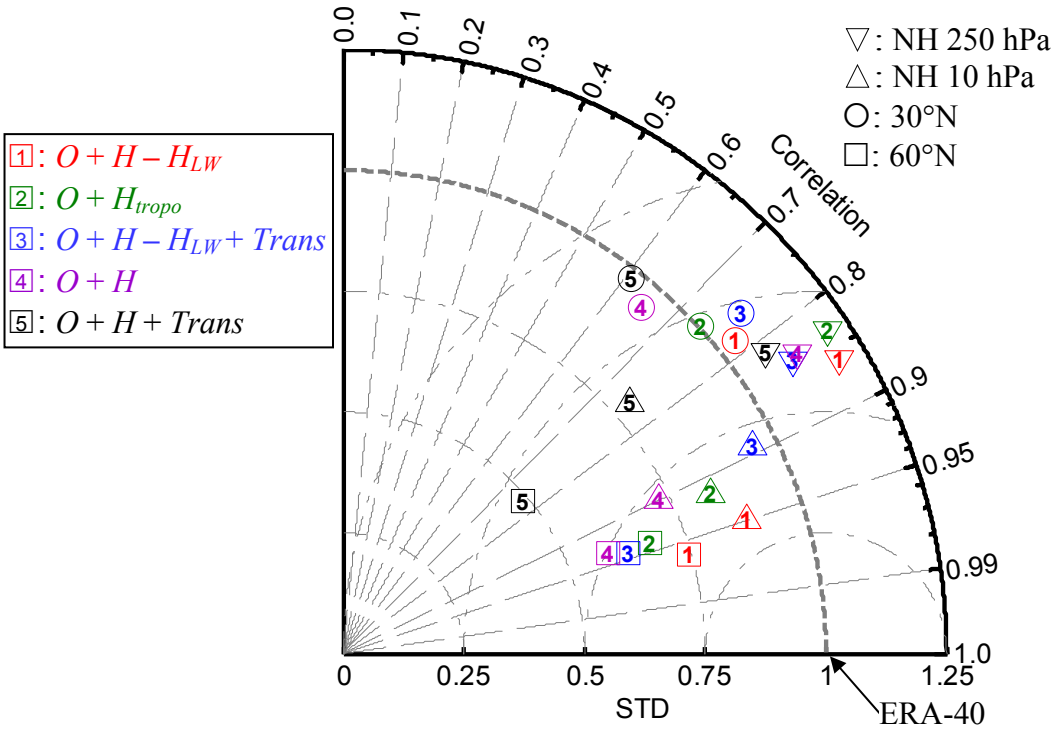

Figure 3.5: Taylor diagram of stationary wave solutions diagnosed by the stationary wave model compared with the ERA-40 NH winter (January 1979–2002) stationary wave climatological mean showing the individual contribution of different combinations of forcings in the ERA-40: 1 $O + H - H_{LW}$ (i.e., topography plus diabatic heating without longwave radiative diabatic heating), 2 $O + H_{tropo}$ (topography plus tropospheric diabatic heating), 3 $O + H - H_{LW} + Trans$ (as in 1 plus the transient wave flux convergences), 4 $O + H$, 5 $O + H + Trans$.

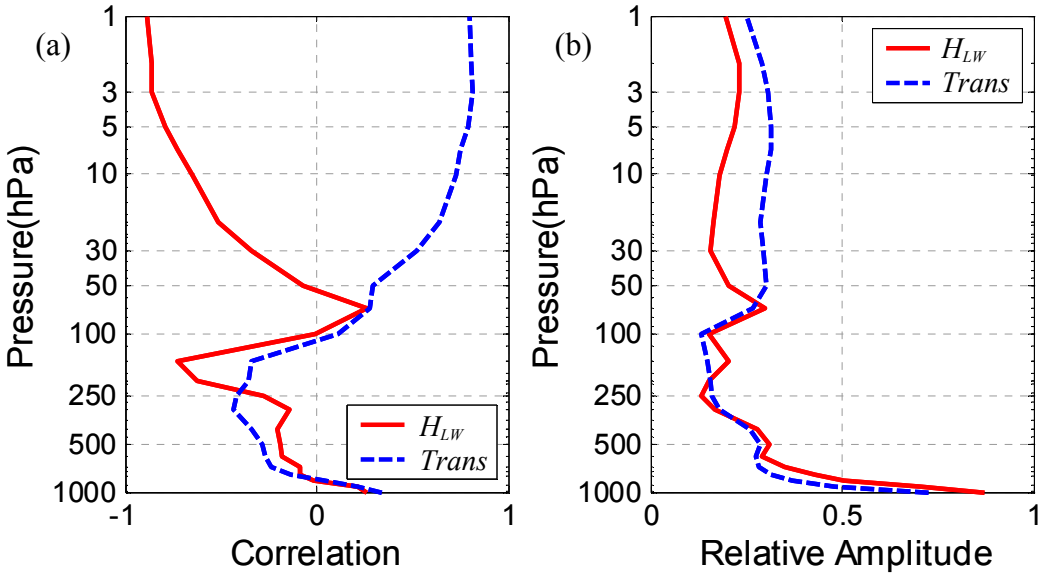

Figure 3.6: Vertical profiles of (a) correlation and (b) relative amplitude examining effects of longwave radiative diabatic heating (H_{LW}) and transient wave flux convergences (*Trans*) in maintaining the NH winter (January 1979–2002) stationary wave field in the ERA-40.

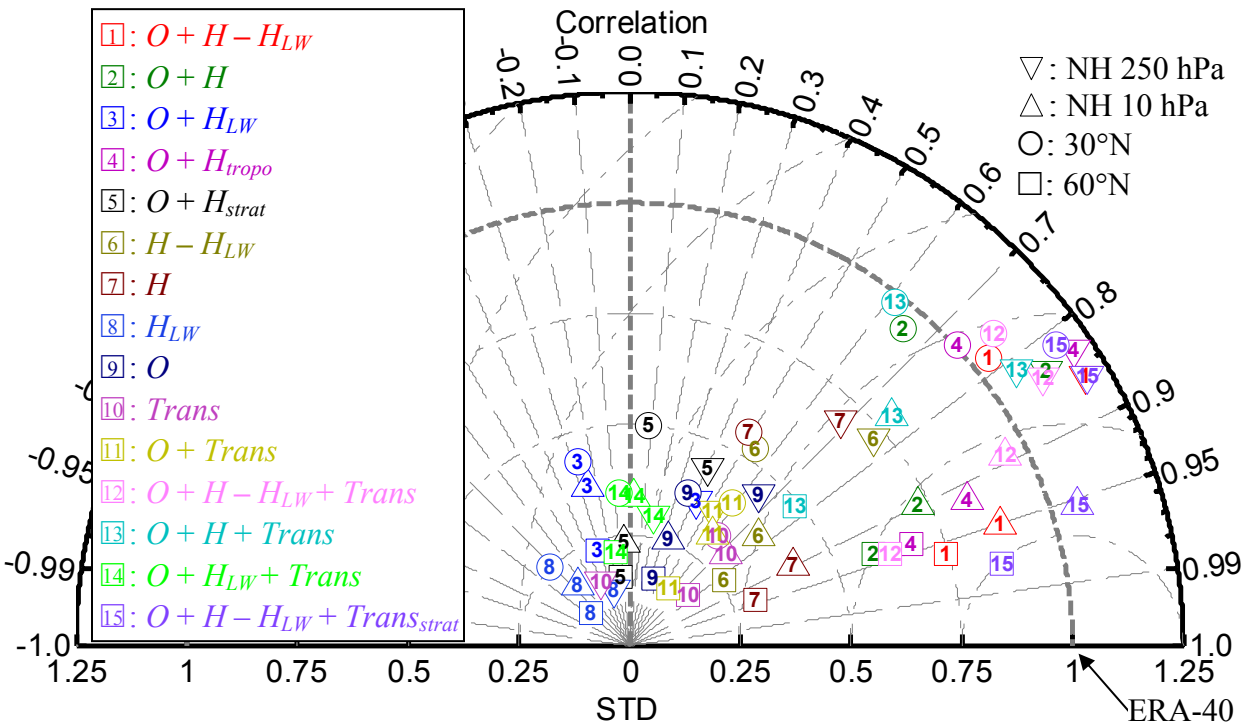

Figure 3.7: Similar to Figure 3.5 but for all the combinations of forcings listed in Table 3.3. Symbols "1" and "15" in ▽ overlap almost completely.

Chapter 4

4 Diagnosing the Stratosphere-Troposphere Stationary Wave Response to Climate Change in a General Circulation Model

4.1 Introduction

After successful development and testing of the stratosphere-troposphere nonlinear stationary wave model (see Chapter 3), in the present chapter this diagnostic tool is applied to study the stationary wave response to climate change simulated by CMAM. This stationary wave model provides partial prognostic information and dynamical insight into the future stationary wave field given knowledge of the future zonal mean state and future zonally asymmetric forcings. The main goal of this chapter is to examine the dynamics of the stationary wave response to climate change.

First, Section 4.2 describes the CMAM and the data used for this study. Section 4.3 presents analysis of the CMAM stationary wave response to climate change and Section 4.4 illustrates the ability of the stationary wave model to capture this response. Section 4.5 presents a diagnosis of the relative importance of changes in the zonal mean basic state and in the zonally asymmetric forcings, and identification of the specific features in the zonal mean flow change that are most responsible for the stationary wave response. Finally, Section 4.6 comprises an analysis of the wave driving (EP-fluxes) associated with the various stationary wave response discussed in Section 4.5. The main findings are summarized in Section 4.7.

4.2 Applying the stationary wave model to the CMAM simulation

The zonal mean basic state and diabatic heating from a CMAM simulation forced by GHG and ODS emissions following the CCMVal REF-2 scenario for the Stratospheric Processes And their Role in Climate project (SPARC) (Erying et al. 2007) are used as input to the stationary wave model. The REF-2 scenario integrates the IPCC 2000 A1b (medium) scenario for GHG, the WMO 2003 Ab scenario for ODS, prescribed SST from a parent model, and fixed solar activity at the mean of a solar cycle. The CMAM is based on the Canadian Centre for Climate Modelling and Analysis (CCCma) general circulation model (Beagley et al. 1997) and its extension to include the middle atmosphere as described in Scinocca et al. (2008). The CMAM REF-2 dynamical and chemistry simulation has been favourably compared with observations relative to the ensemble of CCMs. The CMAM exhibits some common problems in CCMs such as a relatively small decrease in Arctic ozone in the 1980–2000 period, a cold bias in Antarctic late winter / spring, and an associated delayed breakdown of the Antarctic polar vortex (Erying et al. 2007; Shepherd 2008). Furthermore, this version of CMAM does not represent the quasi-biennial oscillation (QBO). But the strength and the locations of the zonal mean tropospheric and stratospheric jets, which are essential for stationary wave propagation (McLandress and Shepherd 2009), are generally realistic (see e.g., Figure 4.5a).

The prescribed zonal mean basic states, including horizontal velocities, temperature, and surface pressure, are interpolated from the original resolution (T32L71 spanning up to 0.0007 hPa) onto the stationary wave model grid (T42L42 with model lid at 0.4 hPa; see Section 3.2). The diabatic heating is available from only one ensemble member out of three, and thus the basic states are also from the same member. The diabatic heating is applied only in the troposphere (see Section 3.4). The time mean transient wave flux convergences are not included in the

diagnoses here because they are also not available and might degrade the stationary wave solutions according to Figure 3.5 and Figure 3.6 (see also Sections 3.3 and 3.4).

The CMAM simulation spans from 1950 to 2099 and the first ten years are discarded as spin-up. Then the time average of the first and last twenty years, 1960–1979 and 2080–2099, are chosen as the "past" and the "future" climate, respectively. The difference between them, i.e., "future" minus "past", is defined as the "response". The response is dominated by radiative forcing from GHG increases because ODS concentrations are similar for both the past and future periods.

The observed NH stationary wave has a strong seasonal cycle with peak wave amplitudes in winter, as introduced in Chapter 1; therefore this study focuses on the wintertime stationary wave. Figure 4.1 plots the long term (20 year) mean of the monthly stationary wave streamfunction on the 10 hPa pressure level for December, January, and February in the past and future and the response. The monthly climatological mean stationary wave fields in CMAM for both the past and future are similar in these three months, but the stratospheric stationary wave response in December is mostly not statistically significant and is quite different from the January-February response. Therefore the long term mean of January and February is chosen as the focus period for the study in this chapter.

4.3 Stationary Wave Response in the CMAM CCM

The past and future stationary wave field in boreal winter (January and February) and the response as simulated by CMAM are shown in Figure 4.2. The NH stationary wave field is shown on representative tropospheric and stratospheric levels: the 250 hPa field is shown in Figure 4.2a–c and the 10 hPa field is shown in Figure 4.2d–f. Figure 4.2 also shows the vertical

structure of the stationary wave field with plots of pressure-longitude sections at 30°N (Figure 4.2g–i), which has a relatively large tropospheric response, and at 60°N (Figure 4.2j–l), which has a relatively large stratospheric response. The left column shows the past period, the middle column shows the future period, and the right column shows the response. The stationary wave responses are generally statistically significant (grey shading in Figure 4.2c, f, i, and l). These fields will be reproduced using the stationary wave model and compared in Section 4.4.

The upper tropospheric stationary wave in CMAM is quite similar to the observations (the ERA-40 and NCEP reanalyses) in both spatial correlation and amplitude (not shown). The 250 hPa NH stationary wave response (Figure 4.2c) consists of a highly structured wave train, characterized approximately by wavenumber 5, and centred in the subtropics. Despite its detailed structure, this basic pattern is found in other settings. It is similar to the stationary wave response in the related CCCma CGCM used in the CMIP3 assessment (see the first panel of Figure 1.5 from this thesis, Figure 3 of Brandefelt and Körnich (2008)). In addition, this pattern has most of the features of group *S*, which characterizes 7 out of 16 IPCC models grouped by the similarity of their response to GHG forcing, in the first panel of Figure 5 of Brandefelt and Körnich (2008). Thus the upper-tropospheric pattern in Figure 4.2c is a robust response to GHG forcing common to many climate models. The structure of the pattern corresponds generally to an eastward shift of several features of the stationary wave field. For example, the negative response over the United States and the positive response over the East Pacific in Figure 4.2c is a result of the eastward shift of the negative centre over the Eastern Pacific, and similarly for the negative response over East Asia and the positive response over the Western Pacific. Many similar dipolar responses belong to this type of shift, and therefore the shift of the past stationary wave field. A zonal Fourier decomposition on the stationary wave shows that the tropospheric stationary wave

averaged over 20–40°N in the past and future primarily comprises wave-1, wave-2, and wave-3 components (36%, 24%, and 16% respectively in the past; 39%, 26%, 10% respectively in the future) and appear as wave-2 dominated structures, while the response has more small scale structures with a relatively strong wave-5 component (20%, 12%, 19%, 14%, 23%, 9% for the first six wavenumber components respectively).

The NH wintertime stratospheric stationary wave is dominated by a wave-1 dipolar structure (Figure 4.2d) and its response to climate change (Figure 4.2e–f) is primarily an enhancement of this dipole plus a shift of roughly 15–20° longitude to the east. The stationary wave averaged over 50–80°N on 10 hPa is dominated by the wave-1 component in the past (71%), the future (79%) and the response (83%). The positive center over Eastern Siberia moves eastward to the Bering Strait; the negative center over Eastern Canada moves eastward to Northern Europe; both centers strengthen in the future, particularly the negative center. The fine structure in the troposphere and the dipolar structure in the stratosphere of the stationary wave response suggests, by Charney-Drazin (1961) theory, that the low-latitude tropospheric wave response will not propagate directly into the stratosphere.

The vertical structure of the stationary wave field in NH extratropics is mainly barotropic in the troposphere and baroclinic in the stratosphere (Figure 4.2 g–h, j–k); the vertical structure of the response is similar, but is characterized by smaller spatial scales (Figure 4.2i, l). The tropospheric stationary wave and its response have larger amplitudes in subtropics than in high-latitudes. The response pattern generally involves an eastward shift of the past stationary wave pattern.

4.4 Stationary wave model diagnoses

The stationary wave field in the past and the future are diagnosed using the stationary wave model with prescribed zonal mean basic state, topography, and zonally asymmetric diabatic heating. The zonally asymmetric transient wave flux convergences are neglected as discussed in Section 3.3. Figure 4.3 shows the Taylor diagram comparing the stationary wave field from the stationary wave model with the CMAM stationary waves on the 250 hPa and 10 hPa pressure levels and in the pressure-longitude cross-sections at 30°N and 60°N for the past, the future, and the response. All these components of the CMAM stationary wave are generally well reproduced in terms of spatial pattern correlation with modest overestimates of the stationary wave amplitude. The response is generally more difficult to reproduce because it consists of small differences between pairs of fields with relatively large amplitude, and because it has a relatively small scale structure compared to those of the past and future stationary waves. The focus will be on which gross features can be captured by the stationary wave model and how these features can be explained dynamically.

Figure 4.4 shows the stationary wave response in CMAM (first column in Figure 4.4, which repeats the last column in Figure 4.2) and in the stationary wave model (second column in Figure 4.4, the notation "*FF – PP*" will be explained in Section 4.5). Although Figure 4.3 shows that the lowest pattern correlation between the stationary wave model and the CMAM response occurs in the case of the 250 hPa pressure level response, the basic features of the wave trains in Figure 4.4a are captured by the stationary wave model in Figure 4.4b, albeit with a weak overall amplitude. The degradation of the spatial correlation is more a result of the mismatch in the amplitude of individual positive and negative centers. For example, the positive center over the

Middle East is weaker than the negative center over East Asia in CMAM while the opposite is found in the stationary wave model response.

The dipolar structure of the stratospheric response in CMAM is captured in the stationary wave model response (Figure 4.4e–f). The location and strength of the positive center over North America is quite close to the counterpart in CMAM, while the negative region is more split and too intense over Siberia. This discrepancy arises from the fact that the wave-2 component decreases slightly in the CMAM stationary wave response but increases in the stationary wave model response.

The vertical structure of the stationary wave response to climate change in CMAM is generally reproduced in the stationary wave model, especially in the stratosphere (Figure 4.4 i–j, m–n). The tropospheric stationary wave model response is not as finely structured as the CMAM response and again the relative strength of individual centers is not quite consistent with their CMAM counterparts, but the positive and negative centers are located at the correct longitudes.

4.5 Analysis of the stationary wave response using the stationary wave model

Having shown that the stationary wave model can capture the basic features of the stationary wave field in observations and in the CMAM simulation, it is now used to better understand the dynamics of the stationary wave response to climate change. In particular, given the available archived output, this section focuses on the impact of changes to the zonal mean basic state (denoted ΔZM) and the zonally asymmetric diabatic heating in the troposphere (denoted ΔH). Table 4.1 lists the stationary wave model experiments designed to investigate the importance of ΔH, ΔZM, and different aspects of ΔZM. In all experiments the topography with

the model grid resolution (T42) is used. In the notation of the table, *P* indicates past, *F* indicates future, and each run is identified by a two-part tag with the first part representing the zonal mean basic state and second part representing the diabatic heating forcing. The past and future stationary wave field in the stationary wave models referred to in Section 4.3 are from *PP* and *FF*, respectively. The total stationary wave response to climate change is thus given by *FF* – *PP*, which is decomposed into the response to ΔZM, *FP* – *PP*, and the response to ΔH, *FF* – *FP*.

As discussed in Section 4.3, most of the major features in the total stationary wave response to climate change in CMAM (the first column in Figure 4.4) are captured by the stationary wave model response *FF* – *PP* (the second column in Figure 4.4). The role of ΔZM can be evaluated by comparing *FF* – *PP* to *FP* – *PP* (the third column in Figure 4.4). The first principal finding of this chapter is that the change in the zonal mean captures most of the upper tropospheric response (Figure 4.4b–c), the lower stratospheric response (Figure 4.4f–g), the 30°N response (Figure 4.4j–k), and the 60°N response (Figure 4.4n–o). Generally speaking, the response to the zonal mean change is somewhat weaker than the total, suggesting that the effects of ΔZM and ΔH reinforce each other, as will be confirmed below in Figure 4.6.

The dynamics is explored further by asking which part of the zonal mean change is most important in shaping the stationary wave response. This part of the study is motivated by the understanding that the zonal mean response can to some extent be broken down into components that are dynamically distinct. Figure 4.5a,e show the zonal mean wind and temperature from the past, and Figure 4.5b,f show the response of these fields, with shading for significance of the response. The temperature response (Figure 4.5f) includes well known features of direct radiative and thermodynamic climate response to greenhouse warming such as tropospheric warming and stratospheric cooling, amplification of the tropospheric warming in the tropical upper

troposphere and towards the poles in the lower troposphere. In the Arctic stratosphere, the cooling is relatively small and statistically insignificant. In the winds, there is a westerly response near the subtropical tropopause in both hemispheres. This response, which is common in many climate simulations, is expected from thermal wind balance, given the direct temperature response to the meridional gradient in radiative forcing. The zonal wind response in the NH polar stratosphere is easterly but statistically insignificant.

Since the subtropical zonal wind response is similar in the two hemispheres, one can reasonably assume that it is independent of stationary wave effects and primarily driven by the direct radiative response to climate change. The high latitude stratospheric zonal mean wind response is quite different and could be greatly influenced by the stationary wave response. Accordingly, after some trial and error experimentation, a stationary wave model experiment (F_aP) is carried out, in which the NH subtropical wind response (ΔZM_a) is imposed in isolation, to see what influence this has on the NH stationary wave pattern. The zonal wind anomaly used is shown in Figure 4.5c. To maintain a consistent thermal wind balance, a temperature field with zero global meridional mean is adopted to balance this zonal wind anomaly. This field is shown in Figure 4.5g; the meridional gradient of this field is proportional to the vertical gradient of the wind anomaly.

In addition to ΔZM_a two other basic state changes are also considered, one corresponding to the total zonal wind response minus the NH subtropical part (ΔZM_b; Figure 4.5d, h) and another corresponding to the residual in the temperature response (ΔZM_c; Figure 4.5i) that consists of zero zonal mean wind response and a mean temperature perturbation with very weak gradients that correspond to very small ageostrophic contributions. By construction, the zonal

wind anomalies in Figure 4.5c–d add up to the zonal wind response in Figure 4.5b, and the temperature anomalies in Figure 4.5g–i add up to Figure 4.5f.

Different basic states taking into account the three subsets of the zonal mean response are input into the stationary wave model, listed as F_aP, F_bP, and F_cP in Table 4.1. The second principal finding of this study is that ΔZM_a is responsible for most of the stationary wave response to climate change in the stratosphere and troposphere. This is evident by comparing the fourth column of Figure 4.4 ($F_aP - PP$) with the second and third columns. The response to the change in the NH subtropical jet brings out some interesting features. For example, this response is associated with an upper tropospheric wave train that appears to arc from the Northwest Pacific across the pole to the North Atlantic Sector in Figure 4.4d; and it appears to enhance the wave-2 component of the response in the stratosphere in Figure 4.4h.

The main results are thus summarized in Figure 4.4: the main features of the CMAM stationary wave response (first column) are captured in the stationary wave model (second column, $FF - PP$); the change in the stationary waves is dominated by the change in the zonal mean circulation (third column, $FP - PP$); and the dominant part of the response is associated with the subtropical jet (fourth column, $F_aP - PP$). Because this kind of subtropical jet response is typical of other models' response to greenhouse warming (e.g., Lorenz and DeWeaver 2007), it will be of interest to see which aspects of these results carry over to other models. The author speculates that the general eastward shift of the stationary wave features seen in the response is tied to the westerly wind response in the subtropics; it perhaps can be understood in terms of an increase in the eastward component of the stationary wave group velocity.

In the exploration of the stationary wave model that has been carried out, other effects are relatively minor but worth considering. The first column of Figure 4.6 ($F_bP - PP$) shows the effects of the zonal mean circulation response without the NH subtropical jet response, and the second column ($F_cP - PP$) shows the case with zero wind response and a thermal perturbation with correspondingly weak temperature gradients. In this case, ΔZM_b induces a stationary wave response that has weaker amplitude and is poorly correlated with the CMAM response in the stratosphere, while the response to ΔZM_c is even weaker and has much poorer spatial correlation. The responses to the individual zonal mean changes generally reinforce each other to some extent except for the stratospheric response to ΔZM_c. It is noted that the responses associated with these three components of the zonal mean change do not perfectly add up to the response associated with the total change in zonal mean flow, indicating modest nonlinearity in this decomposition.

Finally, in the third column of Figure 4.6 ($FF - FP$), the impact of changing the diabatic heating is investigated when the zonal mean is fixed at the future state. In this case, the zonal mean is kept fixed at its future value, so that there is a clean decomposition of the total, i.e., $FF - PP$ (Figure 4.4 second column) is equal to $FF - FP$ (Figure 4.6 third column) plus $FP - PP$ (Figure 4.4 third column). As expected the response in this case is weak but fairly well correlated with the troposphere-stratosphere response, thus suggesting that the heating and zonal mean response reinforce each other. The experiment $PF - PP$ has also been carried out, in which H is changed while the zonal mean is kept constant at its *past* value; this produces similar results.

Taylor diagrams are used to summarize the above findings in a quantitative manner. Figure 4.7 presents the relative contribution of the zonal mean flow change (ΔZM, white symbols in Figure 4.7) and the diabatic heating change (ΔH, black symbols in Figure 4.7) to the total

stationary wave response captured by the stationary wave model ($\Delta ZM + \Delta H$, "1" on the x-axis in Figure 4.7 as the target streamfunction field), which shows clearly that the dominance of ΔZM in the total response $\Delta ZM + \Delta H$. The Taylor diagram in Figure 4.8 presents the further decomposition of the response to ΔZM into three subsets (ΔZM_a, ΔZM_b, and ΔZM_c). The stationary wave response to ΔZM_a is found to explain most of the response to the total zonal mean change ΔZM.

4.6 Analysis of the EP-flux response using the stationary wave model

A challenging test of the stationary wave model is to use it to explain the response in wave driving in the stratosphere, since the wave activity flux depends on the details of the wave propagation and the vertical variation of the phase structure of the waves. The EP-flux of the CMAM past stationary wave shows significant upward propagation of wave activity into the high-latitude stratosphere from the subtropical troposphere (Figure 4.9a), and this feature is enhanced in the future as shown in the response of the EP-flux (Figure 4.9b; the future EP-flux minus the past EP-flux in CMAM, again for the climatological stationary wave). This enhanced wave driving is one of the key contributors to the Brewer Dobson circulation, which in this and many other models increases in response to GHG increases (e.g., Butchart et al. 2006; McLandress and Shepherd 2009; Butchart et al. 2010b). Therefore, the rest of this section will focus on the stratospheric EP-flux response. It is noted, however, that the dominant part of the response occurs in the region of easterly wind response, where the zonal mean wind response is not significant. Thus, while it is reasonable that this enhanced wave driving and EP-flux convergence is associated with the easterly wind response (as will be seen below), the response itself is not statistically robust.

The stationary wave model EP-flux response (Figure 4.9c; *FF* – *PP*) is surprisingly poor considering the ability of the stationary wave model to capture various aspects of the streamfunction response. This EP-flux response has an amplitude that is too large (an overestimation of 310% in the stratospheric EP-flux convergence) due to the overestimated amplitude in the responses of both stationary waves ($\overline{\psi}^*$; an overestimation in NH of 40% on average and up to 109%) and temperature zonal anomalies ($\overline{T}^*$; an overestimation in NH of 59% on average and up to 178%) in the stationary wave model, as EP-flux depends on both $\overline{\psi}^*$ and $\overline{T}^*$. In some ways, the EP-flux response pattern is qualitatively consistent with the CMAM pattern but has an area of EP-flux divergence in the polar stratosphere, inconsistent with the CMAM response (Figure 4.9b).

In tuning the stationary wave model, the author's original strategy was to focus on how the model captures the phase structure of the streamfunction in the troposphere and stratosphere. This is an extension of the classical tuning approach for tropospheric stationary wave modeling to the stratosphere. The motivation appeared reasonable for stratospheric analysis, because the stationary wave field is related to basic salient features of the zonally asymmetric stratospheric circulation. For example, the wave-1 component of the stationary wave is related to the displacement off the pole of the climatological polar vortex, and hence the westward extension of the Aleutian Low at the surface, and the wave-2 component is related to the elongation of the polar vortex; the interannual variability in these features is related to the isolation and robustness of the polar vortex in the presence of transient wave activity fluxes from the troposphere. However, it is seen here that the stationary wave model developed using this strategy is not able to capture one of the most critical aspects of the stratospheric response to climate change, namely the enhanced wave driving and dissipation in the stratosphere. Thus, it becomes apparent that a

flexible approach to tuning the stationary wave model is required if the model is to be a useful applied tool.

To resolve the difficulties the stationary wave model has in capturing the EP-flux response, a new set of simulations have been performed with a different set of damping profiles (see Table 3.2). In the new damping settings (denoted as "CMAM EP-flux" in Table 3.2) only two parameters are different from the CMAM stationary wave settings used above which were designed to optimize the stationary wave streamfunction solution (denoted "CMAM streamfunction" in Table 3.2). First, the Newtonian cooling timescale at the surface (τ_s in Table 3.1) is reduced from 4 days to 1 day, in recognition of the fact that the CMAM diabatic heating forcing near the surface is much stronger than the ERA-40 diabatic heating. The Newtonian cooling timescale in the stratosphere (τ_{strat} in Table 3.1) is reduced from 40 days to 15 days in order to obtain a realistic amplitude of the zonally asymmetric temperature field in the stratosphere. Figure 4.10a shows the impacts on the stationary wave response to climate change by using the "CMAM EP-flux" damping settings in the stationary wave model. These new damping settings reduce significantly the amplitude of the stationary wave solution and have a relatively minor impact on the pattern correlations between the stationary waves diagnosed by the stationary wave model and the CMAM stationary waves (white symbols in Figure 4.10a). The amplitude of the new stationary wave response is very close to the CMAM response (a negligible 1% underestimation on average of the response in $\overline{\psi}^*$ in NH), and the amplitude of the temperature response is more realistic as well (12% overestimation on average of the response in $\overline{T}^*$ in NH).

The dynamics of the stationary wave response to climate change is examined here with the "CMAM EP-flux" damping settings. The zonal mean flow change remains dominant in the

relative importance of the changes to the zonal mean flow and the zonally asymmetric diabatic heating (Figure 4.10b). ΔZM_a is still the major factor explaining the stationary wave response to ΔZM and the effects of ΔZM_c are negligible, while the stationary wave response to ΔZM_b becomes comparable to the effects of ΔZM_a, especially in the troposphere with even larger amplitude than that of ΔZM_a (Figure 4.10c). Figure 4.10d will be discussed later in this section.

The EP-flux response to climate change is diagnosed and decomposed using the stationary wave model with the "CMAM EP-flux" damping settings, similarly to the decomposition of the stationary wave response. Figure 4.11a shows the CMAM EP-flux response to climate change, plotted similarly to Figure 4.9b but with a halved contour interval for the EP-flux divergence. The stationary wave model response $FF - PP$ (or $\Delta ZM + \Delta H$) still overestimates the stratospheric EP-flux response (Figure 4.11b) but its amplitude has been reduced significantly: it was overestimated by 310% in Figure 4.9c but by only 55% in Figure 4.11b (note that the different contour intervals are used in Figure 4.9 and Figure 4.11). Importantly, the pattern of the EP-flux divergence response is more consistent with the CMAM EP-flux response in the stratosphere than the EP-flux response using the "CMAM streamfunction" damping settings (Figure 4.9c). The stratospheric EP-flux response to ΔZM, i.e., $FP - PP$, is reduced in amplitude (note that the EP-flux is a quadratic quantity and its amplitude is roughly proportional to the squared stationary wave amplitude) but has similar pattern, as shown in Figure 4.11c, to the total stationary wave model response in Figure 4.11b and to the CMAM EP-flux response in Figure 4.11a. On the other hand, the stratospheric EP-flux response to ΔH (Figure 4.11d) is only slightly weaker than the response to ΔZM and its pattern is also fairly consistent with the CMAM response (Figure 4.11a). The contributions of ΔZM and ΔH to the total stationary wave EP-flux response ($\Delta ZM + \Delta H$) in the stratosphere are 64% and 42%,

respectively, which are qualitatively consistent with their relative contributions to the total stationary wave response. Thus, in the retuned model, diabatic heating, which is present only in the troposphere, plays a proportionally large role in the wave and wave driving response to climate change.

The EP-flux response to the zonal mean flow change (ΔZM) is decomposed here, similarly to the decomposition of stationary wave response to ΔZM in Section 4.5. Although it has been found that the subtropical jet contribution to the stationary wave field streamfunction response is important, somewhat surprisingly the response of the stratospheric EP-flux to the change in the subtropical jet (ΔZM_a, Figure 4.11e) in the stationary wave model does not capture the main features seen in Figure 4.11d. Instead, these features are more fully captured in the complementary simulation, in which the zonal mean basic state includes the easterly high latitude response but not the westerly subtropical response (ΔZM_b, Figure 4.11f). The suggestion is that the EP-flux convergence feature in around 60°N above 30 hPa is tied strongly to the easterly wind response in that region. Finally, ΔZM_c has a minor contribution to the EP-flux response in the stratosphere (Figure 4.11f). The relative EP-flux contributions of ΔZM_a, ΔZM_b, and ΔZM_c to ΔZM are 38%, 91%, and 19% in the stratosphere, respectively, indicating moderate nonlinearity in this decomposition as the sum of these percentages is about 150% (119% if the cancellation between their EP-flux responses is taken into account).

Another decomposition on the zonal mean response is implemented to explore the contribution of the high latitude easterly response to the EP-flux response. As shown in Figure 4.12, the polar zonal mean zonal wind response and its corresponding temperature response is isolated as ΔZM_d, which is largely driven by enhanced upward propagating stationary wave

activity into the polar stratosphere. The complementary zonal mean zonal wind response and its corresponding temperature response is denoted as ΔZM_e, which satisfies the additivity $\Delta ZM = \Delta ZM_d + \Delta ZM_e + \Delta ZM_c$. The relative contributions of these three subsets to the stationary wave response to ΔZM can be seen in Figure 4.10d. As can be inferred from the effects of $\Delta ZM_{a/b/c}$, ΔZM_d has a minor contribution to the stationary wave response (white symbols in Figure 4.10d); however, this polar easterly response contributes significantly to the stratospheric EP-flux response (Figure 4.11h, 71% of the stratospheric EP-flux response to ΔZM). On the other hand, ΔZM_e (grey symbols in Figure 4.10d) explains most of the stationary wave response to ΔZM, but has a smaller contribution (60%) to the stratospheric EP-flux response to ΔZM (Figure 4.11i), although ΔZM_e dominates the tropospheric EP-flux response, consistent with the expectation that the tropospheric zonal mean flow changes drive changes to the tropospheric stationary waves. There is still moderate nonlinearity in this decomposition; the sum of their percentages is 150% or 111% if the cancellation between their EP-flux responses is taken into account.

An especially striking point about Figure 4.11 is that all the changes to the zonal flow and the diabatic heating result in an essentially similar EP-flux response in the stratosphere: namely, an increase in upwelling wave activity and wave dissipation and driving in the stratosphere. Thus ΔZM_b, ΔZM_d, ΔZM_e, and ΔH all induce an EP-flux pattern similar to the CMAM stratospheric EP-flux response (Figure 4.11a). The stratospheric EP-flux responses to ΔZM_a and ΔZM_c have relatively small amplitudes but agree in sign with the responses to the above components. This indicates that the EP-flux contributions reinforce each other in all decompositions. This point will be further addressed in the discussion in Section 4.7.

4.7 Summary and discussion

A stratosphere-troposphere stationary wave model has been developed to diagnose the stationary wave response to climate change simulated by an interactive Chemistry Climate Model, the CMAM. This stationary wave model is able to capture most of the significant features of the stationary wave and its response to climate change, and can be used to quantify the relative contribution to the total stationary wave response from the changes in the zonal mean flow and the zonally asymmetric forcings. The stationary wave model has been tuned in two different ways to capture different aspects of stationary wave dynamics. The zonal mean flow change is found to be responsible for most of the total response, especially in the stratosphere. A further decomposition of the zonal mean flow change has revealed that the westerly response near the NH subtropical tropopause and its corresponding temperature change are the major factors controlling the stationary wave response. This finding holds most strongly for one of the two tunings that have been used.

The EP-flux analysis highlights unanticipated problems with the standard tuning approach developed in Chapter 3. The stationary wave model optimized for representing the stationary wave streamfunction does not well capture the EP-flux response to climate change. A new tuning is introduced that better captures the EP-flux response. In the retuned simulations, the importance of the zonal mean westerly response near the NH subtropical tropopause to the stationary wave response is reduced, although it is still an important factor. However, the zonal mean changes in the polar region (mostly in the stratosphere) and the diabatic heating change contribute significantly to the EP-flux response. It is noteworthy that for all the decompositions the climate change response involves an increase in the upward propagating EP-flux. The resolved wave (stationary and transient waves) driving contributes to most of the strengthening

of BDC in response to climate change (e.g., more than 60% in Butchart et al. 2006), and stationary wave driving dominants the extra-tropical resolved wave driving in NH winter (McLandress and Shepherd 2009). The contributions of these components to the stationary wave driving reinforce each other, indicating that positive feedbacks play a role in the interactions between the stationary wave responses to individual components. For example, the weakening of the polar jet allows more wave driving propagating into the polar stratosphere, which in return further weakens the polar jet. This mechanism is similar to that of the stratospheric sudden warming, which involves the breakdown of the wintertime polar vortex by wave forcing from the troposphere (e.g., Matsuno 1971).

The dominance of the zonal mean flow change in the stationary wave response to climate change is consistent with previous studies on tropospheric stationary waves (Joseph et al. 2004; Brandefelt and Körnich 2008), and the dominance is even more significant in the stratosphere. Although the model includes two sources of nonlinearity — the dependence on the basic state and the stationary wave nonlinearity — one can roughly quantify how much of the response is explained by the two principal effects investigated here. In particular, the zonal mean change accounts for about half the tropospheric streamfunction response and about 3/4 of the stratospheric response. On the other hand, the diabatic heating change only contributes less than 1/3 to both the tropospheric and the stratospheric streamfunction response. These conclusions are robust in both sets of damping settings. Those parts of the response that the stationary wave model is not able to capture could result from missing forcing terms, such as transient wave flux convergences, and the enhanced damping being introduced in the stationary wave model.

It has proven difficult to improve the dynamical understanding of the enhancement of high latitude stratospheric planetary wave forcing by the stratospheric basic state changes,

beyond what has been deduced by decomposing the response from the nonlinear stationary wave model. For example, the role of nonlinearity is strong in this problem, as shown by a general degradation of the solution when stationary wave nonlinearity is neglected (not shown). The behaviour of the classical planetary wave refractive index has also been examined, and leads to inconclusive results (also not shown). Nevertheless, future dynamical research should explore further the robust enhancement of the stationary wave forcing in response to climate change in this relatively simple case, in order to better understand the enhanced Brewer Dobson Circulation response to climate change seen in almost all CCMs (Butchart et al. 2010a, 2010b).

The zonal mean zonal wind response in CMAM has a barotropic component similar to that of group *S* in Brandefelt and Körnich (2008), which is characterized by a strengthened tropospheric jet, which might explain why the results in this study are consistent with their findings on that group. How the general eastward shift of the stationary wave field is linked to this westerly response is a subject of future research. In light of the recent CCM-based intercomparison and assessment activities, the author intends to test the findings from this study using data from these simulations. (An ongoing pragmatic challenge is that to test the stationary wave model properly the diabatic heating and transient wave flux fields need to be archived, and these are frequently unavailable.) In particular, the author wishes to test the idea that since the acceleration of the zonal mean zonal wind near the subtropical tropopause of both hemispheres is a robust feature of the response to climate change seen in many simulations, which results from radiative warming in the tropical upper troposphere and radiative cooling in the polar stratosphere, it is, in principal, separable from the stationary wave response to climate change and its effects on the stationary wave response could be examined in different CCMs.

The diabatic heating used in this study is not diagnosed through the residual method as in previous studies (e.g., Held et al. 2002; Chang 2009), partly because the transient wave flux convergences are not available in this CMAM simulation, and also because the author would like to extend this study to more simulations with similar limitation on data availability. The residually diagnosed diabatic heating is largely entangled with the thermal transient wave flux convergences because of the nature of the residual method, and therefore forcing the stationary wave model with this diabatic heating absent the thermal transient wave flux convergences often degrades the solution significantly (Ting et al. 2001; Held et al. 2002). On the other hand, the diabatic heating from ERA-40, CMAM or other GCMs typically has relatively large amplitude, and it has been found that a strong Rayleigh friction with a relatively weak Newtonian cooling is able to best combine with this kind of diabatic heating in the absence of transient wave flux convergences. Nevertheless, the diabatic heating amplitude is often model-dependent and tuning of Newtonian cooling is thus required, especially to better capture wave driving. Enhanced Rayleigh friction is used compared to previous practice; this enhanced damping might act to partially parameterize the dissipative effects of tropical transient waves on the stationary wave field, similar to Ting and Held (1990) and Joseph et al. (2004). The approach in this thesis is believed to make diagnosing the stationary wave response to climate change feasible with limited data availability, although an approach that better combines with diabatic heating and transient wave flux forcing is ultimately desirable.

Table 4.1: Climate change experiments

Runs	Zonal Mean	Diabatic Heating
PP	Past	Past
PF	Past	Future
FP	Future	Past
FF	Future	Future
F_aP	Past + ΔZM_a	Past
F_bP	Past + ΔZM_b	Past
F_cP	Past + ΔZM_c	Past
F_dP	Past + ΔZM_d	Past
F_eP	Past + ΔZM_e	Past

The notation ΔZM_a, ΔZM_b, etc. is defined in Sections 4.5 and 4.6.

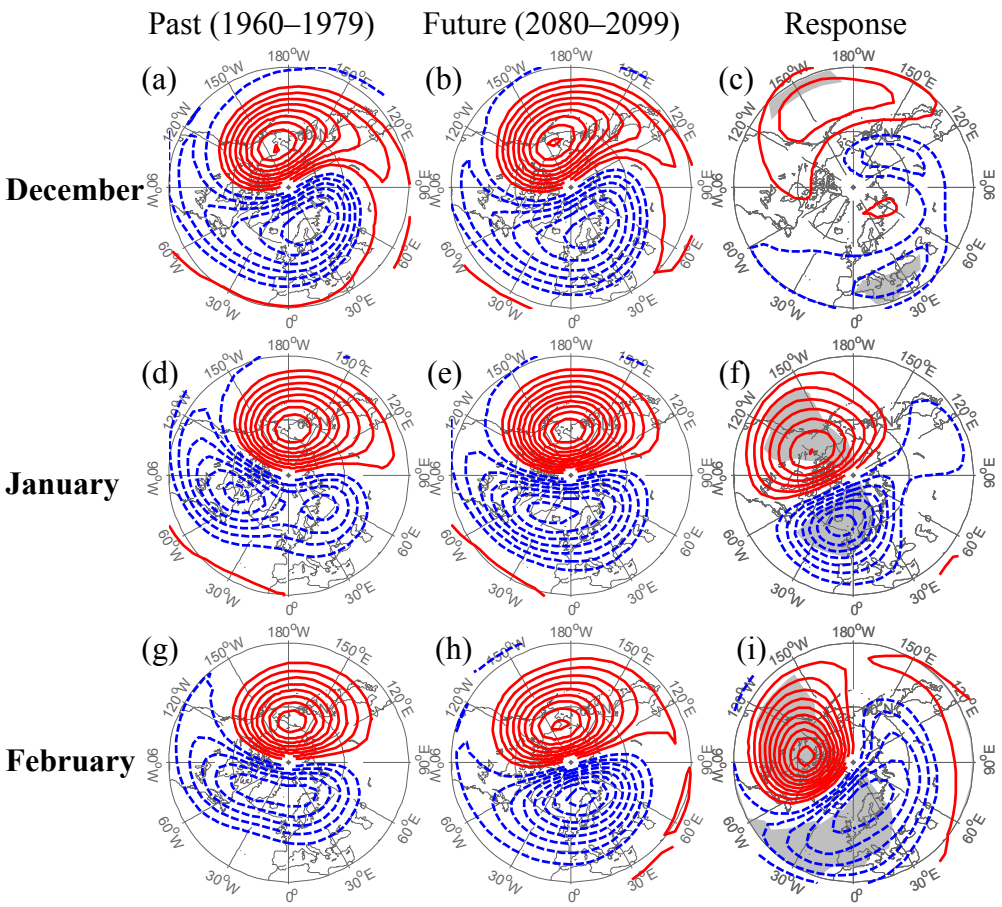

Figure 4.1: NH stationary wave streamfunction simulated by CMAM in the past (1960–1979; left column) and the future (2080–2099; middle column), along with the response (right column) on the 10 hPa pressure level for December (the first row, a–c), January (the second row, d–f), and February (the third row, g–i). Only north of 30°N is shown as the stationary wave amplitude in streamfunction is negligible equatorward of 30°N at 10 hPa. The streamfunction contour is 6×10^6 m^2s^{-1} for the past and the future, and 3×10^6 m^2s^{-1} for the response (hereafter for all streamfunction plots); positive values are plotted in solid / red and negative in dashed / blue (hereafter for all contour plots). The statistical significance of the response is indicated by gray shading at the 5% level by the Student's *t*-test, assuming independence of individual years of the detrended data (hereafter for all plots with statistical significance shading).

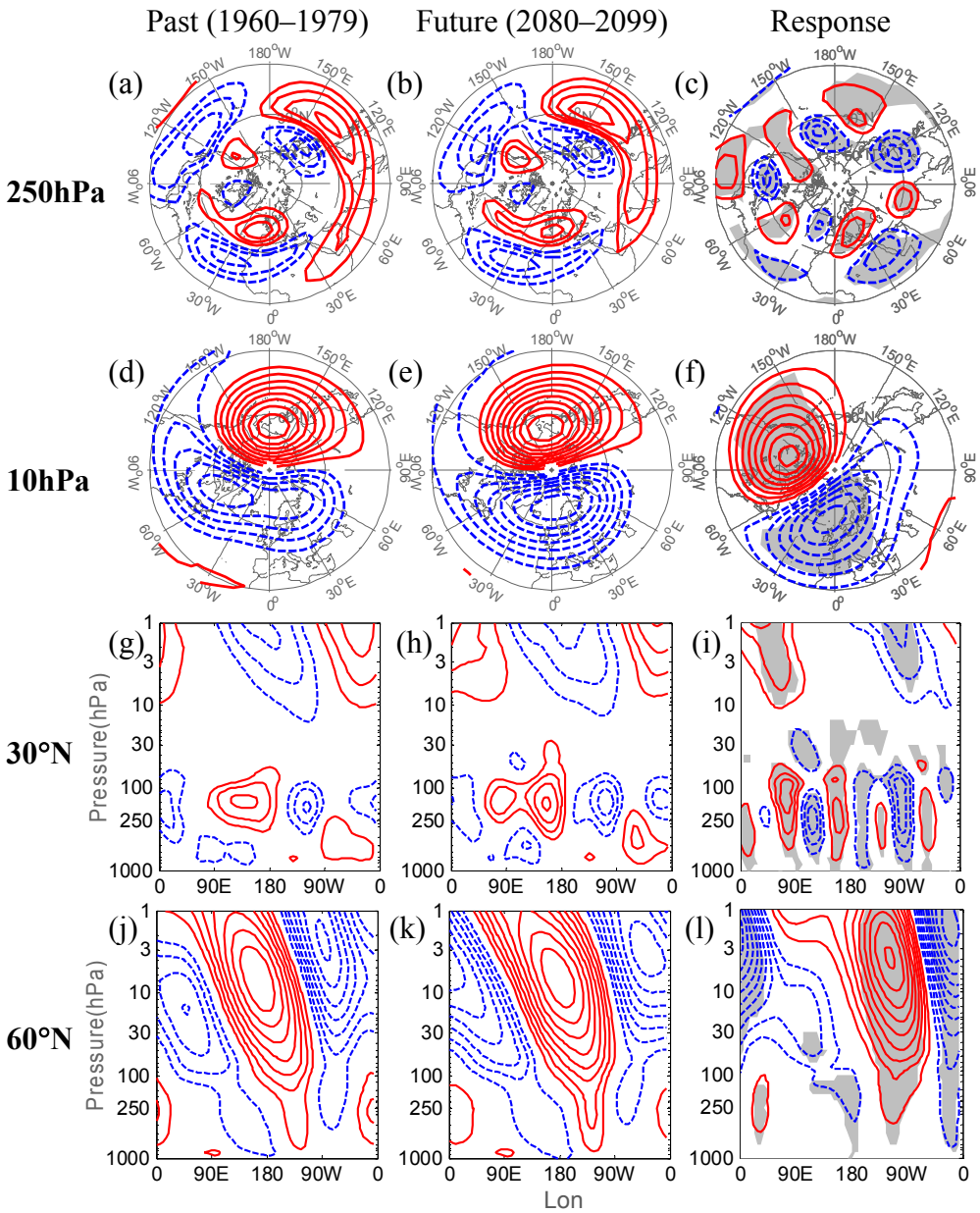

Figure 4.2: NH wintertime (January and February) climatological mean stationary wave streamfunction simulated by CMAM in the past (1960–1979; left column) and the future (2080–2099; middle column), along with the response (right column). The first row (a–c) shows the 250 hPa pressure level, the second row (d–f) shows the 10 hPa pressure level, the third row (g–i) shows the pressure-longitude section at 30°N and the fourth row (j–l) shows the pressure longitude section at 60°N. Note that the 250 hPa plots cover the entire NH, while the 10 hPa plots only show north of 30°N (hereafter for all stereographic plots).

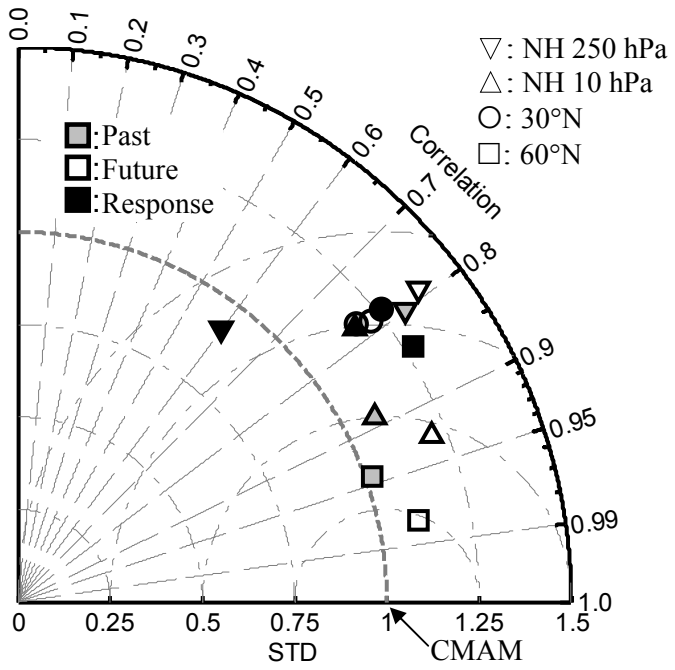

Figure 4.3: Taylor diagram of the past (grey symbols), the future (white symbols) and the response (black symbols) of NH winter stationary waves diagnosed by the stationary wave model compared with their CMAM counterparts (the target; Figure 4.2).

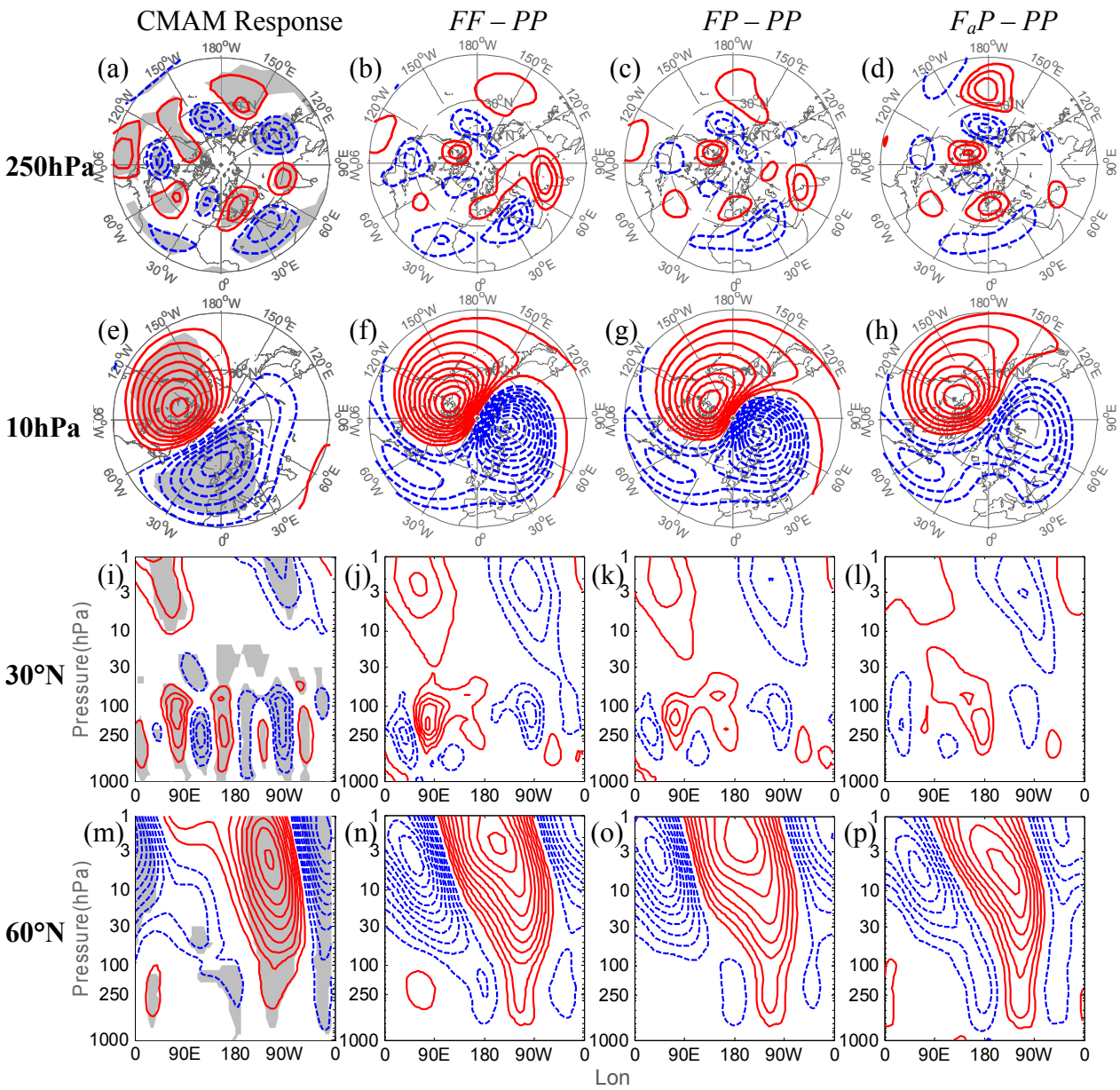

Figure 4.4: Similar to Figure 4.2 but for the NH winter stationary wave streamfunction response to climate change in CMAM (1st column, (a, e, i, m), copied from the right column of Figure 4.2 for ease of comparison), and the response diagnosed by the stationary wave model, to ΔZM and ΔH (2nd column, (b, f, j, n)), to ΔZM (3rd column, (c, g, k, o)), and to ΔZM_a (last column, (d, h, l, p), referring to Figure 4.5c, g).

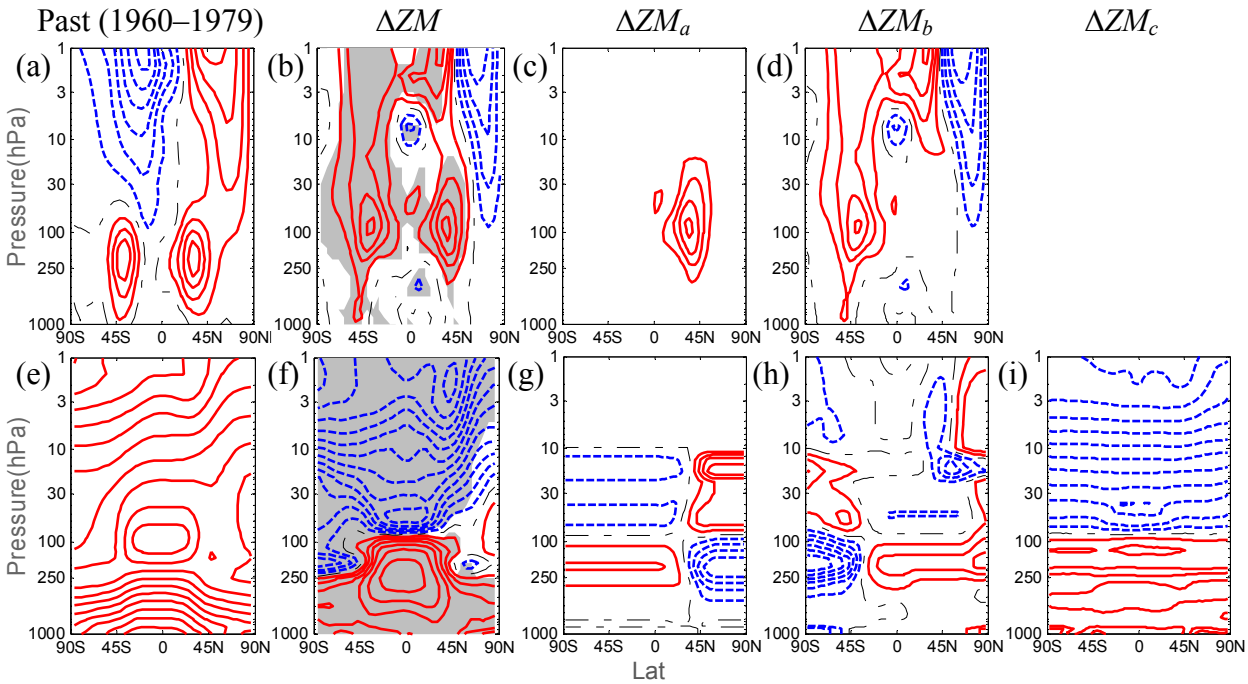

Figure 4.5: CMAM zonal mean zonal wind (upper row) and temperature (lower row) (a, e) in the past and their response to climate change, (b, f) ΔZM, plus three subsets of the response (c, g) ΔZM_a, (d, h) ΔZM_b, and (i) ΔZM_c, which satisfy $\Delta ZM = \Delta ZM_a + \Delta ZM_b + \Delta ZM_c$. Zonal wind contour intervals are 10 m s^{-1} for the past (a) and 2 m s^{-1} for the response (b–d); temperature contour intervals are 10 K for the past (e) and 1 K for the response (f–i).

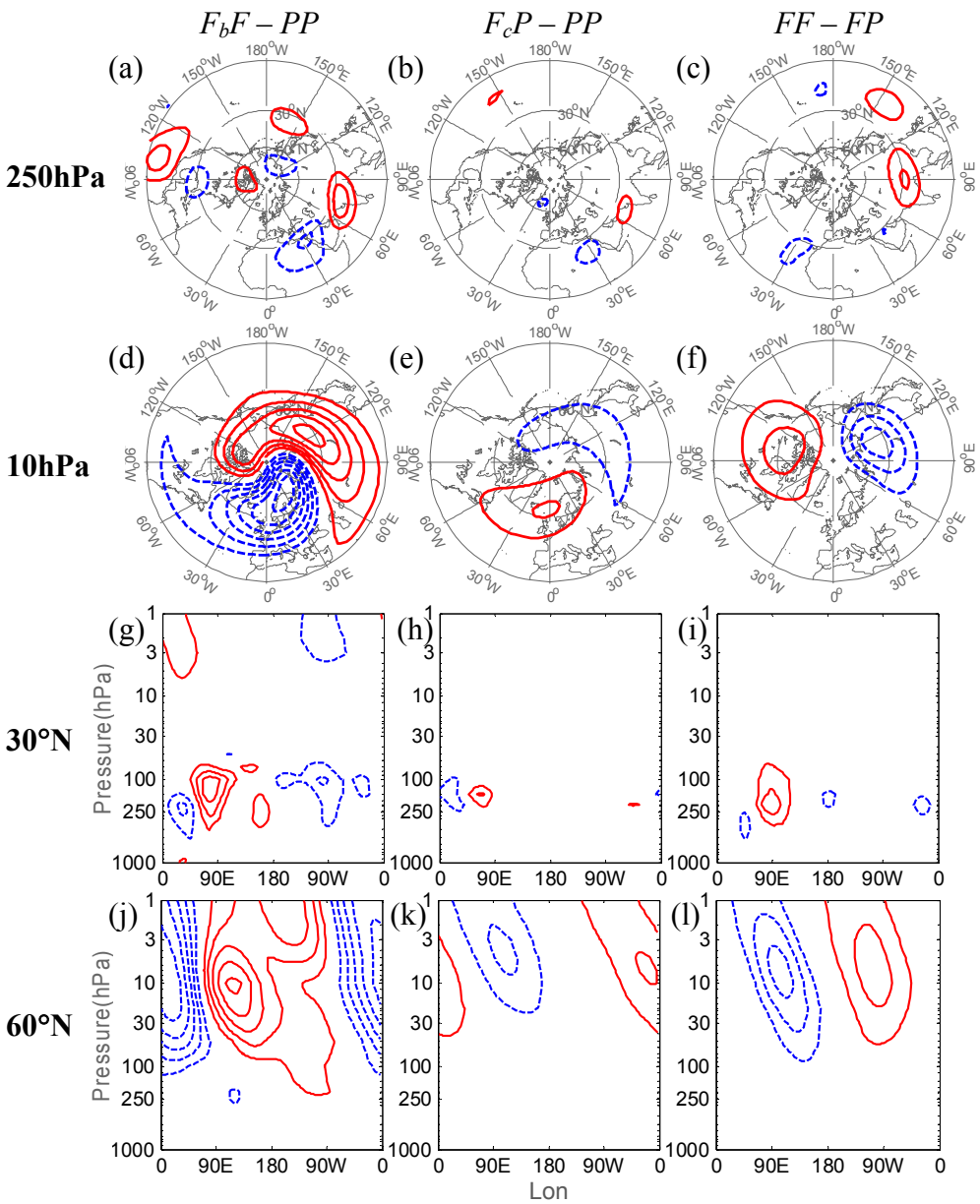

Figure 4.6: Similar to Figure 4.2 but for the response diagnosed by the stationary wave model, to ΔZM_b (left column, (a, d, g, j)), ΔZM_c (middle column, (b, e, h, k)), and ΔH (right column, (c, f, i, l)).

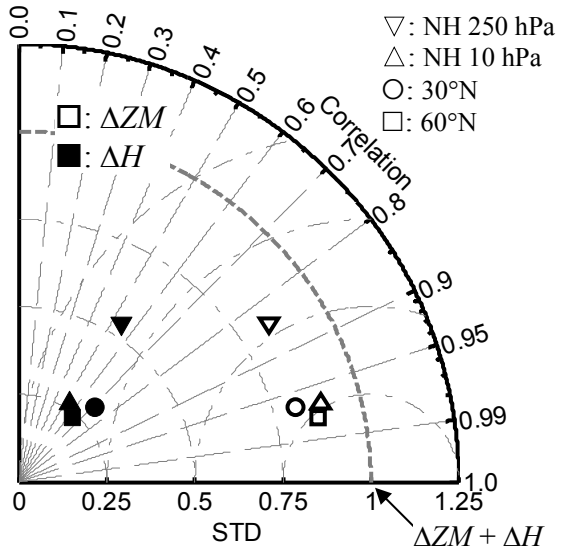

Figure 4.7: Taylor diagram of NH winter stationary wave response to the change in zonal mean basic state (ΔZM, white symbols) and the change in diabatic heating (ΔH, black symbols) compared with the total response to both changes ($\Delta ZM + \Delta H$, the target) diagnosed by the stationary wave model.

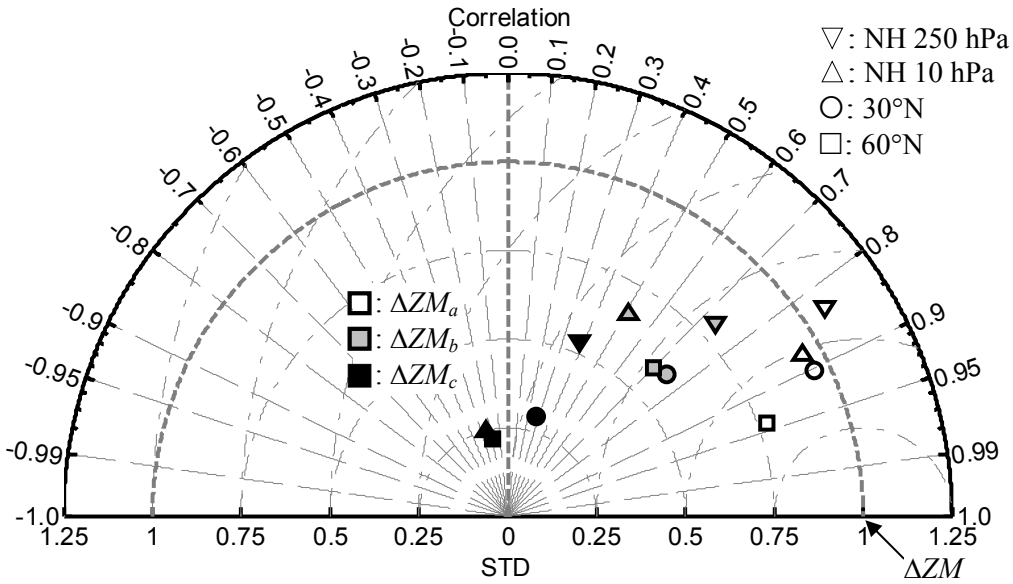

Figure 4.8: Taylor diagram of NH winter stationary wave response to three subsets of the change in the zonal mean basic state: ΔZM_a (white symbols), ΔZM_b (grey symbols), and ΔZM_c (black symbols) compared with the response to the total zonal mean changes (ΔZM, the target) diagnosed by the stationary wave model.

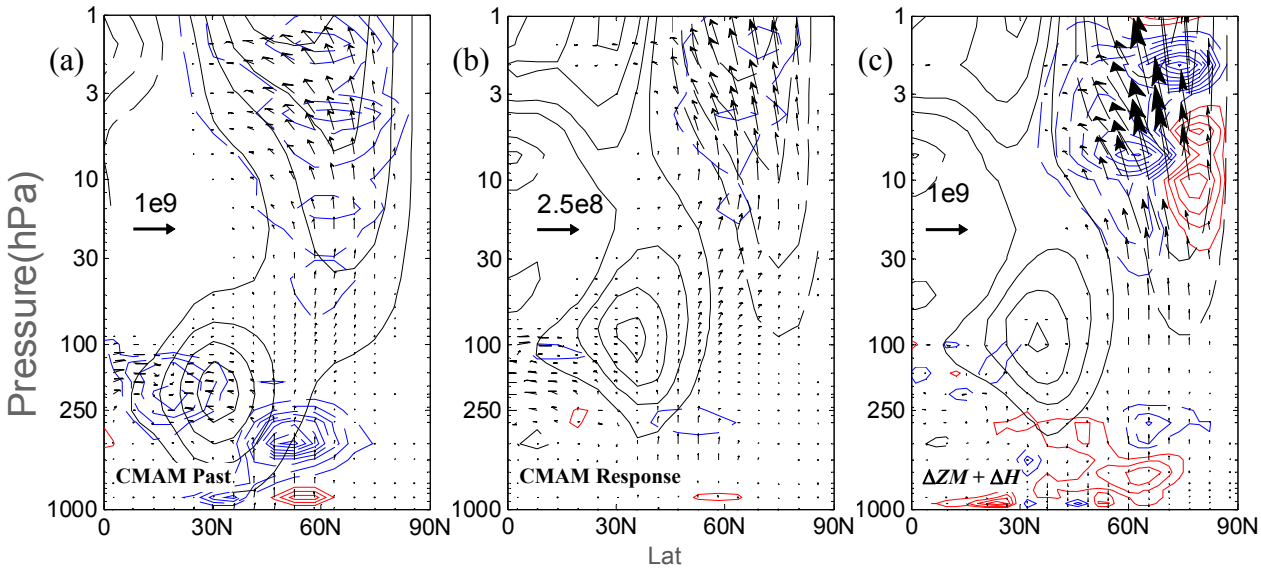

Figure 4.9: (a) The CMAM EP-flux (arrows) of the stationary waves in the past, (b) its response to climate change (Future – Past), and (c) the EP-flux response diagnosed by the stationary wave model (*FF* – *PP* or $\Delta ZM + \Delta H$). Zonal wind (black curves) contour intervals are 10 m s^{-1} for the past (a) and 2 m s^{-1} for the response (b–c); the contour interval of EP-flux divergence (blue and red curves) is 50 m^2s^{-2}.

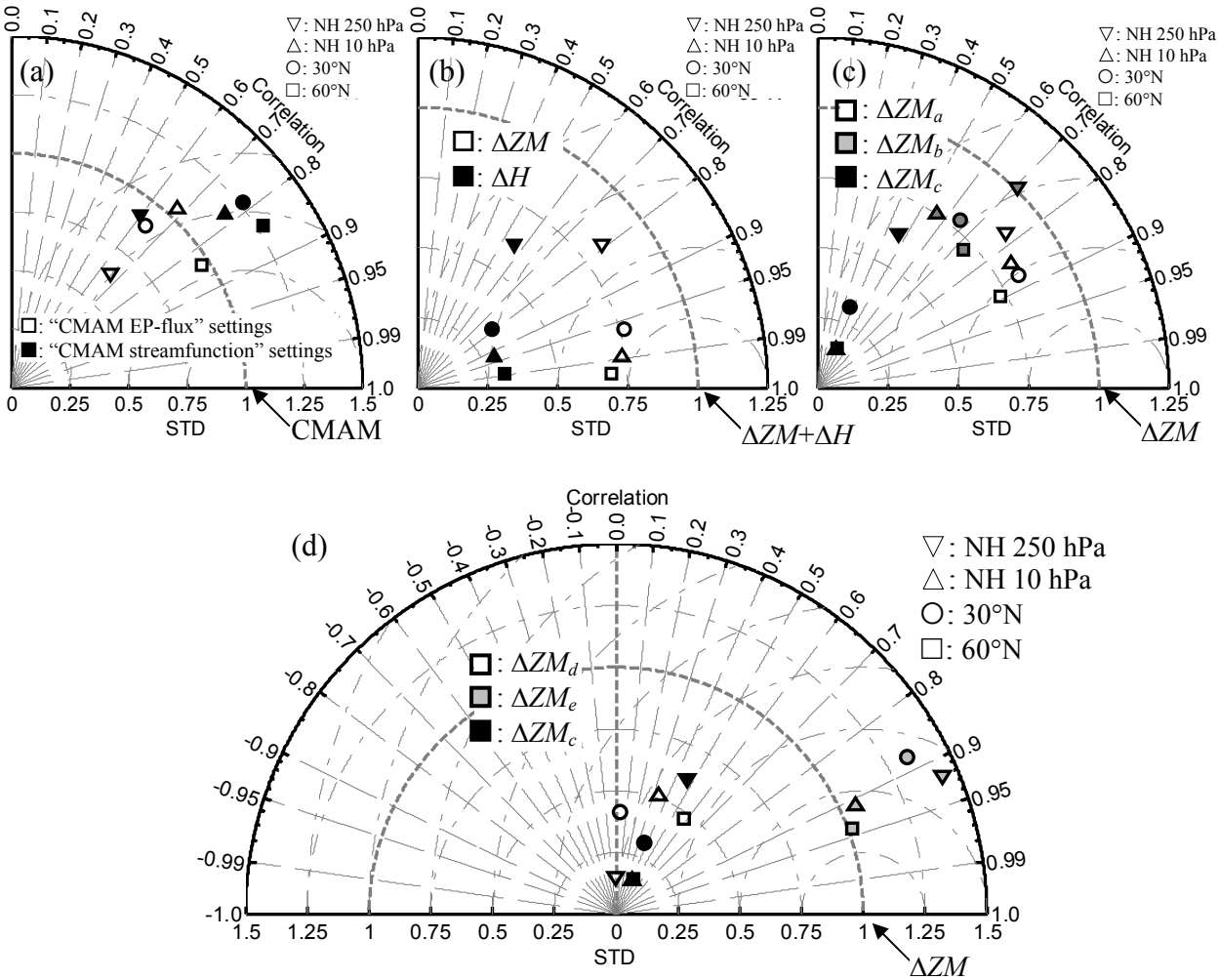

Figure 4.10: (a) Taylor diagram of NH winter stationary wave response to climate change diagnosed by the stationary wave model (ΔZM + ΔH) using the "CMAM streamfunction" damping settings (black symbols; the same as the black symbols in Figure 4.3) and the "CMAM EP-flux" damping settings (white symbols) compared with the CMAM stationary wave response to climate change (the target). (b) Similar to Figure 4.7 but using the "CMAM EP-flux" damping settings.(c) Similar to Figure 4.8 but using the "CMAM EP-flux" damping settings. (d) Similar to (c) but for the stationary wave response to ΔZM_d (white symbols), ΔZM_e (grey symbols), and ΔZM_c (black symbols) compared with the response to the total zonal mean changes (ΔZM, the target; white symbols in (a) or the target "1" in (b)).

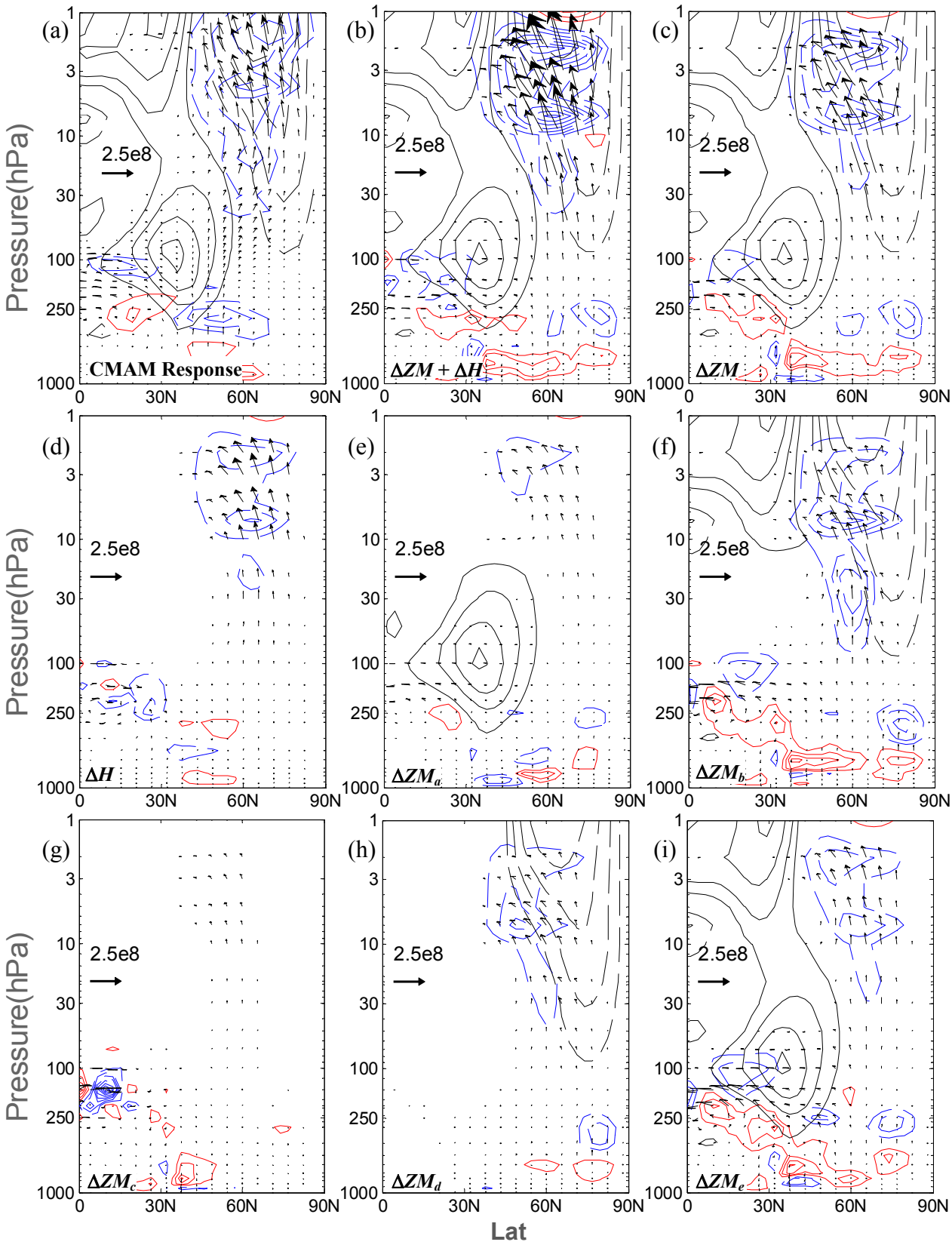
(a)
(b)
(c)
(d)
(e)
(f)
(g)
(h)
(i)
2.5e8
CMAM Response
ΔZM + ΔH
ΔZM
ΔH
ΔZM_a
ΔZM_b
ΔZM_c
ΔZM_d
ΔZM_e
Pressure(hPa)
1
3
10
30
100
250
1000
0
30N
60N
90N
Lat

Figure 4.11: Similar to Figure 4.9, but for (a) the CMAM stationary wave EP-flux (arrows) response to climate change (copied from Figure 4.9b for ease of comparison), and the EP-flux response diagnosed by the stationary wave model using the "CMAM EP-flux" damping settings to (b) $\Delta ZM + \Delta H$, (c) ΔZM, (d) ΔH, (e) ΔZM_a, (f) ΔZM_b, (g) ΔZM_c, (h) ΔZM_d, and (i) ΔZM_e. The contour interval of EP-flux divergence (blue and red curves) is 25 m^2s^{-2}.

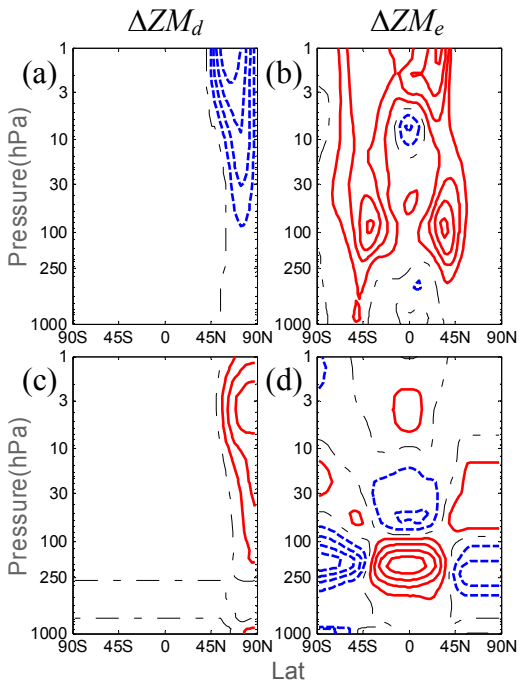

Figure 4.12: Similar to Figure 4.5 but for an alternative decomposition of ΔZM: (a, c) ΔZM_d, (b, d) ΔZM_e, which satisfy $\Delta ZM = \Delta ZM_d + \Delta ZM_e + \Delta ZM_c$.

Chapter 5

5 Conclusions

5.1 Summary

In this thesis stationary wave theory has been explored through analytical and numerical diagnoses of systems from simple barotropic dynamics to full stratosphere-troposphere atmospheric dynamics. The efforts made here have contributed to understanding the role that stationary wave nonlinearity plays in the maintenance of the time mean circulation and to understanding the dynamics of the stationary wave response to climate change in the troposphere and the stratosphere.

In Chapter 2 of this thesis, basic dynamical issues of nonlinear stationary wave dynamics have been investigated in the context of simple barotropic QG dynamics. The large-scale tropospheric time mean flow has a significant barotropic component that can be described with this dynamics, as revealed, for example, in the earliest studies on the topic by Charney and Eliassen (1949) on topographically forced Rossby waves and in the very recent study by Brandefelt and Körnich (2008) on the stationary waves simulated by the IPCC AR4 models and their response to GHG forcing. In this simple framework the dynamical effects of stationary wave nonlinearity have been investigated and found to be strongly related to the stationary wave critical layer reflection in both the absence and presence of transient waves. Stationary wave nonlinearity is the dominant factor in explaining the difference between the nonlinear and linear stationary wave solutions in the absence of transient waves. When the damping is weakened to allow transient waves to develop, the adjustments to the zonal mean in addition to stationary

wave nonlinearity need to be taken into account to accurately capture the character of critical layer reflection in the DNS solution. Neither zonal mean nor zonally asymmetric components of the time mean transient wave flux convergences are found to be responsible for critical layer reflection. Including the zonal mean adjustment to the transient wave forcing does produce reflection of wave activity but with a different pattern than the DNS solution. Stationary wave nonlinearity explains the difference between the nonlinear and linear stationary waves as long as the stationary waves are strong enough to generate localized easterlies and weak PV gradients, even if the zonal mean zonal wind is westerly at any given latitude. Only when the winds are strongly westerly at all latitudes, a regime which is unrealistic and far from the observed mean flow, does the zonal mean adjustment becomes more important than stationary wave nonlinearity.

Also, in Chapter 2, a weakly nonlinear asymptotic theory has been developed to explain the dynamics of the stationary wave nonlinearity for the strongly damped case. This theory demonstrates that, to leading order, stationary wave nonlinearity represents PV advection of the linear response. While there is potential to improve this asymptotic theory (see Section 2.8), this extended theory may not apply directly to the weakly damped case because of the absence of a statistical closure for transient wave flux convergences.

The widely used Ting-Yu nonlinear technique of stationary wave modeling has been tested quantitatively in this simple barotropic setting, demonstrating that the barotropic stationary wave model using this technique is able to well capture the stationary wave in the DNS. Having gained some confidence in the use of the technique, in Chapter 3 of the thesis it is then applied in the baroclinic case to develop a stratosphere-troposphere stationary wave model that is able to capture observed or simulated stationary waves and that is able to diagnose the stationary wave response to climate change simulated by comprehensive GCMs. The stationary wave model has

been tested with ERA-40 data, providing useful experience on how to combine zonally asymmetric stationary forcings such as diabatic heating and transient wave flux convergences in the stationary wave model.

In Chapter 4 of the thesis, the nonlinear stationary wave model is used to analyze the simulated response to climate change in a CCM. The analysis of a CMAM simulation following the CCMVal REF-2 scenario using the stationary wave model has quantified the relative importance of the changes in the zonal mean flow and in the zonally asymmetric forcings. Many aspects of the stationary wave response appear to be tied to changes to the zonal mean flow, consistent with some of the previous studies on tropospheric stationary waves (Joseph et al. 2004; Brandefelt and Körnich 2008). This dominance is even more significant in the stratosphere, which has not been well represented in previous studies. Further decomposition of the zonal mean flow change has identified the westerly response near the NH subtropical tropopause and its corresponding zonal mean temperature change to be one of the major factors controlling the stationary wave response. This is a potentially useful result because this westerly response is common among many models and is understood to be radiatively, rather than dynamically driven, and therefore independent of the stationary wave response itself. This is in contrast to extratropical zonal mean responses which typically have a strong dynamical component.

The analysis in Chapter 4 has also shown that explaining the primary wave response might be simpler than explaining the wave driving response. The EP-flux response is more challenging for the stationary wave model to capture, because it involves detailed structural information in the wind and temperature eddy fields, and appears to be sensitive to many aspects of changes to the basic state. One finding of the analysis in Chapter 4 is that the strategy of tuning on stationary wave amplitude and phase structure, which followed previous practice in

tropospheric stationary wave modeling, leads to a stationary wave model that is unable to capture the key features of the EP-flux response to climate change in CMAM at high latitudes. It is thus necessary to retune the stationary wave model for this application.

The retuned stationary wave model (Section 4.6) agrees better in the wave forcing response with the CMAM simulation. In this case, changes to the zonal mean flow control the EP-flux response, but changes to the diabatic heating also play a non-negligible role. The decomposition of the zonal mean basic state shows that different regions control the stratospheric EP-flux response. In particular, the subtropical jet response is relatively unimportant, and zonal mean changes in the polar stratosphere and the diabatic heating change are relatively more important to the stratospheric EP-flux response. It is noteworthy that the stratospheric EP-flux responses to these components are similar in pattern or at least agree in sign, indicating involvement of positive feedbacks.

Thus, overall, the thesis has provided the following significant and original contributions:

- It has been shown that stationary wave nonlinearity is the dominant factor in explaining the difference between the linear and full nonlinear stationary waves in QG barotropic dynamics, particularly if the zonal-mean flow adjustment to the stationary waves is included. Wave activity analysis shows that stationary wave nonlinearity is associated with localized Rossby wave critical layer reflection, in both QG barotropic dynamics and realistic atmospheric general circulation (at least in the troposphere).

- Furthermore, the stationary wave model developed in this thesis is probably the first realistic stationary wave model with a well resolved stratosphere and is able to capture the observed or simulated stationary waves.

- In addition, this stationary wave model is applied to diagnose and quantify the NH wintertime stationary wave response to climate change simulated by a CCM, the CMAM. In this CMAM simulation the response of the zonal mean basic state to climate change alone is responsible for more than half of the stationary wave response, especially in the stratosphere. This part of the stationary wave response is primarily controlled by changes of the zonal mean circulation in the NH subtropical upper troposphere.

- Finally, the stratospheric wave driving response is found to be also affected significantly by other aspects of the zonal mean flow response and by the diabatic heating response. These climate change related effects appear to contribute robustly to an increased wave activity flux into the stratosphere. Some of these effects reinforce each other, likely through wave-mean flow interactions.

5.2 Future research topics

While the work presented in this thesis has improved the understanding of the stationary wave dynamics, many aspects of the topic remain to be clarified. As introduced in Section 1.3, state-of-the-art comprehensive GCMs and CCMs do not capture some of the essential characteristics of the observed atmospheric stationary wave field, especially in the stratosphere where there is a large spread in the simulated stationary wave amplitude. This point is also demonstrated in Figure 5.1 which shows Taylor diagrams comparing the NH wintertime

stationary waves in the CCMVal-2 REF-B2 simulations and the stationary wave solution diagnosed by the stationary wave model to ERA-40 data. For the stationary wave model it is necessary to prescribe zonal mean basic state and zonally asymmetric forcing (corresponding to symbol “15” in Figure 3.7) from ERA-40 data. The NCEP stationary wave field is included as a rough measure of the uncertainty in observations; its correlation with the ERA-40 field is better than 0.95. Even the best CCMs are well separated from the observations given the observational uncertainty. CCMs capture the observed stationary wave relatively well in the troposphere and subtropics (Figure 5.1a, c), but in the stratosphere and high latitudes there is a large spread of both correlation and amplitude (Figure 5.1b, d). On the other hand, in the upper troposphere and subtropics the stationary wave model is not far from the CCMs (Figure 5.1a, c), and in the stratosphere and high latitudes it performs as well as the CCMs (Figure 5.1b, d). This comparison indicates that increased complexity of a model does not guarantee increased realism and that in some situations simple models might be sufficient to capture essential dynamics.

The fact is that the complexity of state-of-the-art GCMs and CCMs keeps increasing as more and more components are added into models. Most of these components represent physical or chemical processes, which have feedbacks onto the atmospheric general circulation to a greater or lesser degree. Including these components is certainly necessary to improve the prediction of future climate, but is not guaranteed to improve the understanding of fundamental dynamics or the accuracy in simulating the observations. The interactions between the circulation and these components are often complicated and not well understood. For example, the climatological mean temperature biases in CCMVal-2 models (Butchart et al. 2010b) have been barely improved in general compared with those biases in CCMVal models (Eyring et al. 2006). Another common weakness in CCMs is the representation of the QBO. The QBO is a

dominant mode of natural stratospheric variability in tropics, and has significant influence on extra-tropical stratospheric circulation as well through modulation of winds and extra-tropical wave propagation (see review in Baldwin et al. 2001). Most of the current CCMs, however, do not simulate a QBO; the investigation of extra-tropical dynamical influence of QBO still largely relies on simplified models (e.g., Holton and Tan 1980, 1982; Holton and Austin 1991; Naito et al. 2003; Hampson and Haynes 2006). The NH winter zonal mean wind difference between the westerly phase QBO years and easterly phase QBO years is up to 14 m s^{-1} in the polar stratosphere (Baldwin and Dunkerton 1998) and its structure is similar to the zonal wind response of ΔZM_d in Figure 4.12a. This zonal mean difference may not have strong impacts on the stationary wave field but may influence the stratospheric wave activity significantly, similarly to the findings in Section 4.6 of this thesis. The impact of the zonal mean wind difference in the two QBO phases on the extra-tropical circulation is a possible application of the stationary wave model developed in this thesis.

There are also other important issues that can be addressed with the current stationary wave model. For example, in light of the recent CCMVal-2 intercomparison and assessment activities, a natural extension of the work in this thesis is to test the findings of this study in those CCM simulations. It would be strongly preferable if the diabatic heating and transient wave flux fields were archived for these models and available for use in this analysis, although the analysis of Chapter 4 was able to proceed with some compromises without these fields for the CMAM simulations (see Chapter 4). To date the full diabatic heating field has been obtained by the author from only one of the CCMVal-2 models and this has been used to carry out preliminary tests regarding the dynamics of the stationary wave response to climate change (not shown here). Moreover, the stationary wave driving (EP-fluxes) decomposed in Chapter 4 has not been

directly attributed to the mean overturning circulation, i.e., the BDC, which can be diagnosed through the downward control principle (Haynes et al. 1991) similarly to Butchart et al. (2006) and McLandress and Shepherd (2009). This attribution can quantify the relative contribution to the BDC from the zonal mean flow change and its components as well as changes to the zonally asymmetric diabatic heating.

In addition, the spread in the stratospheric stationary wave response to climate change has not been quantitatively evaluated as in Brandefelt and Körnich (2008). Diabatic heating and transient wave fluxes from each model would permit this evaluation. In particular, the author wishes to test the effects of the acceleration of the zonal mean zonal wind near the subtropical tropopause in different CCMs. This feature is a robust response in both hemispheres to enhanced GHG forcing as a result of radiative warming in the tropical upper troposphere and radiative cooling in the polar stratosphere, which as discussed above is in principle separable from the stationary wave response. Moreover, the strengthening of the tropospheric jet in CMAM has a barotropic component similar to that of group *S* in Brandefelt and Körnich (2008). How the general eastward shift of the stationary wave field found in CMAM simulation (perhaps from other models as well, e.g., CCSM, GFDL0, MPI, MRI, PCM, and GISS in Figure 1.5) is dynamically linked to this zonal mean zonal wind response is another subject of future research.

The author has diagnosed long term trends in the seasonal stationary waves in the CCMVal-2 models and compared them with the ERA-40 and NCEP reanalyses (see also Butchart et al. 2010b). Few statistically significant trends in the observed seasonal stationary wave field are found, apart from a trend towards stronger zonal asymmetry in the SH stratosphere in the period 1980–1999. Figure 5.2 shows the trends in the SH stationary waves on 10 hPa for CCMVal-2 REF-B2 simulations as well as NCEP reanalysis and ERA-40 data. Both

the NCEP and ERA-40 trends are positive and statistically significant. Although almost all simulated trends are also positive, they are generally statistically insignificant except for the multi-model mean trend. Nevertheless there is a consistency between the simulations and observations which is possibly linked to zonally asymmetric trends in the SH ozone depletion (Crook et al., 2008); a possible mechanism is that the photochemical ozone loss within a displaced Antarctic vortex could strengthen the vortex and thus enhance the stationary wave field. This effect would reverse under ozone recovery, and in all the models the positive trend shown in Figure 5.2 weakens or switches sign from the period of 1980–1999 to the period of 2050–2099, though again, only a few of these trends and the multi-model mean trend are statistically significant. The stationary wave model developed in Chapters 3 and 4 can be used to study in detail the role of the chemistry-circulation interaction in these trends by diagnosing the effects of the diabatic heating due to the Antarctic ozone depletion and recovery on the stratospheric stationary wave field.

The stationary wave model can also be used to diagnose other feedbacks in the climate system. For example, the representation of snow-albedo feedback (SAF) is responsible for a significant fraction of variability among the predictions by IPCC AR4 models for future summertime climate change over cryospheric areas (Qu and Hall 2007). Fletcher et al. (2009a) find that SAF has a nonlocal influence on the NH summertime extratropical circulation: the increased land surface warming in models with stronger SAF induces large-scale sea-level pressure anomalies over the Pacific and Atlantic oceans and a poleward intensification of the NH subtropical jet. This response of the NH subtropical jet bears some similarity to the CMAM response to climate change, although it is much weaker and a little different in structure. Its effects on the stationary wave field can be diagnosed by the stationary wave model (similar to

Chapter 4) and compared with the circulation response simulated by GCM. In addition, Fletcher et al. (2009b) have designed another experiment to investigate the teleconnection between the variability in the extent of fall season snow cover over Northern Eurasia and the wintertime northern annular mode pattern. In this second experiment a wintertime coupled stratosphere-troposphere response is found to occur even without the persistence of the fall season snow forcing into winter. This response is also related to the wave-mean flow interaction which involves primarily quasi-stationary planetary waves. Thus one would expect the stationary wave model to be an appropriate diagnostic tool to identify proper mechanisms for this kind of dynamical coupling between the stratosphere and the troposphere.

On the other hand, one should not stop at the level of simple models such as the stationary wave models introduced in this thesis in order to better understand the dynamics of the stationary wave field or the atmospheric general circulation, but must go beyond prescribing forcings that are ingredients of the atmospheric circulation themselves. Intermediate models (e.g., Chang 2006) which lie between stationary wave models and GCMs, may provide more insight. Such models better approximate the coupling between elements such as stationary and transient waves, which is often crudely parameterized as linear damping in simple models. Held (2005) suggests that a hierarchy of intermediate models should fill the gap between simple models and comprehensive climate models. Current development of such intermediate models includes those in which simpler representations of moist processes are added and carefully tested (Frierson et al. 2006, 2007). A possible extension of the stationary wave model along this kind of development is to create a stationary wave model based on the Frierson et al. models, and thus to prognose empirically the diabatic heating response to climate change from the SST response simulated by

climate models. This extension can decrease the dependence of stationary wave models on prescribed diabatic heating.

Other extensions are also possible to the stationary wave theory and modelling discussed in this thesis. For example, the cancellation between the effects of stationary and transient waves in maintaining the zonal mean flow in barotropic dynamics suggests that care needs to be taken in separating their effects in both barotropic and baroclinic systems. Diagnosing systematically the roles of stationary and transient waves in maintaining the observed zonally symmetric and asymmetric time mean flow may improve the fundamental understanding of the dynamics of the general circulation.

Moreover, there certainly exists other types of dynamical effects due to stationary wave nonlinearity, such as the nonlinear interaction between topographically and diabatic-heating forced stationary waves (see review in Held et al. 2002). It would be interesting to explore the effects of this kind of nonlinearity quantitatively, which might be important not only locally in the troposphere but also remotely in the stratosphere. This kind of nonlinearity might also be important in shaping the zonal mean flow if wave-mean flow interactions are included in the stationary wave model. This point may be especially true in the stratosphere where the zonal mean flow and waves are not well separated as in the troposphere (e.g., Figure 1.1b,d).

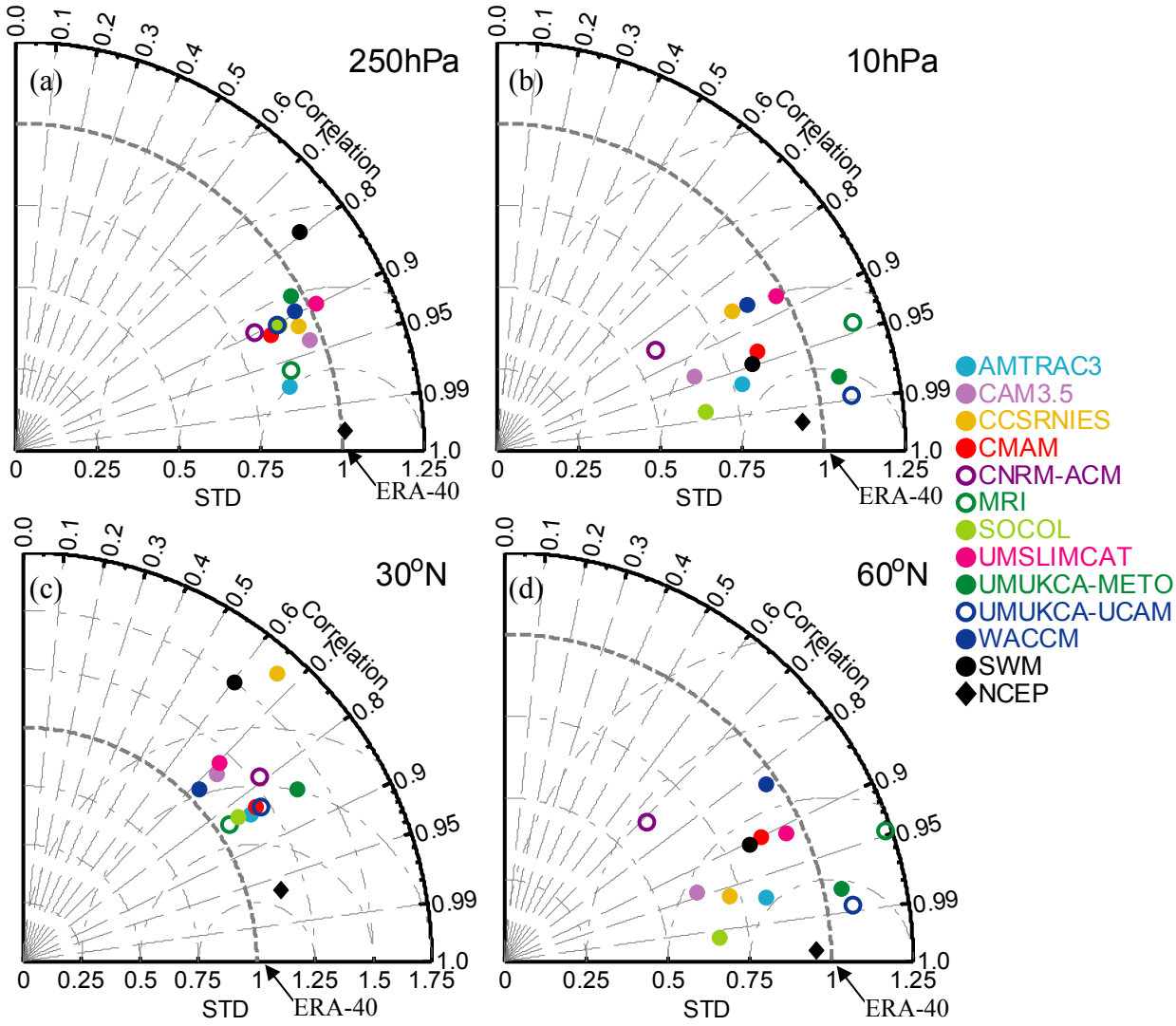

Figure 5.1: Taylor diagrams of stationary waves in CCMVal-2 REF-B2 simulations (color circles) and the stationary wave solution diagnosed by the stationary wave model forced by $O + H - H_{LW} + Trans_{strat}$ (equivalent to symbol "15" in Figure 3.7; black circles) compared with the ERA-40 stationary wave climatological mean (a) on 250 hPa, (b) on 10 hPa, (c) at 30°N, (d) at 60°N. The NCEP stationary wave field (black diamonds) is included as a measure of the uncertainty in observations. All stationary wave fields are in geopotential height. Data are based on NH winter (January 1980–1999) climatological mean geopotential heights for the CCMVal-2 models, the stationary wave model in Section 3.3, ERA-40, and NCEP reanalysis.

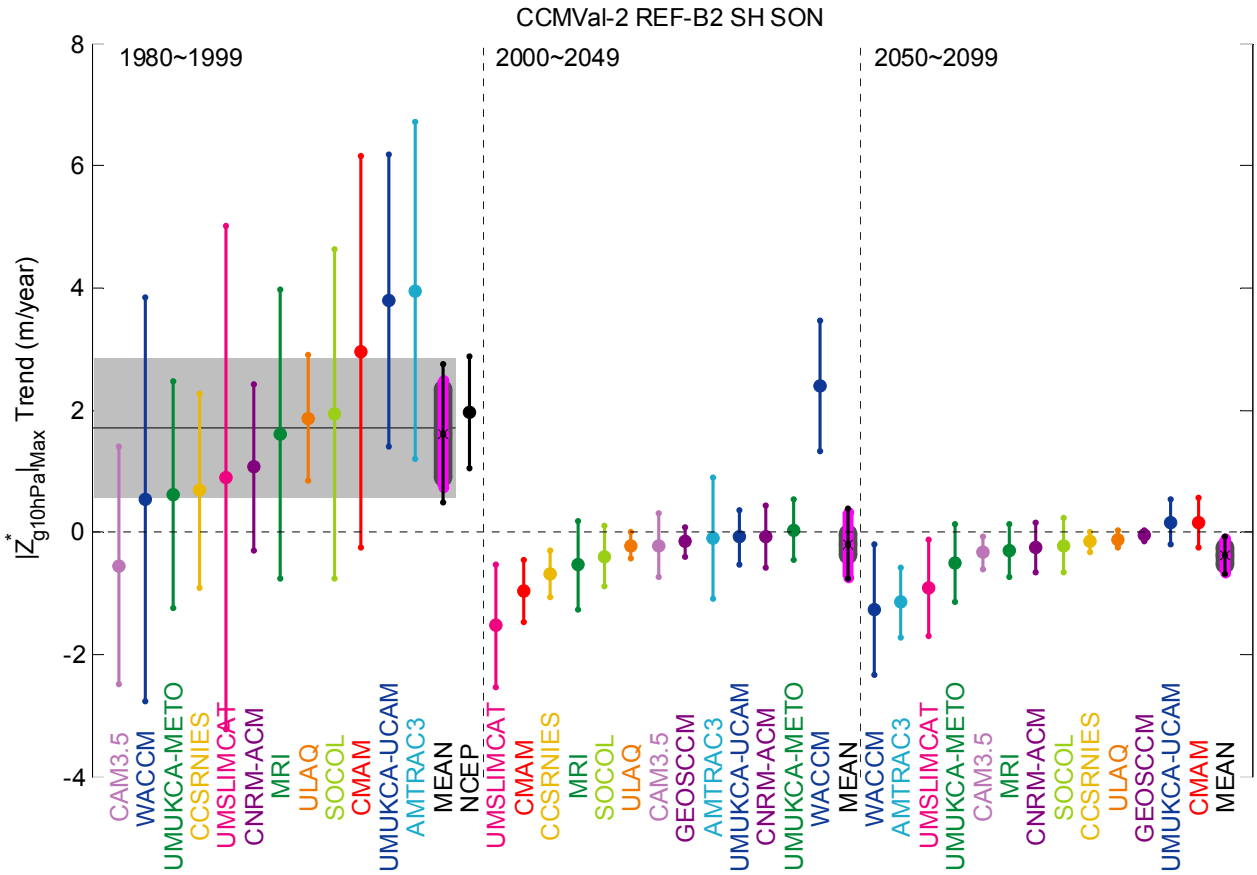

Figure 5.2: Trends in the amplitude of the seasonal-mean stationary wave for the periods 1980–1999, 2000–2049, and 2050–2099 in the CCMVal-2 REF-B2 simulations, ERA-40 (shaded) and NCEP data from 1980 to 1999. The trends for model simulations and NCEP data are plotted in filled circles with the error bars representing the uncertainties in these trends, and the ERA-40 trend is plotted as the horizontal solid line with its uncertainty in grey shading. The linear trend is calculated using least square estimates, and the *t*-distribution is used to test the two-sided hypothesis that the true trend is within the estimated trend plus or minus an uncertainty for a given significance level (p=0.05 here). The multi-model mean trend (indicated as "x") is simply the average of the trends of individual models, where its error bar in magenta indicates the inter-model spread (based on the *t*-test at the 0.05 significance level), its thick error bar in dark grey represents the uncertainty due to the confidence intervals of individual models, and the black thin error bar represents the combination of the above two errors via root sum square.

Bibliography

Baldwin, M.P. and T.J. Dunkerton, 1998: Quasi-biennial modulation of the southern hemisphere stratospheric polar vortex. *Geophys. Res. Lett.*, **25**, 3343-3346.

Baldwin, M.P. et al., 2001: The quasi-biennial oscillation. *Rev. Geophys.*, **39**, 179-229.

Barlow, M., S. Nigam, and E. H. Berbery, 2001: ENSO, Pacific decadal variability, and the U.S. summertime precipitation, drought, and streamflow. *J. Climate*, **14**, 2105–2128.

Beagley, SR, J. de Grandpré, J. N. Koshyk, N. A. McFarlane, and T. G. Shepherd, 1997: Radiative-dynamical climatology of the first-generation Canadian Middle Atmosphere Model. *Atmos. Ocean*, **35**, 293–331.

Boyle, J., 2006: Upper level atmospheric stationary waves in the twentieth century climate of the Intergovernmental panel on climate change simulations. *J. Geophys. Res.,* **111**, D14101, doi:10.1029/2005JD006612.

Brandefelt, J., and H. Körnich, 2008: Northern hemisphere stationary waves in future climate projections. *J. Climate*, **21**, 6341–6353.

Branstator, G. and S. E. Haupt, 1998: An empirical model of barotropic atmospheric dynamics and its response to tropical forcing. *J. Climate*, **11**, 2645–2667.

Branstator, G., 1992: The maintenance of low-frequency atmospheric anomalies. *J. Atmos. Sci.*, **49**(20), 1924–1946

Branstator, G., and J. Frederiksen, 2003: The seasonal cycle of interannual variability and the dynamical imprint of the seasonally varying mean state. *J. Atmos. Sci.*, **60**, 1577–1592.

Brunet, G. and P. Haynes, 1996: Low-Latitude Reflection of Rossby Wave Trains. *J. Atmos. Sci.*, **53**, 482–496.

Butchart, N., A. A. Scaife, M. Bourqui, J. de Grandpré, S.H.E. Hare, J. Kettleborough, U. Langematz, E. Manzini, F. Sassi, K. Shibata, D. Shindell, and M. Sigmond, 2006: Simulations of anthropogenic change in the strength of the Brewer-Dobson circulation. *Clim. Dynam.*,**27**, 727-741, doi:10.1007/s00382-006-0162-4.

Butchart, N., I. Cionni, V. Eyring, T. G. Shepherd, D. W. Waugh, H. Akiyoshi, J. Austin, C. Brühl, M. P. Chipperfield, E. Cordero, M. Dameris, R. Deckert, S. Dhomse, S. M. Frith, R. R. Garcia, A. Gettelman, M. A. Giorgetta, D. E. Kinnison, F. Li, E. Mancini, C. McLandress, S. Pawson, G. Pitari, D. A. Plummer, E. Rozanov, F. Sassi, J. F. Scinocca, K. Shibata, B. Steil and W. Tian, 2010a: Chemistry-climate model simulations of 21st century stratospheric climate and circulation changes. *J. Climate*, **23**, doi: 10.1175/2010JCLI3404.1.

Butchart, N., A. J. Charlton-Perez, I. Cionni, S. Hardiman, K. Krüger, P. J. Kushner, P. Newman, S. M. Osprey, J. Perlwitz, F. Sassi, M. Sigmond and L. Wang, 2010b: Stratospheric Dynamics, in *SPARC CCMVal*, *SPARC CCMVal Report on the Evaluation of Chemistry-Climate Models*, edited by V. Eyring, T. G. Shepherd, D. W. Waugh, SPARC Report No. 5, WCRP-X, WMO/TD-No. X, http://www.atmosp.physics.utoronto.ca/SPARC, 2010.

Butchart, N., A. J. Charlton-Perez, I. Cionni, S. C. Hardiman, K. Krüger, P. Kushner, P. A. Newman, S. M. Osprey, J. Perlwitz, F. Sassi, M. Sigmond, L. Wang, H. Akiyoshi, J. Austin, S. Bekki, A. Baumgartner, G. Bodeker, P. Braesicke, C. Brühl, M. Chippereld, M. Dameris, S. Dhomse, H. Garny, P. Jöckel, J.-F. Lamarque, M. Marchand, M. Michou, O. Morgenstern, T. Nakamura, S. Pawson, T. Peter, D. Plummer, J. Pyle, E. Rozanov, J.

Scinocca, T. G. Shepherd, K. Shibata, D. Smale, R. Stolarski, H. Teyssèdre, W. Tian, and Y. Yamashita, 2010c: Multi-model climatologies of the middle atmosphere. In preparation.

Chang, E. K. M., 2009: Diabatic and orographic forcing of northern winter stationary waves and storm tracks. *J. Climate*, **22**, 670–688.

Charney, J. G., and A. Eliassen, 1949: A numerical method for predicting the perturbations of the midlatitude westerlies. *Tellus*, **1**, 38–54.

Charney, J. G., and P. G. Drazin, 1961: Propagation of planetary scale disturbances from the lower into the upper stratosphere. *J. Geophys. Res.*, **66**(1), 83–109, doi:10.1029/JZ066i001p00083.

Crook, J. A., N. P. Gillett, and S. P. E. Keeley, 2008: Sensitivity of Southern Hemisphere climate to zonal asymmetry in ozone, *Geophys. Res. Lett.*, **35**, L07806, doi:10.1029/2007GL032698.

Davey, M. K., 1980: A quasi-linear theory for rotating flow over topography. I - Steady beta-plane channel. *J. Fluid Mech.*, **99**, 267-292.

DeWeaver, E. and S. Nigam, 2004: On the forcing of ENSO teleconnections by anomalous heating and cooling. *J. Climate*, **17**, 3225–3235.

Egger, J., 1976: The linear response of a hemispheric two–level primitive equation model to forcing by topography. *Mon. Wea. Rev.*, **104**(4), 351–364.

Eyring, V., N. Butchart, D. W. Waugh, H. Akiyoshi, J. Austin, S. Bekki, G. E. Bodeker, B. A. Boville, C. Brühl, M. P. Chipperfield, E. Cordero, M. Dameris, M. Deushi, V. E. Fioletov, S. M. Frith, R. R. Garcia, A. Gettelman, M. A. Giorgetta, V. Grewe, L.

Jourdain, D. E. Kinnison, E. Mancini, E. Manzini, M. Marchand, D. R. Marsh, T. Nagashima, P. A. Newman, J. E. Nielsen, S. Pawson, G. Pitari, D. A. Plummer, E. Rozanov, M. Schraner, T. G. Shepherd, K. Shibata, R. S. Stolarski, H. Struthers, W. Tian, and M. Yoshiki, 2006: Assessment of temperature, trace species and ozone in chemistry-climate model simulations of the recent past, *J. Geophys. Res.*, **111**, D22308, doi:10.1029/2006JD007327.

Eyring, V., D. W. Waugh, G. E. Bodeker, E. Cordero, H. Akiyoshi, J. Austin, S. R. Beagley, B. Boville, P. Braesicke, C. Brühl, N. Butchart, M. P. Chipperfield, M. Dameris, R. Deckert, M. Deushi, S. M. Frith, R. R. Garcia, A. Gettelman, M. Giorgetta, D. E. Kinnison, E. Mancini, E. Manzini, D. R. Marsh, S. Matthes, T. Nagashima, P. A. Newman, J. E. Nielsen, S. Pawson, G. Pitari, D. A. Plummer, E. Rozanov, M. Schraner, J. F. Scinocca, K. Semeniuk, T. G. Shepherd, K. Shibata, B. Steil, R. Stolarski, W. Tian, and M. Yoshiki, 2007: Multimodel projections of stratospheric ozone in the 21st century, *J. Geophys. Res.*, **112**, D16303, doi:10.1029/2006JD008332.

Fletcher, C. G., S. C. Hardiman, P. J. Kushner, and J. Cohen, 2009: The dynamical response to snow cover perturbations in a large ensemble of atmospheric GCM integrations, *J. Climate*, **22**, 1208-1222. doi:10.1175/2008JCLI2505.1.

Fletcher , C. G., P. J. Kushner, A. Hall, and X. Qu, 2009: Circulation responses to snow albedo feedback in climate change, *Geophys. Res. Lett.*, **36**, L09702, doi:10.1029/2009GL038011

Frierson, D. M. W., I. M. Held, and P. Zurita-Gotor, 2006: A gray-radiation aquaplanet moist GCM. Part I: Static stability and wave scale. *J. Atmos. Sci.*, **63**, 2548–2566.

Frierson, D. M. W., I. M. Held, and P. Zurita-Gotor, 2007: A gray-radiation aquaplanet moist GCM. Part II: Energy transports in altered climates. *J. Atmos. Sci.*, **64**, 1680–1693.

Gritsun, A. and G. Branstator, 2007: Climate response using a three-dimensional operator based on the fluctuation–dissipation theorem. *J. Atmos. Sci.*, **64**, 2558–2575.

Grose, W. L. and B. J. Hoskins. 1979: On the influence of orography on the large-scale atmospheric flow. *J. Atmos. Sci.*, 36, 223–234.

Hampson, J. and P. Haynes, 2006: Influence of the equatorial QBO on the extratropical stratosphere. J. Atmos. Sci., 63:936–951.

Harnik, N., and R. S. Lindzen, 2001: The effect of reflecting surface on the vertical structure and variability of stratospheric planetary waves. *J. Atmos. Sci.*, **58**, 2872-2894.

Haynes, P. H., and M. E. McIntyre, 1987: On the representation of Rossby-wave critical layers and wave breaking in zonally truncated models. *J. Atmos. Sci.*, **44**, 2359--2382.

Haynes, P. H., M. E. McIntyre, T. G. Shepherd, C. J. Marks, and K. P. Shine, 1991: On the "downward control" of extratropical diabatic circulations by wave-induced mean zonal forces. *J. Atmos. Sci.*, **48**, 651-680.

Held, I. M., 1983: Stationary and quasi-stationary eddies in the extratropical troposphere: theory. In *Large-scale Dynamical Processes in the Atmosphere*, eds. B. J. Hoskins and R. P. Pearce, Academic Press, 127-168, London; New York.

Held, I. M., 1985: Pseudomomentum and the orthogonality of modes in shear flows. *J. Atmos. Sci.*, **42**, 2280–2288.

Held, I. M., 2005: The gap between simulation and understanding in climate modeling. *Bull. Amer. Meteor. Soc.*, **11**, 1609-1614.

Held, I. M, M. F. Ting, and H. L. Wang, 2002: Northern Winter Stationary Waves: Theory and Modeling. *J. Climate*, **15**(16), 2125–2144.

Held, I. M. and M. F. Ting, 1990: Orographic versus thermal forcing of stationary waves: The importance of the mean low-level wind. *J. Atmos. Sci.*, **47**(4), 495–500.

Held, I. M., and M. J. Suarez, 1994: A Proposal for the Intercomparison of the Dynamical Cores of Atmospheric General Circulation Models. *Bull. Amer. Meteor. Soc.*, **75**, 1825–1830.

Held, I. M., and P. J. Phillips, 1987: Linear and nonlinear barotropic decay on the sphere. *J. Atmos. Sci.*, **44**, 200–207.

Held, I. M., W. Lyons, and S. Nigam, 1989: Transients and the extratropical response to El Niño. *J. Atmos. Sci.*, **46**, 163–174.

Hendon, H. H. and D. L. Hartmann, 1982: Stationary Waves on a Sphere: Sensitivity to Thermal Feedback. *J. Atmos. Sci.*, **39**(9), 1906–1920.

Holton, J. R. and J. Austin, 1991: The influence of the equatorial QBO on sudden stratospheric warmings. *J. Atmos. Sci.*, **48**, 607–618.

Holton, J. R., P. H. Haynes, M. E. McIntyre, A. R. Douglass, R. B. Rood and L. Pfister, 1995: Stratosphere-troposphere exchange. *Rev. Geophys.*, **33**(4), 403–439, doi:10.1029/95RG02097.

Holton, J. R. and H. C. Tan, 1980: The influence of the equatorial quasi-biennial oscillation on the global circulation at 50 mb. *J. Atmos. Sci.*, **37**, 2200–2208.

Holton, J. R. and H. C. Tan, 1982: The quasi-biennial oscillation in the Northern Hemisphere lower stratosphere. *J. Meteor. Soc. Japan*, **60**, 140–148.

Hoskins, B. J. and D. J. Karoly, 1981: The steady linear response of a spherical atmosphere to thermal and orographic forcing. *J. Atmos. Sci.*, **38**(6), 1179–1196.

Hoskins, B.J., and T. Ambrizzi, 1993: Rossby wave propagation on a realistic longitudinally varying flow. *J. Atmos. Sci.*, **50**, 1661–1671.

Hoskins, B. J. and M. J. Rodwell, 1995: A Model of the Asian Summer Monsoon. Part I: The Global Scale. *J. Atmos. Sci.*, **52**(9), 1329–1340.

Intergovernmental Panel on Climate Change, 2007: *The Physical Science Basis*: Working Group I Contribution to the Fourth Assessment Report of the IPCC. Cambridge University Press, Cambridge, UK and New York, NY, USA, 1009pp.

Jin, F. F., and B. J. Hoskins, 1995: The Direct Response to Tropical Heating in a Baroclinic Atmosphere. *J. Atmos. Sci.*, **52**, 307–319.

Joseph, R., M. F. Ting, and P. J. Kushner, 2004: The global stationary wave response to climate change in a coupled GCM. *J. Climate*, **17**(3), 540–556.

Kalnay, E., M. Kanamitsu, R. Kistler, W. Collins, D. Deaven, L. Gandin, M. Iredell, S. Saha, G. White, J. Woollen, Y. Zhu, A. Leetmaa, R. Reynolds, M. Chelliah, W. Ebisuzaki, W. Higgins, J. Janowiak, K. C. Mo, C. Ropelewski, J. Wang, R. Jenne, and D. Joseph, 1996: The NCEP/NCAR 40-Year Reanalysis Project. *Bull. Amer. Meteor. Soc.*, **77**, 437–471.

Karoly, D. J., 1983: Rossby wave propagation in a barotropic atmosphere. *Dyn. Atmos. Oceans*, **7**, 111-125.

Körnich, H., G. Schmitz, and E. Becker, 2006: The role of stationary waves in the maintenance of the northern annular mode as deduced from model experiments. *J. Atmos. Sci.*, **63**, 2931–2947.

Kushner, P. J., and L. M. Polvani, 2004: Stratosphere–Troposphere coupling in a relatively simple AGCM: The role of Eddies. *J. Climate*, 17(3), 629-639.

Leith, C. E., 1975: Climate response and fluctuations, *J. Atmos. Sci.*, **32**, 2022–2026.

Lin, B-D., 1982: The behavior of winter stationary planetary waves forced by topography and diabatic heating. *J. Atmos. Sci.*, **39**, 1206–1226.

Lindzen, R. S. and H. L. Kuo, 1969: A reliable method for the numerical integration of a large class of ordinary and partial differential equations. *Mon. Wea. Rev.*, **97**, 732-734.

Lindzen, R. S. and T. Matsuno, 1968: On the nature of large scale wave disturbances in the equatorial lower stratosphere. *J. Met. Soc. Japan*, **46**, 215-221.

Liu, A. Z., M. Ting, and H. Wang, 1998: Maintenance of circulation anomalies during the 1988 drought and 1993 floods over the United States. *J. Atmos. Sci.,* **55,** 2810–2832.

Lorenz, D. J., and E. T. DeWeaver, 2007: Tropopause height and zonal wind response to global warming in the IPCC scenario integrations, *J. Geophys. Res.*, **112**, D10119, doi:10.1029/2006JD008087.

Matsuno, T., 1970: Vertical propagation of stationary planetary waves in the winter northern hemisphere, *J. Atmos. Sci.*, **27**, 871–883.

Matsuno, T., 1971: A dynamical model of the stratospheric sudden warming. *J. Atmos. Sci.*, **28**, 1479–1494.

McLandress, C., and Shepherd, T. G., 2009: Simulated anthropogenic changes in the Brewer-Dobson circulation, including its extension to higher latitudes. *J. Climate*, **22**, 1516-1540.

Naito, Y., M. Taguchi, and S. Yoden, 2003: A parameter sweep experiment on the effects of the equatorial QBO on stratospheric sudden warming events. *J. Atmos. Sci.*, **60**, 1380–1394.

Nigam, S., and I. M. Held, 1983: The influence of a critical latitude on topographically forced stationary waves in a barotropic model. *J. Atmos. Sci.*, **40**, 2610–2622.

Nigam, S., I. M. Held and S. W. Lyons, 1986: Linear simulation of the stationary eddies in a GCM. Part I: The no-mountain model. *J. Atmos. Sci.*, **43**(23), 2944–2961.

Nigam, S., I. M. Held and S. W. Lyons, 1988: Linear simulation of the stationary eddies in a GCM. Part II: The "mountain" model. *J. Atmos. Sci.*, **45**(9), 1433–1452.

Pan, Z., M. Segal, R. W. Arritt, T. C. Chen and S. P. Weng, 1999: A method for simulating effects of quasi-stationary wave anomalies on the regional climate. *J. Climate*, **12**, 1336–1343.

Peixoto, J. P., and A. H. Oort, 1992: *Physics of Climate*. American Institute of Physics, 520 pp, New York, USA.

Plumb, R. A., 1985: On the three-dimensional propagation of stationary waves. *J. Atmos. Sci*, **42**, 217–229.

Polvani, L.M. and P. J. Kushner, 2002: Tropospheric response to stratospheric perturbations in a relatively simple general circulation model. *Geophys. Res. Lett.*, **29**, 2001GL014284.

Qin, J. and W. A. Robinson, 1993: On the Rossby wave source and the steady linear response to tropical forcing. *J. Atmos. Sci.*, **50**, 1819–1823.

Qu, X., and A. Hall, 2007: What controls the strength of snow-albedo feedback? *J. Clim.*, **20**(15), 3971–3981, doi:10.1175/JCLI4186.1.

Ringler, T. D. and K. H. Cook, 1997: factors controlling nonlinearity in mechanically forced stationary waves over orography. *J. Atmos. Sci.*, **54**(22), 2612–2629.

Robinson, W. A., 1986: Interactions between Stationary Planetary Waves in the Stratosphere. *J. Atmos. Sci.*, **43**(10), 1006–1016.

Rodwell, M. J., and B. J. Hoskins, 1996: Monsoons and the dynamics of deserts. *Quart. J. Roy. Meteor. Soc.,* **122**, 1385-1404.

Rosenlof, K. H. and J. R. Holton, 1993: Estimates of the stratospheric residual circulation using the downward control principle, *J. Geophys. Res.*, **98**(D6), 10,465–10,479.

Rossby, C. G., 1939: Relation between variations and the intensity of the zonal circulation of the atmosphere and the displacements of the semi-permanent centers of action. *J. Mar. Res.*, **2**, 38–55.

Rossby, C. G., 1940: Planetary flow patterns in the atmosphere. *Quart. J. Roy. Meteor. Soc.* (suppl), **66**, 68-87.

Scinocca, J. F., N. A. McFarlane, M. Lazare, J. Li, and D. Plummer, 2008: The CCCma third generation AGCM and its extension into the middle atmosphere. *Atmos. Chem. Phys.*, **8**, 7055-7074.

Shaman, J. and E. Tziperman, 2005: The effect of ENSO on Tibetan Plateau snow depth: A stationary wave teleconnection mechanism and implications for the South Asian monsoons. *J. Climate*, **18**, 2067–2079.

Shepherd, T.G., 2008: Dynamics, stratospheric ozone, and climate change. *Atmos.-Ocean*, **46**, 371-392.

Shutts, G. J., 1978: Quasi-geostrophic planetary wave forcing. *Quart. J. Roy. Meteor. Soc.*, **104**, 331-350.

Simmons, A. J., 1974: Planetary-scale disturbances in the polar winter stratosphere. *Quart. J. Roy. Meteor. Soc.*, **100**, 76–108.

Simmons, A. J., J. M. Wallace, and G. W. Branstator, 1983: Barotropic wave propagation and instability and atmospheric teleconnection patterns. *J. Atmos. Sci.*, **40**, 1363-1392.

Smagorinsky, J., 1953: The dynamical influences of large-scale heat sources and sinks on the quasi-stationary mean motions of the atmosphere. *Quart. J. Roy. Meteor. Soc.*, **79**, 342–366.

SPARC CCMVal, 2010: SPARC Report on the Evaluation of Chemistry-Climate Models, V. Eyring, T. G. Shepherd, D. W. Waugh (Eds.), SPARC Report No. 5, WCRP-132, WMO/TD-No. 1526, http://www.atmosp.physics.utoronto.ca/SPARC.

Stephenson D. B., and I. M. Held, 1993: GCM response of Northern winter stationary waves and storm tracks to increasing amounts of carbon dioxide. *J. Climate*, **6**, 1859–1870.

Taylor, K. E., 2001, Summarizing multiple aspects of model performance in a single diagram. *J. Geophys. Res.*, **106**, 7183–7190, doi:10.1029/2000JD900719.

Ting, M. F. and L. H. Yu, 1998: Steady Response to Tropical Heating in Wavy Linear and Nonlinear Baroclinic Models. *J. Atmos. Sci.*, **55**(24), 3565–3582.

Ting, M. F. and P. D. Sardeshmukh, 1993: Factors determining the extratropical response to equatorial diabatic heating anomalies. *J. Atmos. Sci.*, **50**(6), 907–918.

Ting, M. F., 1994: Maintenance of northern summer stationary waves in a GCM. *J. Atmos. Sci.*, **51**, 3286–3308.

Ting, M. F., H. L. Wang and L. H. Yu, 2001: Nonlinear Stationary Wave Maintenance and Seasonal Cycle in the GFDL R30 GCM. *J. Atmos. Sci.*, **58**(16), 2331–2354.

Uppala, S. M., P. W. Kaallberg, A. J. Simmonds, and 42 co-authors, 2005: The ERA-40 re-analysis. *Quart. J. Roy. Meteor. Soc.*, **131**(612), 2961–3012.

Valdes, P. J. and B. J. Hoskins, 1991: Nonlinear orographically forced planetary waves. *J. Atmos. Sci.*, **48**(18), 2089–2106.

Valdes, P. J. and B. J. Hoskins, 1989: Linear stationary wave simulations of the time-mean climatological flow. *J. Atmos. Sci.*, **46**(16), 2509–2527.

Vallis, G. K., 2006: *Atmospheric and oceanic fluid dynamics*. Cambridge University Press, 745 pp.

Walker, C. C., and G. Magnusdottir, 2003: Nonlinear planetary wave reflection in an atmospheric GCM. *J. Atmos. Sci.*, **60**, 279–286.

Wallace, J. M., and D. S. Gutzler, 1981: Teleconnections in the geopotential height field during the Northern Hemisphere Winter. *Mon. Wea. Rev.,* **109,** 784-812.

Wang, L., and P.J. Kushner, 2010: Interpreting stationary wave nonlinearity in barotropic dynamics. *J. Atmos. Sci.*, **67**(7), 2240–2250, DOI: 10.1175/2010JAS3332.1.

Waugh, D.W., R.A. Plumb, and L.M. Polvani, 1994: Nonlinear, barotropic response to a localized topographic forcing: formation of a “tropical surf zone” and its effect on interhemispheric propagation. *J. Atmos. Sci.*, **51**, 1401–1416.

Wirth, V., 1991: What causes the seasonal cycle of stationary waves in the southern stratosphere? *J. Atmos. Sci*, **48**, 1194–1200.

Yulaeva, E., J. R. Holton and J. M. Wallace, 1994: On the Cause of the Annual Cycle in Tropical Lower-Stratospheric Temperatures. *J. Atmos. Sci.*, **51**(2), 169–174.

Copyright Acknowledgements

Figure 1.5 is from Figure 3 in Brandefelt, J., and H. Körnich, 2008: Northern hemisphere stationary waves in future climate projections. *J. Climate*, **21**, 6341–6353. ©American Meteorological Society. Reprinted with permission.

Chapter 2 is based on Wang, L., and P.J. Kushner, 2010: Interpreting stationary wave nonlinearity in barotropic dynamics. *J. Atmos. Sci.*, **67**(7), 2240–2250, DOI: 10.1175/2010JAS3332.1. ©American Meteorological Society. Reprinted with permission.

Figure 1.3 and Figure 5.2 are from the lower left panel of Figure 4.5, Figure 4.8, respectively, in *SPARC CCMVal*, *SPARC CCMVal Report on the Evaluation of Chemistry-Climate Models*, edited by V. Eyring, T. G. Shepherd, D. W. Waugh, SPARC Report No. 5, WCRP-X, WMO/TD-No. X, http://www.atmosp.physics.utoronto.ca/SPARC, 2010. Reprinted with permission.